Immunomodulatory Contribution of Mast Cells to the Biomaterial Microenvironment

Short Title: Mast Cell Response to Immunomodulatory Biomaterial

Raymond M. Wang[a], Jessica Ungerleider[a], Yu Kawakami[b,c], Yuko Kawakami[b,c], Toshiaki Kawakami[b,c], Karen L. Christman[a]*

Affiliations:

[a]Department of Bioengineering, Sanford Consortium of Regenerative Medicine, University of California San Diego, 2880 Torrey Pines Scenic Drive, La Jolla, CA, 92037, USA.

[b]Division of Cell Biology, La Jolla Institute for Immunology, La Jolla, California, 92037, USA.

[c]Department of Dermatology, University of California San Diego, School of Medicine, La Jolla, CA, 92093, USA.

***Corresponding Author:**

Karen L. Christman, PhD

UC San Diego

Sanford Consortium for Regenerative Medicine

2880 Torrey Pines Scenic Drive

La Jolla, CA 92037

Telephone: (858) 822-7863

Fax: (858) 534-5722

Email: christman@eng.ucsd.edu

Abstract:

Immunomodulatory biomaterials have been shown to promote tissue repair and regeneration mainly through interaction with macrophages and T cells. In this study, we investigated the role of mast cells in the regulation of the immune response to decellularized biomaterial scaffolds. In mast cell-deficient mice, there was dysregulation of the expected M1 to M2 macrophage transition. Polarization progression deviated in a sex specific manner with an early transition to an M2 profile in female mice, while the male response was unable to properly transition past a pro-inflammatory M1 state. Both were reversed with adoptive mast cell transfer. Further investigation of the later stage immune response in male mice determined a sustained pro-inflammatory gene expression profile in deficient mice consisting of members from the IL-1 cytokine family, IL-6, IL-17, and related downstream pathways. These results highlight mast cells as another important cell type that influences the immune response to biomaterials.

Teaser: This study demonstrates the contribution of mast cells in immunomodulatory biomaterial therapies.

Introduction:

The immune response is known to have a necessary role in tissue homeostasis, remodeling, and repair, and our understanding of the involved immune populations and their phenotypic state improves our capacity to treat adverse disease conditions. Mast cells are tissue resident granulocytes classically associated in host defense, proinflammatory responses and various immune disorders (*1*). The granules of mast cells are known to contain a variety of immune mediators demonstrated to contribute to pathological responses such as allergic reactions, inflammatory cell recruitment (*2*), and fibrosis (*3*). While mast cells are also known to secrete a plethora of pro-remodeling/anti-inflammatory cytokines that are relevant for tissue repair, their role in tissue regenerative therapies has not been studied.

Biomaterial scaffolds that influence the immune response are emerging as a viable clinical strategy for tissue repair and regeneration (*4*). Although this immunomodulatory influence associated with improved tissue outcomes has been rigorously evaluated with macrophage (*5, 6*) and T cell populations (*7, 8*), potential contribution of mast cells to the immunomodulatory effect of naturally derived biomaterials has been largely ignored. *In vitro* culture of human mast cell lines has demonstrated that interaction in the decellularized extracellular matrix (ECM) microenvironment promotes mast cell differentiation, maturation, and viability compared to collagen controls (*9*). However, *in vivo* studies have mainly just evaluated shifts in mast cell numbers associated with biomaterial deployment, though their general low numbers in tissue make it difficult to determine conclusive results from this approach (*10, 11*). Early studies with synthetic materials have focused on their functional role and mainly produced results characteristic of a classical mast cell phenotype highlighting contributions to early acute inflammatory cell infiltration (*2*), and fibrous capsule formation (*12*). Thus, there is limited investigation on the influence of mast cells from a pro-regenerative biomaterial stimulus *in vivo*.

From a general tissue disease perspective, several studies have similarly emphasized the detrimental role of mast cells to tissue remodeling outcomes (*13-15*). However, research

has also produced confounding results (*16-19*) or evidence of their beneficial contributions to select cases of native tissue repair or inflammatory resolution (*17, 20, 21*), suggesting a greater functional complexity and potential to be utilized in therapeutic design. Given the recent clinical and rapidly expanding pre-clinical use of decellularized biomaterials derived from isolated tissue extracellular matrix, which are known to induce pro-remodeling and pro-regenerative effects based on immunomodulatory mechanisms in macrophages and T cells (*5, 7, 8*), we chose to evaluate this class of biomaterial scaffold in mast cell-deficient mice, and compared the biomaterial induced immune response to wild-type and mast cell engrafted responses. Based on recent evidence suggesting that mast cells can have beneficially influences on native tissue remodeling outcomes, we hypothesized mast cells play a role in regulation of decellularized ECM biomaterial scaffold-induced immunomodulatory responses, and demonstrated in this investigation its critical regulatory contribution to the pro-inflammatory to pro-remodeling immunomodulatory transition, which deviates in a sex specific manner.

Results:

Similar or Increased Leukocyte Recruitment Despite Lack of Mast Cell Contribution

To study the contribution of mast cells to the immunomodulatory response of ECM biomaterials, mast cell deficient mice $Kit^{W\text{-}sh/W\text{-}sh}$ mice were utilized as they are highly deficient in mast cells across various tissues and in the skin by 10-12 weeks while maintaining relatively normal levels of a broad range of lymphocyte and myeloid lineages (*22*), though some evidence of neutrophilia has been observed (*23*). For our investigation of the interaction with a biomaterial scaffold, we used an injectable hydrogel form of myocardial matrix, which was previously shown to be immunomodulatory (*24, 25*) and recently progressed through a Phase I clinical trial in post-myocardial infarction patients (*26*).

To study the influence of mast cells on the immune response to biomaterial scaffolds, we subcutaneously injected the ECM hydrogel into the dorsal region of male and female $Kit^{W\text{-}sh}$

mast cell-deficient mice, and compared the recruitment of surrounding immune cell populations to wild-type C57BL6/J mice. Day 1 isolated subcutaneous injections showed mast cell presence at low cellular density as early as day 1 post-injection in wild-type mice. Mast cells were non-degranulated or minimally degranulated based on toluidine blue staining while deficient mice showed no mast cell presence in the material or throughout the skin (Fig. 1A, B). Similar characteristics of mast cells along with greater inward infiltration were observed for the ECM scaffold isolated at 3 days post-injection (Fig. S1A, B). Comparison with subcutaneous injection of commercial milled urinary bladder matrix showed a similar non-degranulated state of mast cells bordering the material at day 3 post-injection demonstrating that these observations were not specific to the ECM hydrogel (Fig. S1C, D). Similar to a previous study utilizing human mast cell lines to study influence of decellularized ECM on mast cell viability (*9*), *in vitro* assessment of the interaction of differentiated bone marrow derived FcεRI^{+}c-kit^{+} mast cells (Fig. S2) with the ECM hydrogel material in solution at non-gelling concentrations in comparison to collagen and media only controls showed higher alamarBlue™ readings confirming matrix interaction enhanced differentiated mast cell viability (Fig. S3). Quantification of total cellular infiltration into the ECM hydrogel scaffold along with staining for Ly-6G/Ly-6C^{+} neutrophil (Fig. 1C) and F4/80^{+} macrophage populations (Fig. 1D) showed similar or greater infiltration in deficient mice compared to wild-type mice (Fig. 1E-J).

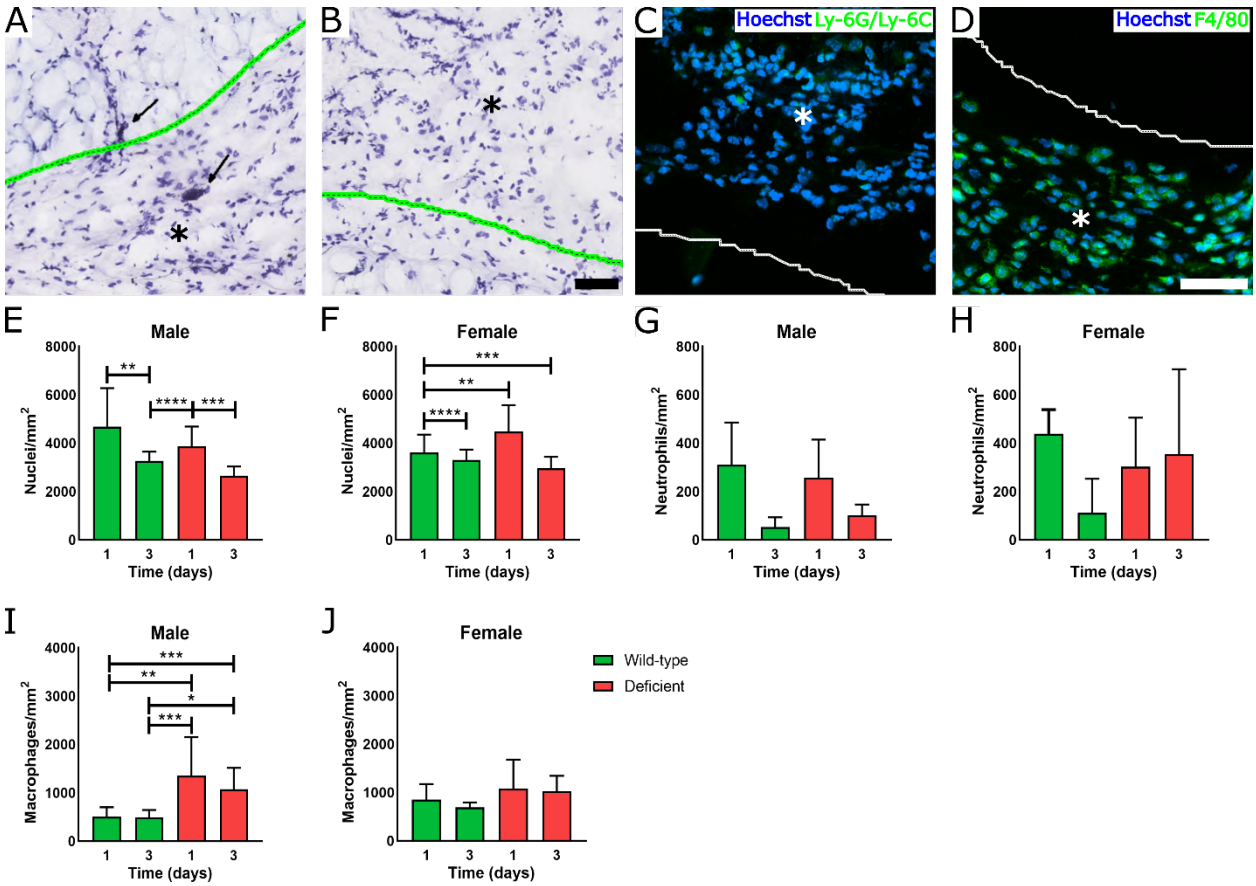

Figure 1: ECM scaffold promotes early immune cell infiltration with or without mast cells. Representative images of toluidine blue staining of ECM scaffold (green outlined with asterisk where material is present) and neighboring dermal tissue in wild-type (A) and mast cell-deficient (B) mice at day 1 post-injection. Mast cells can be found as early as day 1 showing lack of or minimal degranulation (black arrow). Representative fluorescent images of injected biomaterial (white outlined with asterisk) with Ly-6G/Ly-6C^{+} neutrophil (C) and F4/80^{+} pan-macrophage staining (D) in green, and Hoechst nuclei counterstain in blue. Quantification of total nuclei (E, F), neutrophil (G, H) and macrophage (I, J) density at one and three days post-injection for male and female wild-type (green) and deficient (red) mice. Scale bar of 50 μm in toluidine blue (A-B) and fluorescent images (C, D, G, H). (*$p < 0.05$, **$p < 0.01$, ***$p < 0.001$ and ****$p < 0.0001$).

Induced Macrophage Polarization and Pro-inflammatory Cytokine Expression is Dysregulated and Rescued based on Mast Cell Presence

As ECM scaffold injection allowed for cellular infiltration similar to wild-type mice despite the lack of mast cells (Fig. 1), a screen of immune cell populations and polarized phenotypes through flow cytometry (Fig. S4-S5) and gene expression markers (Table S1) was utilized to assess if these infiltrating cells were affected by loss of regulatory contributions from mast cells. To confirm that this shift was mast cell specific, mast cell-engrafted mice were also similarly assessed where adoptive transfer of bone marrow derived mast cells differentiated *in vitro* were implanted subcutaneously into deficient mice to reconstitute the local resident mast cell population (*22, 27*). Mast cell engraftment was confirmed by toluidine blue staining showing presence of mast cells in dermal tissue and extracted ECM scaffold injections (Fig. S6).

Transient polarization of immune cells from a pro-inflammatory to a pro-remodeling phenotype is a characteristic of wound healing responses (*6, 28, 29*) and the immunomodulatory effect of ECM scaffolds promotes this transition (*8, 30*). Macrophage polarization assessment based on ratio of M2 pro-remodeling and M1 pro-inflammatory phenotypic markers in male mice showed a significant lack of polarization shift towards M2 for mast cell-deficient mice at day 11 post-injection that was observed in wild-type mice (Fig. 2A) and in previous studies (*25*). Mast cell engrafted mice showed a restoration of the M2 shift, which was significant to the deficient group (Fig. 2A). Assessing the individual percentages of M2 and M1 macrophages showed similar percentages of M2 macrophages and those simultaneously displaying both M2 and M1 markers (M2+1; Fig. S7C, G) for the wild-type and deficient mice while a higher relative number of M1 macrophages were present in deficient male mice at the day 11 (Fig. S7E). Notably, addition of mast cells in the engrafted mice had a significantly greater percentage of M2 macrophages compared to deficient mice (Fig. S7C). This result further supports an alternative mast cell phenotype from ECM scaffold interaction as opposed to a classically activated phenotype that would promote greater M1 macrophage

presence. In contrast, mast cell deficient female mice showed an M2 dominant presence at the early day 3 timepoint (Fig. 2B), which arose from a higher relative percentage of M2 macrophages (Fig. S7D) and not from differences in M1 percentage (Fig. S7F). Notably, there were no changes in either sex in total macrophage numbers (Fig. S7) and other assayed populations including T-cell subpopulations (Fig. S8), B cells (Fig. S9), and dendritic cells (Fig. S10). Percentages of mast cells were likewise equivalent in wild-type and engrafted mice (Fig. S11). Thus, the results stemmed from phenotypic changes in immune cell polarization versus differences in general immune cell numbers between models (Fig. 1).

A gene expression screen of select pro-inflammatory and pro-remodeling/anti-inflammatory markers between the male wild-type and deficient group showed only a significant increase in anti-inflammatory Il38 in deficient compared to wild-type at day 3 post-injection (Fig. S12A). At day 11 when significant shifts based on flow cytometry were observed, significant differences in the IL-1 family were found including increases in pro-inflammatory Il1b and Il33 expression, and a decrease in Il38 (Fig. S12B). Further comparison of mast cell deficient mice with engrafted mice showed that increased expression of Il1B (Fig. 2C) and IL33 (Fig. 2D) and decreased expression of the IL-1 receptor antagonist Il1rn relative to IL1b expression (Fig. 2E) in deficient mice were reversed in the engrafted mice supporting mast cell influence on the IL-1 cytokine family response. Additionally, expression of Cd206 was significantly upregulated in engrafted mice compared to wild-type controls, matching previous flow cytometry results of an increased M2 macrophage transition from mast cell interaction with the ECM scaffold (Fig. 2F, Fig. S7C). Similar assessment for female mice at day 3 (Fig. S13) when dysregulation of macrophage polarization was observed by flow cytometry (Fig. 2B) determined only a significant upregulation of M1 marker Nos2 in deficient mice compared to wild-type that was reversed in engrafted mice (Fig. 2G).

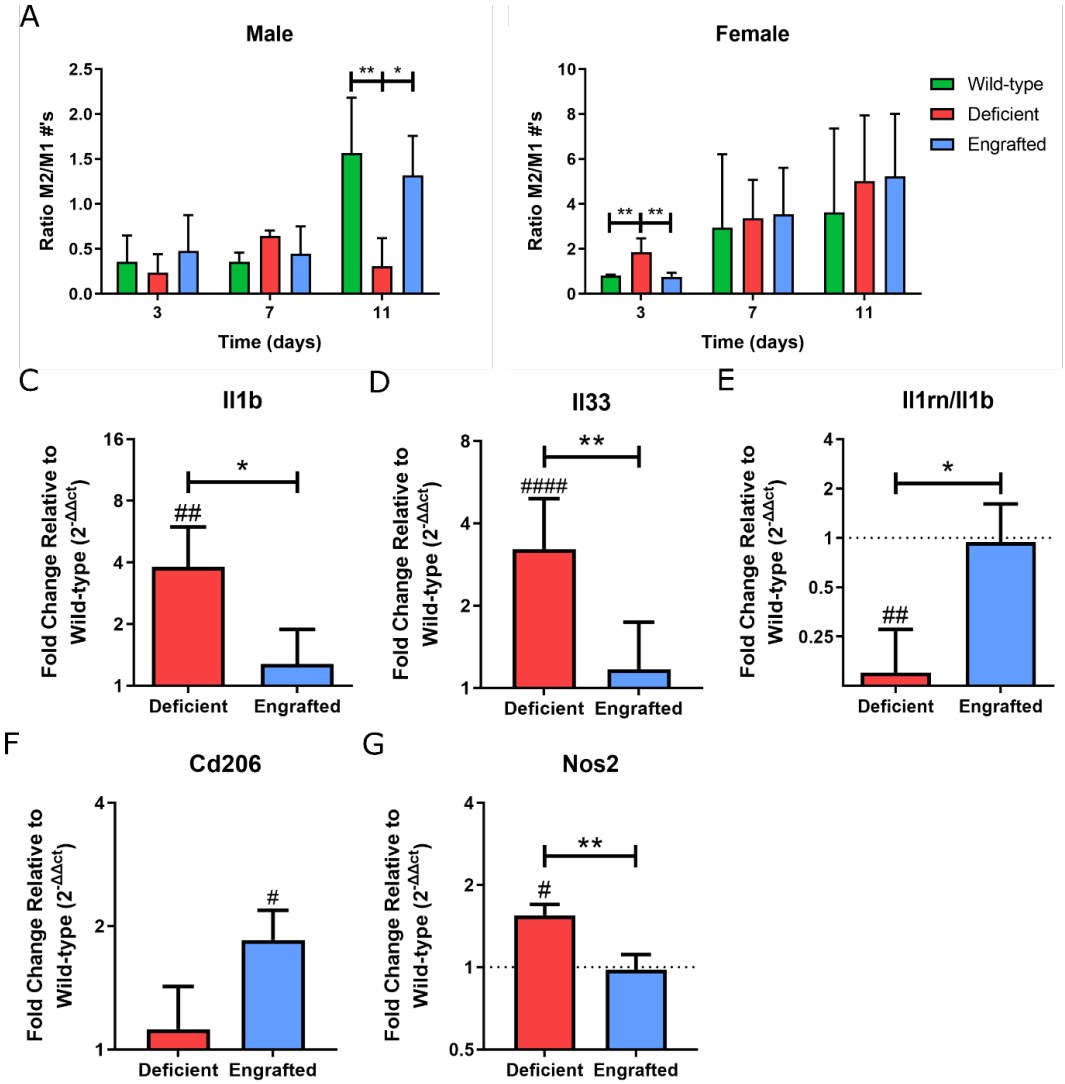

Figure 2: Transition from a pro-inflammatory to pro-remodeling macrophage and cytokine immune profile is dysregulated in a sex specific manner. Flow cytometry quantification for macrophages polarization based on a ratio of $CD206^+$ M2 versus $CD86^+$ M1 macrophage counts was assessed at three, seven, and eleven days post-injection between wild-type (green), mast cell-deficient (red), and mast cell-engrafted (blue) male (A) and female mice (B). Relative gene expression normalized to wild-type expression at day 11 in male mice measured by qPCR for (C) Il1b and (D) Il33 relative to housekeeping gene, Gapdh. (E) Gene expression ratio of IL-1 receptor antagonist, Il1rn, to Il1b. (F) Gene expression for Cd206. (G) Relative gene expression at day 3 in female mice measured by qPCR for Nos2 relative to

Gapdh housekeeping gene. # indicates significance relative to wild-type expression; * indicates significance between deficient and engrafted; gene expression plotted as mean ± SEM. ($^{\#}p < 0.05$, $^{\#\#}p < 0.01$, $^{\#\#\#\#}p < 0.0001$, $^{*}p < 0.05$, and $^{**}p < 0.01$).

Differential Inflammatory Expression Profile is based on Mast Cell Presence

As mast cells are known to secrete and influence a broad spectrum of immune responses, a more comprehensive multiplex analysis was carried out through a Nanostring panel allowing direct probing of the RNA molecular content for 546 immune related targets. Day 11 male mouse samples were assessed as results supported a lack of beneficial pro-inflammatory resolution in deficient mice at this timepoint. PCA analysis of the top 50% of genes based on variance showed that the majority of wild-type and engrafted samples clustered in separate groups along PC1 with some samples dispersed between the two groups. Mast cell deficient samples were more distinct along PC2 and not as tightly clustered conveying increased variance due to removal of regulatory influence from mast cells (Fig. S14). Multi-group differential expression analysis of the deficient compared to the wild-type and engrafted response determined differentially upregulated genes for a host of pro-inflammatory cytokines (Il1a, Il1b, Il6, Il33, Tnf) and chemokines (Ccl2, Ccl3, Ccl4, Ccl7, Cxcl1, Cxcl3, Cxcl10) (Fig. 3, Table S2). Across samples based on Z-score heatmap visualization of differentially expressed genes, a differing immune profile in deficient samples compared to wild-type and engrafted samples was apparent, with the most distinct differences in the upper and lower clusters (Fig. 4), notably, for a host of pro-inflammatory cytokines and chemokines.

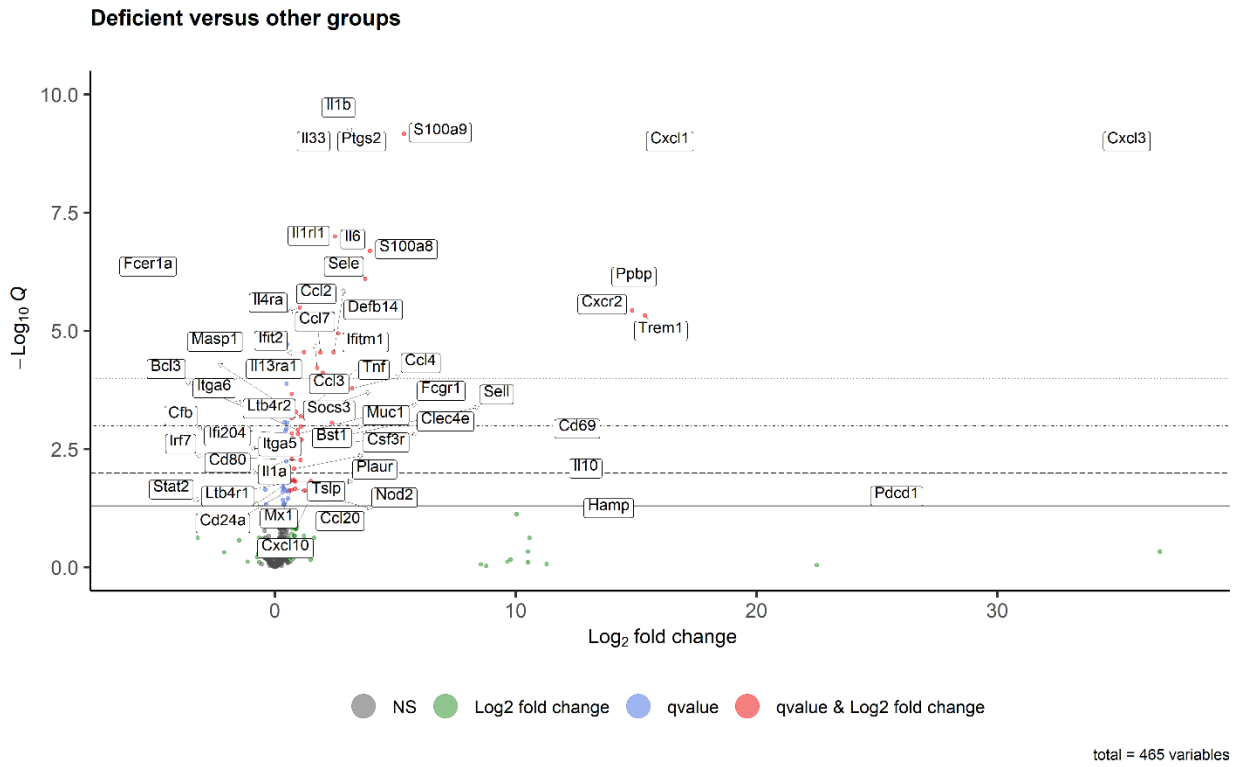

Figure 3: Mast cell-deficient male mice maintain late pro-inflammatory response profile to biomaterial implantation. Differential expression with dots indicating false discovery rate less than 0.05 (blue, red), absolute fold change greater than 1.5 (green, red) or non-significant (black). Dashed lines indicating different significance thresholds (*$q < 0.05$, **$q < 0.01$, ***$q < 0.001$ and ****$q < 0.0001$).

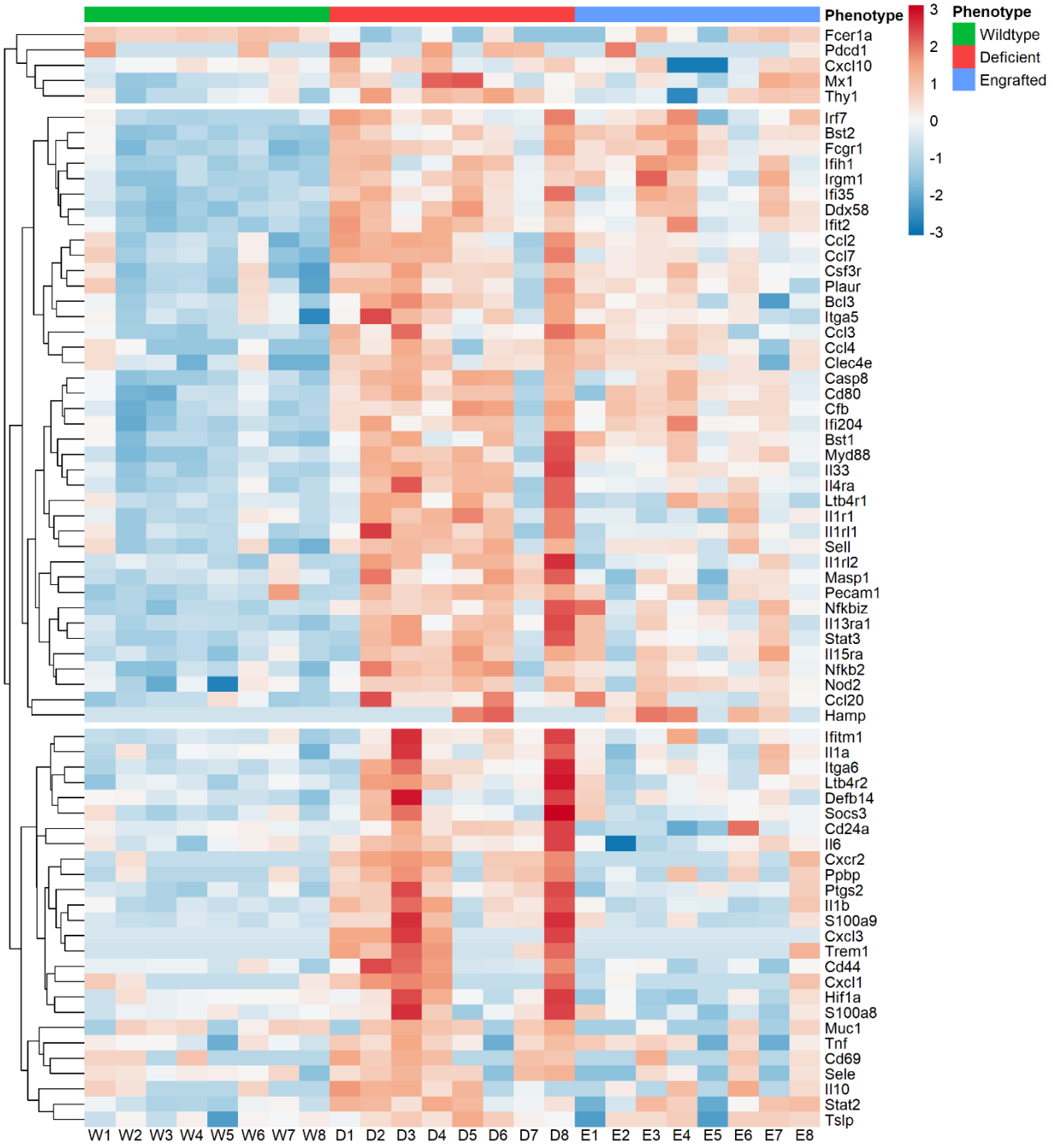

Figure 4: Heatmap of wild-type, deficient, engrafted mice gene expression. *Z*-scores of Nanostring nCounter gene expression data normalized based on the NanostringDiff package (*31*) method and displayed with pheatmap package (*32*) in R. Sample ID of wild-type (W1-W8, green), deficient (D1-D8, red), and engrafted mouse samples (E1-E8, blue) for male mice at day 11 post-injection. Upregulated expression in red and downregulated in blue.

Pairwise analysis showed a similar pro-inflammatory differential response profile comparing deficient with wild-type alone (Fig. S15A, Table S3). While total number of differentially expressed genes between mast cell deficient and engrafted samples (Fig. S15B, Table S4) was limited to just 34 genes, these predominantly consisted of the various pro-inflammatory cytokines and chemokines such as IL1 family of genes that were also highlighted in the multi-group analysis. These results were paralleled with the pairwise comparison between the engrafted and wild-type samples. Differential expression analysis determined 220 significant genes that lacked pro-inflammatory markers particularly associated with the IL1 cytokine family and instead mainly consisted of cellular processes, cell cycle, and migration markers (Fig. S16, Table S5). Notably, the mast cell marker, Fcer1a, was also significantly decreased for the mast cell deficient samples compared to both the wild-type and engrafted samples, but not between the wild-type and engrafted samples (Table S3-S5), thus, supporting successful engraftment.

KEGG pathway gene enrichment over-representation analysis of male day 11 deficient versus both the wild-type and engrafted (Table S5) or individual pair-wise comparisons (Table S6, S7) highlighted association with several pro-inflammatory pathways related to TNF, IL-17, NOD-like receptors, and viral protein-like interactions along with cellular stress pathways such as necroptosis and HIF-1 signaling pathway. In contrast, enrichment analysis between engrafted and wild-type groups highlighted simple cellular processes such as the phagosome, and antigen processing and presentation (Table S9) despite the high percentage of genes from the panel that were significantly differentially regulated suggesting similar resolution of the inflammatory response between $Kit^{W\text{-}sh}{}_{mice}$ with mast cell engraftment and wild-type mice. Likewise, GO term gene enrichment analysis of mast cell deficient to non-deficient groups (Fig. 5, Table S10-S12) showed enrichment of inflammatory response pathways related to neutrophils, IL-6, bacterium or microbial-like responses. Diverging from these comparisons,

pairwise enrichment analysis between engrafted and wild-type samples mainly consisted of pathways related to standard biological and cellular processes to a xenogeneic ECM therapeutic such as antigen processing and presentation, general immune, defense and other organism responses, response to biotic and organic stimulus, and phagocytosis (Fig. 5, Table S13)

Figure 5: Mast cell-deficient male mice maintain late pro-inflammatory response to biomaterial implantation while mast cell engraftment restores physiological cellular responses to biomaterial stimuli. Bubble plot of simplified biological process GO terms

enrichment between groups based on differentially expressed genes with a false discovery rate of q-value < 0.05 and absolute fold change greater than 1.5 between groups. Point size representing differentially expressed gene counts related to each pathway and color representing q-value.

Discussion:

Biomaterials have gained momentum as pro-regenerative therapies through modulation of the innate and adaptive immune response, particularly macrophages and T cells, during tissue remodeling progression. In this study, we demonstrated the contribution of mast cells to the immunomodulatory response of a decellularized ECM biomaterial. Within a short time following subcutaneous deployment of various decellularized bioscaffolds, non-degranulated mast cells were identified in the nearby surrounding tissue, at the bioscaffold-tissue border, and in the core of the material, contrasting the activated degranulated states observed with synthetic biomaterial implants. Implantation of the ECM biomaterial in male and female $Kit^{W\text{-}sh}$ mast cell deficient mice demonstrated similar or greater total and immune subpopulation specific infiltration, despite the lack of mast cells releasing secretory factors such as histamine for vasodilation and chemokines that are known to contribute to driving the early immune response. Given that ECM components contain signals for promoting immune cell recruitment and migration (*33*), stimuli for immune cell recruitment might have been partially compensated. Previously mentioned potential neutrophilia in this deficient model did not manifest in significant differences in observed neutrophil infiltration in this experimental context.

Given that similar immune infiltrate was observed in both the deficient and wild-type animals, we then investigated whether subpopulation identity and phenotypic characteristics of these infiltrating immune cells differed. Although percentages alone conveyed limited changes amongst the various immune cell populations for the timepoints assessed, it was determined

that the ratio of alternatively activated M2 and classically activated M1 macrophages significantly differed between the wild-type and mast cell deficient mice. However, these observations were not consistent based on sex as male mice showed this dysregulation at the later day 11 timepoint while female mice showed altered ratios at the early day 3 timepoint. Additional comparison with deficient mice engrafted with *in vitro* differentiated bone marrow derived mast cells to confirm whether this difference was mast cell specific demonstrated a restoration of the wild-type ratios in each scenario. Looking at the M2 and M1 percentages individually, each of these altered ratios were observed to involve a heightened presence of M1 macrophages in males at day 11 post-injection and M2 macrophages in females at day 3 post-injection. The early observation of a M2 dominant response could result from influences of female hormones such as estrogen, which has been demonstrated to accelerate resolution of pro-inflammatory responses (*34*). Furthermore, female hormones are known to influence mast cell activation contributing to the enhanced host defense and greater incidents of autoimmune disease in females that is likely mitigated with mast cell deficiency (*1, 35*).

Investigation of the cytokine gene expression profile at timepoints when altered M2/M1 ratios by flow cytometry were observed showed limited distinct differences at the early day 3 timepoint for female mice except for the increased expression of Nos2. Though this result could be considered contradictory to the flow cytometry results suggesting a greater M2 profile at this timepoint, studies on the influence of female hormones have shown specific upregulated expression of Nos2 (*36, 37*), potentially suggesting the known interaction of mast cells with female hormones helps to regulate these responses (*38*). For the day 11 timepoint in male mice samples, a host of pro-inflammatory cytokines between mast cell deficient and non-deficient mice were determined, most notably including the pro-inflammatory IL-1 family, IL-6, and Tnf. Compensatory upregulation of anti-inflammatory markers such as Il10, Il19, and Cxcl10 was also observed, which commonly occur in cases of pathological tissue remodeling and foreign body responses (*39, 40*). This was further emphasized based on gene enrichment

analysis based on GO terms or KEGG pathways emphasizing inflammatory response and pro-inflammatory cytokine signaling pathways, neutrophil responses, cellular stress pathways, and viral protein-like responses. This cytokine and pathway profile greatly differed in the deficient mice from expectations for a decellularized bioscaffold at this timepoint where a transition from a pro-inflammatory to pro-remodeling state would be expected such as in the wild-type control and as demonstrated in previous studies (*5, 7, 8, 25*).

Comparison between the engrafted and deficient groups determined a modest number of differentially expressed genes, however, these genes were highly predominated with pro-inflammatory markers leading to similar gene and pathway enrichment results. Furthermore, comparison between the engrafted and wild-type groups determined the highest number of differentially expressed genes and despite the use of a Nanostring panel enriched for immune cell markers, there was a lack of GO terms or KEGG pathways associated specifically with inflammatory response. Instead, enrichment analysis highlighted pathways mainly associated with antigen processing, phagocytosis, recognition of a xenogeneic biological stimuli, and general immune response. Ultimately, these distinct differences in macrophage ratios, pro-inflammatory cytokine gene expression, and enrichment analysis between comparisons from mast cell deficient versus engrafted groups supports that mast cells play a crucial role regulating the immunomodulatory transition of surrounding immune cellular processes in response to ECM based biomaterial scaffolds.

In contrast to previous *in vivo* studies of the mast cell response to biomaterials, which showed involvement in acute inflammation and fibrous capsule formation (*2, 12*), this study demonstrated that mast cells contribute to the dynamic immunomodulatory response to pro-regenerative biomaterial scaffolds. This work highlights the need to examine the role of other immune cells beyond macrophages and T cells as well as sex differences in pro-regenerative therapies, and supports the potential of mast cells as a critical immune regulatory element that can be manipulated for stimulating endogenous tissue repair.

Materials and Methods:

All procedures in this study were performed in accordance with the guidelines established by the Committee on Animal Research at the University of California, San Diego and the Association for the Assessment and Accreditation of Laboratory Animal Care.

ECM Hydrogel Preparation

An ECM hydrogel was generated from porcine left ventricular tissue based on previously established protocols (*44*). In brief, porcine left ventricular tissue was isolated and minced into small pieces. The tissue was decellularized under mechanical agitation in a solution of phosphate buffered saline (PBS) containing 1% (wt/vol) sodium dodecyl sulfate (SDS) (Fischer Scientific, Fair Lawn, NJ) with 0.5% 10,000 U/mL penicillin streptomycin (PS) (Gibco, Life Technologies, Grand Island, NY) until fully decellularized based on previously established criteria(*44*). Once decellularized, the decellularized ECM was thoroughly rinsed to remove residual SDS, lyophilized, and milled into a fine powder. ECM powder was partially digested with 1 mg/mL pepsin in 0.1M HCL solution for 48 hours before solution was neutralized to pH of 7.4 and reconstituted to physiological salt concentrations. Partially digested ECM solution was aliquoted, lyophilized and stored at -80°C until re-suspending with sterile water prior to injection which self-assemble into hydrogels *in vivo*.

Mast Cell-Deficient Mouse Model

Homozygous mast cell-deficient mouse, w-sh mice: B6.Cg-*Kit*$^{W\text{-}sh}$/HNihrJaeBsmJ (Jackson Laboratory, Sacramento, CA) were breed in UCSD vivarium up to 11-13 weeks before being designated for subcutaneous procedures. Both male and female mice were utilized for investigation. Age matched wild-type C57BL6/J mice were used as control animals.

Bone Marrow Derived Differentiated Mast Cell Culture

Bone marrow derived cells were harvested from wild-type C57BL6/J mice that were euthanized by CO2 and cervical dislocation. Each femur was isolated and bone marrow was flushed with 10 mL of media, collected and pipetted into culture flasks incubated in cell culture incubator at 37ºC and 5% CO_2. Mast cell differentiation media consisting of DMEM media (Gibco) with 10% FBS (Gibco), 1% penicillin streptomycin (Gibco), sterile filtered conditioned culture medium from D11 hybridoma cells as a source of IL3, 100 uM MEM nonessential amino acids (Lonza), 1mM sodium pyruvate (Gibco), 0.1 mM HEPES (Gibco), and 55 uM β-mercaptoethanol (Gibco). Non-adherent cells were passaged at day 3, 7, 10, 14, 18, 22 and 28 before differentiation of mast cells was assessed by flow cytometry with antibody markers for CD117 APC and FcεRI PE (Biolegend, San Diego, CA). Cells at greater than ~95% purity were utilized up to 4-6 weeks from initial isolation before mast cell functionality was expected to subside.

For assessment of cell viability, 100,000 mast cells were plated into a 48 well plate (n = 4) with ECM hydrogel material at nongelling concentrations of 0.6 mg/mL or neutralized Collagen I, Rat Tail at concentrations of equivalent stiffness and collagen content of 0.25 mg/mL concentration (*45*) (Corning®, Corning, NY) doped into culture media. Media only culture was used as a control. AlamarBlue™ Cell Viability Reagent (Invitrogen, Waltham, MA) was added to each well at a tenth the volume totaling 400 µL solution, and cells were incubated in a 37ºC, 5% CO_2 cell culture incubator. At 0, 2, 4, and 8 hours after plate set-up, fluorescent plate readings for alamarBlue signal at 560 nm excitation and 590 emission were read on a Synergy™ H4 multi-mode microplate reader and Gen5™ software (Biotek®. Wilnooski, VT). Experimental set-up was repeated to demonstrated relative reproducibility of the results.

Mast Cell-Engrafted Model Generation

For injection procedures, animals were briefly put under anesthesia at 2% isoflurane on a nose cone and mice went placed upright to expose the dorsal region. The dorsal region was

shaved and cleaned with 3 intervals of betadine and 70% ethanol. Mast cell-engrafted mice were created by subcutaneous injections consisting of a total of 4 million bone marrow differentiated mast cells in DMEM in 100 μL volumes at evenly spaced intervals throughout the dorsal region of 4-6 week old deficient mice. Subsequent procedures were done in engrafted mice at 11-13 weeks old. Toluidine blue staining of subcutaneous tissue and injections confirmed presence of mast cells in engrafted mice at the time of subcutaneous procedures and harvest (Fig. S6). Age matched deficient mice were injected with DMEM alone at similar timepoints for comparative studies. For comparisons with engrafted mice, age matched mast cell deficient mice and wild-type mice were utilized as controls.

Biomaterial Injection and Harvesting

For biomaterial injections, animals were briefly put under anesthesia using 2% isoflurane on a nose cone and each mouse was injected with ECM hydrogel material receiving two evenly spaced 200 μL subcutaneous injections in the upper and lower dorsal region. At one, three, seven, and eleven days post-injection, mice were euthanized by CO_2 and cervical dislocation. Timepoints were selected based on observation of consistent material retention and clear visibility up to the later timepoints. General dorsal skin tissue was cut and flipped to expose the underside to observe location and area of material injection. The injections, along with neighboring dermal tissue, were excised. Each harvested injections were divided into multiple parts for analysis by flow cytometry, staining or gene expression analysis as described below (n= 5-8 mice per group, 10-16 injections per group). Samples were collected across 2-3 experimental batches of animals for demonstrating consistency of results.

Flow Cytometry

Excised subcutaneous injections were minced in ice-cold HBSS (Gibco) and enzymatically digested in a solution consisting of 1:1 solution of HBSS (calcium and magnesium

supplemented) and 1% bovine serum albumin in PBS with 1 μM HEPES (Gibco), 300 U/mL collagenase type IV (Worthington Biochemical), 60 U/mL hyaluronidase (Sigma-Aldrich) and 10 U/mL DNase I (Sigma-Aldrich). Material in enzymatic digestion solution were incubated at 37ºC under mechanical agitation at 750 rpm on a thermomixer (Benchmark Scientific) for 45 minutes. Solutions were then kept in ice and FACs buffer consisting of 1% bovine serum albumin and 1mM EDTA in DPBS lacking calcium and magnesium added to inhibit further enzyme reaction. Digested tissue was filtered through a 100μm cell strainer. Cells were centrifuged at 400 rcf centrifugation at 4ºC and resuspended in HBSS. Cell suspension was stained with LIVE/DEAD™ Fixable Aqua (ThermoFisher Scientific) for 10 minutes at 4ºC and excess dye was quenched with FACs buffer. Cells were fixed and permeabilized by BD Cytofix/Cytoperm™ Buffer (BD Biosciences) for 10 minutes and washed in BD Perm/Wash™ Buffer (BD Biosciences). Cells were counted by hemocytometer and stained with antibody panels for immune cell subpopulations. General immune cell populations were stained with the following antibody panel: CD11c BV421 (Biolegend), F4/80 BUV395 (BD Biosciences), CD3 PerCp/Cy5.5 (Biolegend), CD117 APC (Biolegend), FcεRI PE (Biolegend), and CD19 APC-Cy7 (Biolegend). An antibody panel for macrophage and T cell polarization was also stained for consisting of: F4/80 BUV395 (BD Biosciences), CD86 BV786 (Biolegend), CD206 PE (Biolegend), CD3 PerCp/Cy5.5 (Biolegend), CD4 APC (Biolegend), CD8 Alexa Fluor 488 (Biolegend), and FoxP3 BV421 (Biolegend). Antibodies and IgG isotype controls were stained in BD Perm/Wash™ Buffer for 30 minutes at 4ºC before rinsing and resuspending in FACs buffer consisting of 1% bovine serum albumin and 1 mM EDTA in PBS for analysis. Stained cells were analyzed on a BD FACSCanto™ II and BD LSRFortessa™ X-20 (BD Biosciences). Gating was set based on positive, isotype and fluorescence minus one controls utilizing a mixed single cell suspension control sample derived from seven day post-injection biomaterial, isolated spleen cells, and four week differentiated mast cells to ensure all cells of interest were present in distinguishable amounts. Gating and flow data were processed in FlowJo (FlowJo LLC, Ashland, OR).

Quantitative Real-Time Polymerase Chain Reaction (qRT-PCR)

Flash frozen samples or tissue samples treated in RNAlater™ (Invitrogen) were homogenized with a mechanical rotator and then run through a RNeasy Mini kit (Qiagen, Germantown, MD) to extract RNA based on manufacturer instructions with an on-column DNase I digestion (Qiagen) for minimizing genomic DNA contamination. Superscript IV Reverse Transcriptase kit (Applied Biosystems, Foster City, MA) was used to synthesize cDNA with thermocycler settings of 65ºC for 5 minutes, 23ºC for 10 minutes, 55ºC for 10 minutes and 80ºC for 10 minutes. Eva Green Master Mix (Biotium, Fremont, CA) was used with custom-made forward and reverse primers (Table 1) at a final concentration of 0.2 μM for qPCR reactions. Samples were run in technical duplicate along with negative controls without template cDNA to confirm lack of contamination from qPCR reagents. PCR reactions were run on a CFX95™ Real-Time System (Bio-Rad, Hercules, CA) with the following thermal cycler settings: 30s at 50°C, 2 min at 95°C, 40 cycles of 10s at 95°C, and 30s at 55-65°C based on pre-determined optimal primer efficiency amplification temperature. After completing 40 cycles of PCR amplification, automated melting curve analysis, consisting of increasing the thermal cycler temperature from 50°C to 95°C at 5°C increments lasting 5s each, for confirming singular amplicon product in each reaction vessel. Bio-Rad CFX Manager™ 3.0 (Bio-Rad) was used for determining cycle threshold values from recorded signal based on a preset threshold.

Nanostring Multiplex Gene Expression Analysis

For comprehensive evaluation of the whole immune profile, RNA samples were analyzed by Nanostring nCounter® MAX Analysis System with nCounter® Immunology Panel (Mouse) allowing for multiplexed assessment of 546 genes (*46, 47*). Samples were processed according to manufacturer instructions. In brief, RNA sample concentrations were measured on a Qubit 3.0 Fluorometer with a Qubit™ RNA HS Assay kit. 70 μL of hybridization buffer was

mixed with Immunology Panel Reporter CodeSet solution, and 8 μL of this master mix was mixed in a separate reaction vessel with 100 ng of RNA per tissue sample and RNA-free water up to 13 μL total. 2 μL of Capture ProbeSet was added to each vessel, mixed and placed on a thermocycler at 65ºC for 16-48 hours before being maintained at 4ºC for less than 24 hours. Nanostring nCounter Prep Station performed automated fluidic sample processing to purify and immobilize hybridized sample to cartridge surface. Digital barcode reads were analyzed by Nanostring nCounter® Digital Analyzer. Results were analyzed by manufacturer nSolver™ Analysis Software 4.0 and custom R scripts. Gene expression normalization and differential expression was determined by the NanostringDiff package (*31*) with average probe count below negative control probes excluded from analysis and significance set with a false discovery rate Benjamini-Hochberg method correction for calculating q-value < 0.05 and an absolute fold change threshold of 1.5. Heatmap of significant differentially expressed genes was displayed with the pheatmap package (*32*). Volcano plots created with the EnhancedVolcano package(*48*) with a threshold at a false discovery rate of qvalue < 0.05. Gene enrichment over-representation analysis was performed on differentially expressed gene criteria compared to total panel probe targets as background gene set with the clusterprofiler package (*49*) for Gene Ontology (GO) terms with redundancy reduced with the GOSemSim package (*50*) and Kyoto Encyclopedia Encyclopedia of Genes and Genomes (KEGG) pathways with images created with the Pathview package(*51*). KEGG pathways related to disease gene sets were excluded with gageData package(*52*) and significance was set to p-value < 0.05.

Immunohistochemistry

Harvested samples were embedded into Tissue-Tek O.C.T. Compound (Sakura®, Torrance, CA) for cryosectioning. Cryosections from three different evenly spaced locations were used for all immunohistochemistry. Transverse sections were taken to obtain a cross-section of the biomaterial injection and neighboring dermal tissue. Histological evaluation of

total cell and mast cell infiltration were taken from sections stained with Toluidine Blue Stain, 1% w/v (Ricca Chemical, Arlington, TX) and scanned with a Leica Aperio ScanScope® CS^2 (Leica, Buffalo Brove, IL) system. For fluorescent staining, slides were fixed with 4% paraformaldehyde in PBS (Thermo Scientific™) and blocked with a buffered solution containing 3% bovine serum albumin (Gemini Bio-Products, Inc., West Sacramento, CA)and 0.1% Triton X-100 (Sigma) in PBS. The primary antibodies, pan-macrophage marker anti-mouse F4/80 (eBioscience, San Diego, CA) and anti-mouse Ly-6G/Ly-6C (eBioscience), were incubated for 12-18 hours at 4°C: Secondary antibody Alexa Fluor 488 with Hoechst 33342 (Thermo Scientific™) counterstain was incubated for 30-40 minutes at room temperature. Coverslips were mounted with Fluoromount™ Aqueous Mounting Medium (Sigma) and allowed to dry protected from light. Fluorescent images were scanned with the Leica Ariol® DM6000B system (Leica). Cellular density and co-staining quantification were done with custom MATLAB scripts (Mathworks, Natick, MA).

Statistical Analysis

All data and plots are presented as mean ± SD unless noted otherwise. Statistics were performed in Prism 8 (GraphPad Software, San Diego, CA) or custom R scripts. For two group assessments, an unpaired student's *t*-test was performed while assessments across three or more groups was evaluated with a one-way ANOVA with a Tukey post-hoc with significance taken at $p < 0.05$. For analysis of differential expression of Nanostring data, a false discovery rate threshold of $q < 0.05$ and fold change threshold of greater than 1.5 based on the Benjamini-Hochberg method was utilized. Gene enrichment analysis utilized p-value < 0.05 for KEGG pathway over-representation analysis and q-value of 0.05 for GO term enrichment analysis.

References

1. A. L. Christy, M. A. Brown, The Multitasking Mast Cell: Positive and Negative Roles in the Progression of Autoimmunity. *The Journal of Immunology* **179**, 2673 (2007).
2. L. Tang, T. A. Jennings, J. W. Eaton, Mast cells mediate acute inflammatory responses to implanted biomaterials. *Proceedings of the National Academy of Sciences* **95**, 8841 (1998).
3. P. T. Thevenot, D. W. Baker, H. Weng, M. W. Sun, L. Tang, The pivotal role of fibrocytes and mast cells in mediating fibrotic reactions to biomaterials. *Biomaterials* **32**, 8394-8403 (2011).
4. K. L. Christman, Biomaterials for tissue repair. *Science* **363**, 340 (2019).
5. S. F. Badylak, J. E. Valentin, A. K. Ravindra, G. P. McCabe, A. M. Stewart-Akers, Macrophage Phenotype as a Determinant of Biologic Scaffold Remodeling. *Tissue Eng Pt A* **14**, 1835-1842 (2008).
6. J. W. Godwin, A. R. Pinto, N. A. Rosenthal, Macrophages are required for adult salamander limb regeneration. *Proceedings of the National Academy of Sciences* **110**, 9415 (2013).
7. A. J. Allman, T. B. McPherson, S. F. Badylak, L. C. Merrill, B. Kallakury, C. Sheehan, R. H. Raeder, D. W. Metzger, XENOGENEIC EXTRACELLULAR MATRIX GRAFTS ELICIT A TH2-RESTRICTED IMMUNE RESPONSE. *Transplantation* **71**, (2001).
8. K. Sadtler, K. Estrellas, B. W. Allen, M. T. Wolf, H. Fan, A. J. Tam, C. H. Patel, B. S. Luber, H. Wang, K. R. Wagner, J. D. Powell, F. Housseau, D. M. Pardoll, J. H. Elisseeff, Developing a pro-regenerative biomaterial scaffold microenvironment requires T helper 2 cells. *Science (New York, N.Y.)* **352**, 366-370 (2016).
9. E. W. Ozpinar, A. L. Frey, G. K. Arthur, C. Mora-Navarro, A. Biehl, D. B. Snider, G. Cruse, D. O. Freytes, Dermal Extracellular Matrix-Derived Hydrogels as an In Vitro Substrate to Study Mast Cell Maturation. *Tissue Eng Pt A*, (2020).

10. K. N. Methe, N. Nayakawde, D. Banerjee, C. Sihlbom, C. Agbajogu, G. Travnikova, M. Olausson, Differential Activation of Immune Cells for Genetically Different Decellularized Cardiac Tissues. *Tissue Eng Pt A*, (2020).

11. M. Ibrahim, J. Bond, M. A. Medina, L. Chen, C. Quiles, G. Kokosis, L. Bashirov, B. Klitzman, H. Levinson, Characterization of the Foreign Body Response to Common Surgical Biomaterials in a Murine Model. *Eur J Plast Surg* **40**, 383-392 (2017).

12. M. N. Avula, A. N. Rao, L. D. McGill, D. W. Grainger, F. Solzbacher, Foreign body response to subcutaneous biomaterial implants in a mast cell-deficient Kitw-Sh murine model. *Acta Biomaterialia* **10**, 1856-1863 (2014).

13. K. Bhattacharya, K. Farwell, M. Huang, D. Kempuraj, J. Donelan, D. Papaliodis, M. Vasiadi, T. C. Theoharides, Mast cell deficient W/Wv mice have lower serum IL-6 and less cardiac tissue necrosis than their normal littermates following myocardial ischemia-reperfusion. *Int J Immunopathol Pharmacol* **20**, 69-74 (2007).

14. A. Arac, M. A. Grimbaldeston, A. R. B. Nepomuceno, O. Olayiwola, M. P. Pereira, Y. Nishiyama, A. Tsykin, G. J. Goodall, U. Schlecht, H. Vogel, M. Tsai, S. J. Galli, T. M. Bliss, G. K. Steinberg, Evidence that Meningeal Mast Cells Can Worsen Stroke Pathology in Mice. *The American Journal of Pathology* **184**, 2493-2504 (2014).

15. S. Jolly, J. Detilleux, D. Desmecht, Extensive mast cell degranulation in bovine respiratory syncytial virus-associated paroxystic respiratory distress syndrome. *Vet Immunol Immunopathol* **97**, 125-136 (2004).

16. J. S. Janicki, G. L. Brower, S. P. Levick, The emerging prominence of the cardiac mast cell as a potent mediator of adverse myocardial remodeling. *Methods in molecular biology (Clifton, N.J.)* **1220**, 121-139 (2015).

17. B. C. Wulff, T. A. Wilgus, Mast cell activity in the healing wound: more than meets the eye? *Exp Dermatol* **22**, 507-510 (2013).

18. S. A. Legere, I. D. Haidl, J.-F. Légaré, J. S. Marshall, Mast Cells in Cardiac Fibrosis: New Insights Suggest Opportunities for Intervention. *Frontiers in Immunology* **10**, (2019).

19. S. Willenborg, B. Eckes, J. Brinckmann, T. Krieg, A. Waisman, K. Hartmann, A. Roers, S. A. Eming, Genetic Ablation of Mast Cells Redefines the Role of Mast Cells in Skin Wound Healing and Bleomycin-Induced Fibrosis. *Journal of Investigative Dermatology* **134**, 2005-2015 (2014).

20. E. M. Lennon, L. B. Borst, L. L. Edwards, A. J. Moeser, Mast Cells Exert Anti-Inflammatory Effects in an IL10 Model of Spontaneous Colitis. *Mediators of Inflammation* **2018**, 7817360 (2018).

21. N. Shiota, Y. Nishikori, E. Kakizoe, K. Shimoura, T. Niibayashi, C. Shimbori, T. Tanaka, H. Okunishi, Pathophysiological Role of Skin Mast Cells in Wound Healing after Scald Injury: Study with Mast Cell-Deficient W/W^V Mice. *International Archives of Allergy and Immunology* **151**, 80-88 (2010).

22. M. A. Grimbaldeston, C.-C. Chen, A. M. Piliponsky, M. Tsai, S.-Y. Tam, S. J. Galli, Mast cell-deficient W-sash c-kit mutant Kit W-sh/W-sh mice as a model for investigating mast cell biology in vivo. *The American journal of pathology* **167**, 835-848 (2005).

23. P. A. Nigrovic, D. H. D. Gray, T. Jones, J. Hallgren, F. C. Kuo, B. Chaletzky, M. Gurish, D. Mathis, C. Benoist, D. M. Lee, Genetic inversion in mast cell-deficient (Wsh) mice interrupts corin and manifests as hematopoietic and cardiac aberrancy. *The American journal of pathology* **173**, 1693-1701 (2008).

24. J. W. Wassenaar, R. Gaetani, J. J. Garcia, R. L. Braden, C. G. Luo, D. Huang, A. N. DeMaria, J. H. Omens, K. L. Christman, Evidence for Mechanisms Underlying the Functional Benefits of a Myocardial Matrix Hydrogel for Post-MI Treatment. *J Am Coll Cardiol* **67**, 1074-1086 (2016).

25. R. M. Wang, T. D. Johnson, J. He, Z. Rong, M. Wong, V. Nigam, A. Behfar, Y. Xu, K. L. Christman, Humanized mouse model for assessing the human immune response to xenogeneic and allogeneic decellularized biomaterials. *Biomaterials* **129**, 98-110 (2017).

26. J. H. Traverse, T. D. Henry, N. Dib, A. N. Patel, C. Pepine, G. L. Schaer, J. A. DeQuach, A. M. Kinsey, P. Chamberlin, K. L. Christman, First-in-Man Study of a Cardiac Extracellular Matrix Hydrogel in Early and Late Myocardial Infarction Patients. *JACC: Basic to Translational Science* **4**, 659 (2019).

27. T. Ando, W. Xiao, P. Gao, S. Namiranian, K. Matsumoto, Y. Tomimori, H. Hong, H. Yamashita, M. Kimura, J.-i. Kashiwakura, Tissa R. Hata, K. Izuhara, Michael F. Gurish, A. Roers, Nicholas M. Rafaels, Kathleen C. Barnes, C. Jamora, Y. Kawakami, T. Kawakami, Critical Role for Mast Cell Stat5 Activity in Skin Inflammation. *Cell Reports* **6**, 366-376 (2014).

28. S. Nassiri, I. Zakeri, M. S. Weingarten, K. L. Spiller, Relative Expression of Proinflammatory and Antiinflammatory Genes Reveals Differences between Healing and Nonhealing Human Chronic Diabetic Foot Ulcers. *J Invest Dermatol* **135**, 1700-1703 (2015).

29. T. Hasegawa, C. J. Hall, P. S. Crosier, G. Abe, K. Kawakami, A. Kudo, A. Kawakami, Transient inflammatory response mediated by interleukin-1β is required for proper regeneration in zebrafish fin fold. *Elife* **6**, (2017).

30. L. Huleihel, J. L. Dziki, J. G. Bartolacci, T. Rausch, M. E. Scarritt, M. C. Cramer, T. Vorobyov, S. T. LoPresti, I. T. Swineheart, L. J. White, B. N. Brown, S. F. Badylak, Macrophage phenotype in response to ECM bioscaffolds. *Semin Immunol* **29**, 2-13 (2017).

31. H. Wang, C. Horbinski, H. Wu, Y. Liu, S. Sheng, J. Liu, H. Weiss, A. J. Stromberg, C. Wang, NanoStringDiff: a novel statistical method for differential expression analysis based on NanoString nCounter data. *Nucleic Acids Research* **44**, e151-e151 (2016).

32. K. R., pheatmap: Pretty heatmaps [Software]. (2015).

33. P. Chen, M. Cescon, G. Zuccolotto, L. Nobbio, C. Colombelli, M. Filaferro, G. Vitale, M. L. Feltri, P. Bonaldo, Collagen VI regulates peripheral nerve regeneration by modulating macrophage recruitment and polarization. *Acta Neuropathologica* **129**, 97-113 (2015).

34. A. Villa, N. Rizzi, E. Vegeto, P. Ciana, A. Maggi, Estrogen accelerates the resolution of inflammation in macrophagic cells. *Scientific Reports* **5**, 15224 (2015).

35. H. Vliagoftis, V. Dimitriadou, W. Boucher, J. J. Rozniecki, I. Correia, S. Raam, T. C. Theoharides, Estradiol augments while tamoxifen inhibits rat mast cell secretion. *Int Arch Allergy Immunol* **98**, 398-409 (1992).

36. H. J. You, J. Y. Kim, H. G. Jeong, 17 beta-estradiol increases inducible nitric oxide synthase expression in macrophages. *Biochem Biophys Res Commun* **303**, 1129-1134 (2003).

37. R. Dai, R. A. Phillips, E. Karpuzoglu, D. Khan, S. A. Ahmed, Estrogen regulates transcription factors STAT-1 and NF-kappaB to promote inducible nitric oxide synthase and inflammatory responses. *J Immunol* **183**, 6998-7005 (2009).

38. O. Zierau, A. C. Zenclussen, F. Jensen, Role of female sex hormones, estradiol and progesterone, in mast cell behavior. *Frontiers in immunology* **3**, 169-169 (2012).

39. A. B. Aurora, E. R. Porrello, W. Tan, A. I. Mahmoud, J. A. Hill, R. Bassel-Duby, H. A. Sadek, E. N. Olson, Macrophages are required for neonatal heart regeneration. *J Clin Invest* **124**, 1382-1392 (2014).

40. D. M. Higgins, R. J. Basaraba, A. C. Hohnbaum, E. J. Lee, D. W. Grainger, M. Gonzalez-Juarrero, Localized Immunosuppressive Environment in the Foreign Body Response to Implanted Biomaterials. *The American Journal of Pathology* **175**, 161-170 (2009).

41. A. Ngkelo, A. Richart, J. A. Kirk, P. Bonnin, J. Vilar, M. Lemitre, P. Marck, M. Branchereau, S. Le Gall, N. Renault, C. Guerin, M. J. Ranek, A. Kervadec, L. Danelli, G.

Gautier, U. Blank, P. Launay, E. Camerer, P. Bruneval, P. Menasche, C. Heymes, E. Luche, L. Casteilla, B. Cousin, H.-R. Rodewald, D. A. Kass, J.-S. Silvestre, Mast cells regulate myofilament calcium sensitization and heart function after myocardial infarction. *Journal of Experimental Medicine* **213**, 1353-1374 (2016).

42. A. Widiapradja, E. J. Manteufel, H. M. Dehlin, J. Pena, P. H. Goldspink, A. Sharma, L. L. Kolb, J. D. Imig, J. S. Janicki, B. Lu, S. P. Levick, Regulation of Cardiac Mast Cell Maturation and Function by the Neurokinin-1 Receptor in the Fibrotic Heart. *Scientific Reports* **9**, 11004 (2019).

43. M. Sawaguchi, S. Tanaka, Y. Nakatani, Y. Harada, K. Mukai, Y. Matsunaga, K. Ishiwata, K. Oboki, T. Kambayashi, N. Watanabe, H. Karasuyama, S. Nakae, H. Inoue, M. Kubo, Role of Mast Cells and Basophils in IgE Responses and in Allergic Airway Hyperresponsiveness. *The Journal of Immunology* **188**, 1809-1818 (2012).

44. J. M. Singelyn, J. A. DeQuach, S. B. Seif-Naraghi, R. B. Littlefield, P. J. Schup-Magoffin, K. L. Christman, Naturally derived myocardial matrix as an injectable scaffold for cardiac tissue engineering. *Biomaterials* **30**, 5409-5416 (2009).

45. J. L. Ungerleider, T. D. Johnson, N. Rao, K. L. Christman, Fabrication and characterization of injectable hydrogels derived from decellularized skeletal and cardiac muscle. *Methods* **84**, 53-59 (2015).

46. L. Jardine, S. Wiscombe, G. Reynolds, D. McDonald, A. Fuller, K. Green, A. Filby, I. Forrest, M.-H. Ruchaud-Sparagano, J. Scott, M. Collin, M. Haniffa, A. J. Simpson, Lipopolysaccharide inhalation recruits monocytes and dendritic cell subsets to the alveolar airspace. *Nature Communications* **10**, 1999 (2019).

47. S. Hussain, C. G. Johnson, J. Sciurba, X. Meng, V. P. Stober, C. Liu, J. M. Cyphert-Daly, K. Bulek, W. Qian, A. Solis, Y. Sakamachi, C. S. Trempus, J. J. Aloor, K. M. Gowdy, W. M. Foster, J. W. Hollingsworth, R. M. Tighe, X. Li, M. B. Fessler, S.

Garantziotis, TLR5 participates in the TLR4 receptor complex and promotes MyD88-dependent signaling in environmental lung injury. *Elife* **9**, (2020).

48. R. S. Blighe K, Lewis M., EnhancedVolcano: Publication-ready volcano plots with enhanced colouring and labeling. R package version 1.6.0. (2020).

49. G. Yu, L.-G. Wang, Y. Han, Q.-Y. He, clusterProfiler: an R Package for Comparing Biological Themes Among Gene Clusters. *OMICS: A Journal of Integrative Biology* **16**, 284-287 (2012).

50. G. Yu, F. Li, Y. Qin, X. Bo, Y. Wu, S. Wang, GOSemSim: an R package for measuring semantic similarity among GO terms and gene products. *Bioinformatics* **26**, 976-978 (2010).

51. W. Luo, C. Brouwer, Pathview: an R/Bioconductor package for pathway-based data integration and visualization. *Bioinformatics* **29**, 1830-1831 (2013).

52. L. W., *gageData: Auxillary data for gage package. R package version 2.28.0.*, (2020).

Acknowledgements: The authors would like to thank Drs. Thomas Gilbert and Adam Young from ACell, Inc. for kindly providing the milled urinary bladder matrix. We would also like to acknowledge Dr. Elsa Molina, Director of the UC San Diego Stem Cell Genomics Core, for technical assistance of NanoString experiments, and Jesus Olvera and Cody Fine of the UC San Diego Human Embryonic Stem Cell Core Facility for technical assistance of flow cytometry experiments with all made possible in part by the CIRM Major Facilities grant (FA1-00607) to the Sanford Consortium for Regenerative Medicine. **Funding:** This work was supported by the NIH NHLBI (R01HL113468, R01HL146147). R.M.W. and J.L.U. were supported by NIH NHLBI pre-doctoral fellowships (F31HL137347, F31HL136082). **Author contributions:** R.M.W. contributed to the project conceptualization, design, experimental work, data analysis, and

manuscript write-up. J.U. contributed to project conceptualization, implementation of mast cell culture and breeding colony, and initial pilot data. Yu K. contributed to initial training and feedback on mast cell methods. Yuko K. contributed to initial training, reagents for mast cell work, and feedback on mast cell methods. T.K. contributed guidance for project design and experimental work, feedback on data, and evaluation of manuscript. K.L.C. contributed to project conceptualization, guidance for project design and experimental work, feedback on data, and evaluation of manuscript. All authors edited the manuscript. **Competing interests:** KLC is co-founder, consultant, board member, and holds equity interest in Ventrix, Inc. Other authors declare that they have no competing interests. **Data and materials availability:** All data for the conclusions in the paper are available in the main manuscript and/or the Supplementary Materials. Additional data may be requested from the authors.

Supplement

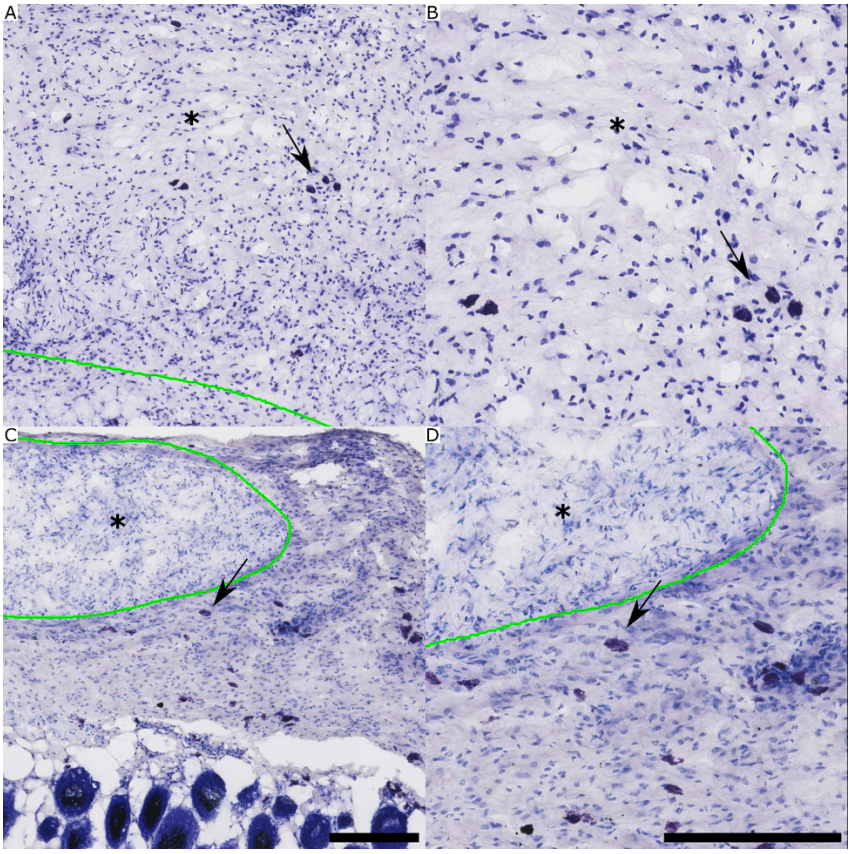

Figure S1: Toluidine blue staining of subcutaneously injected ECM hydrogel and urinary bladder matrix powder. Representative images of toluidine blue staining of (A, B) ECM hydrogel scaffold and (C, D) milled urinary bladder matrix (material outlined in green with asterisk on side where material is present) and neighboring dermal tissue in male wild-type 3 days post-injection. Mast cells staining is indicated by a black arrow. Scale bar is 200 μm.

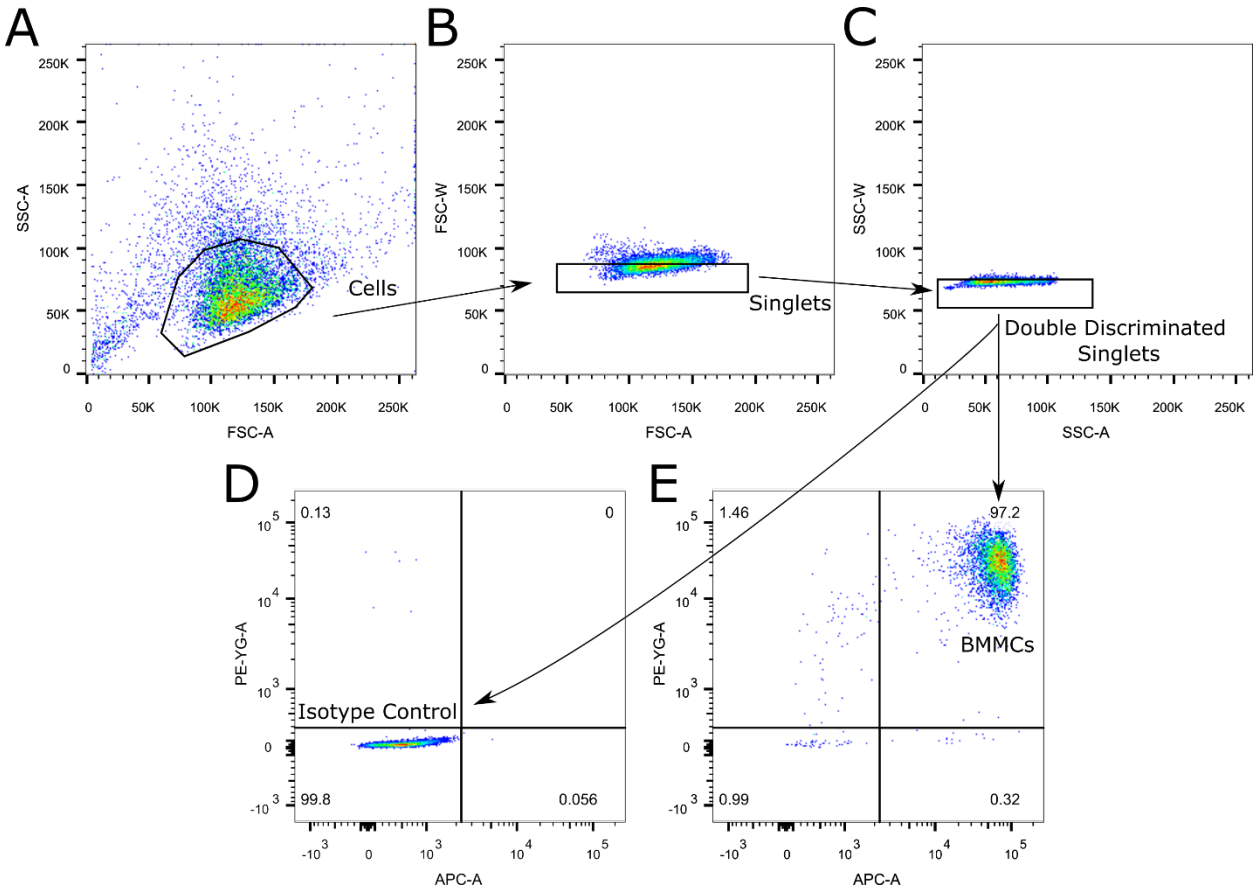

Figure S2: Gating scheme for bone marrow derived differentiated mast cell culture purity. Representative gating of mast cells for assessing purity at four to six weeks of differentiation protocol. (A) Cells and (B-C) double discrimination of singlets based on forward and side scatter. Quadrant gating cut-offs were set relative to (D) isotype control for (E) CD117^{+}FcƐRI^{+} mast cells.

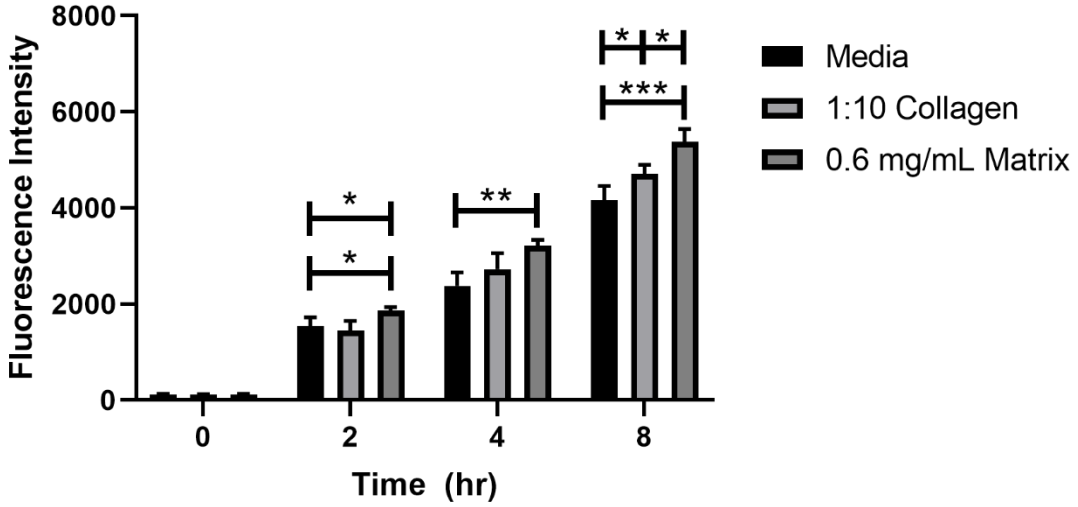

Figure S3: Viability assay of mast cells incubated with ECM hydrogel. Four week differentiated bone marrow derived mast cells were incubated ECM hydrogel material, collagen or culture media control. AlamarBlue™ fluorescent readings were taken at 0, 2, 4, and 8 hours following plate set-up (n = 4 per group). (*$p < 0.05$, **$p < 0.01$, ***$p < 0.001$).

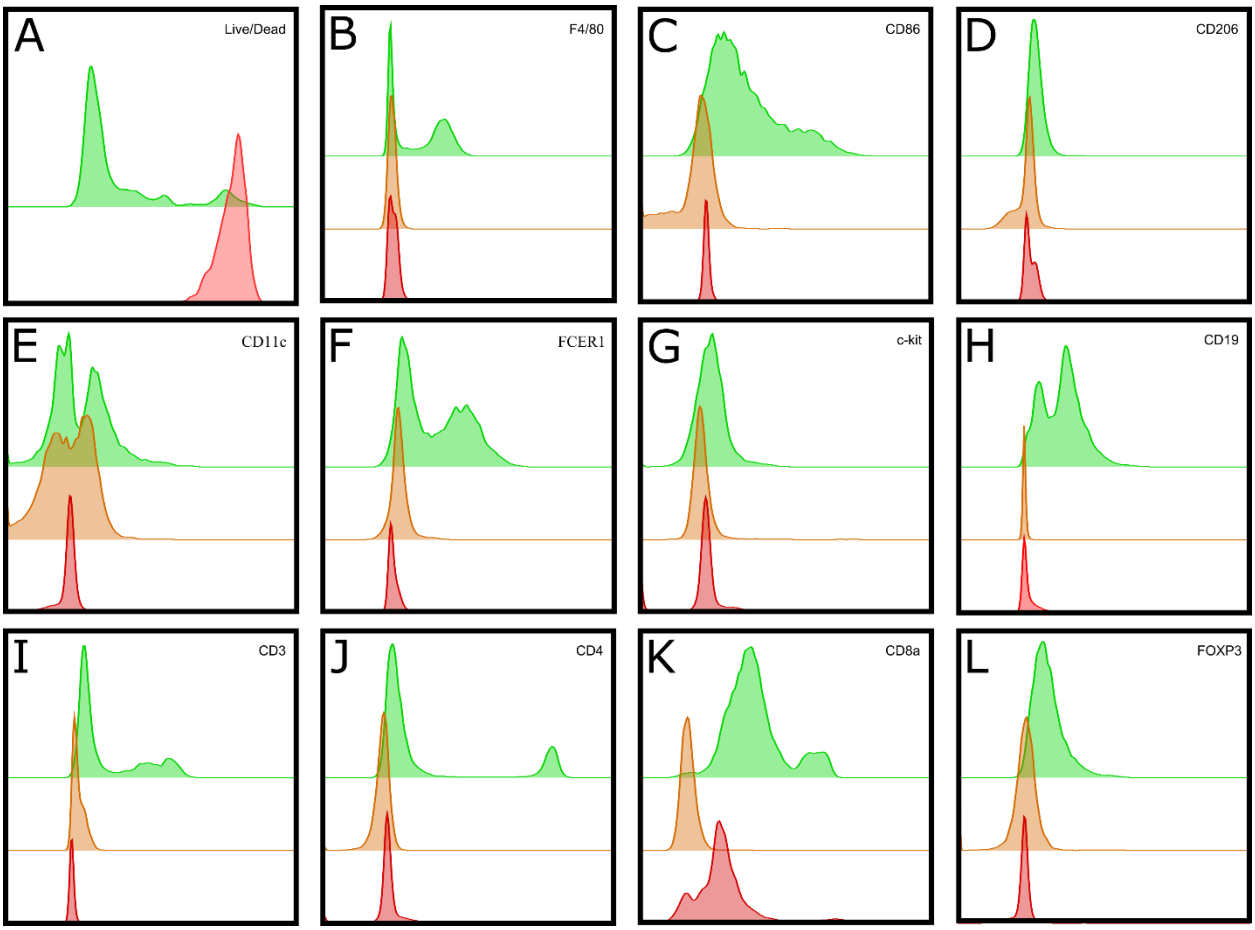

Figure S4: Gating controls for flow cytometry markers. (A) LIVE, DEAD™ Aqua thresholds utilized ethanol fixed sample as control (red) for determining live cell gating (green). (B-L) Gating for fluorescent antibody markers was set for positive signal (green) based on isotype (red) and fluorescence minus one controls (orange).

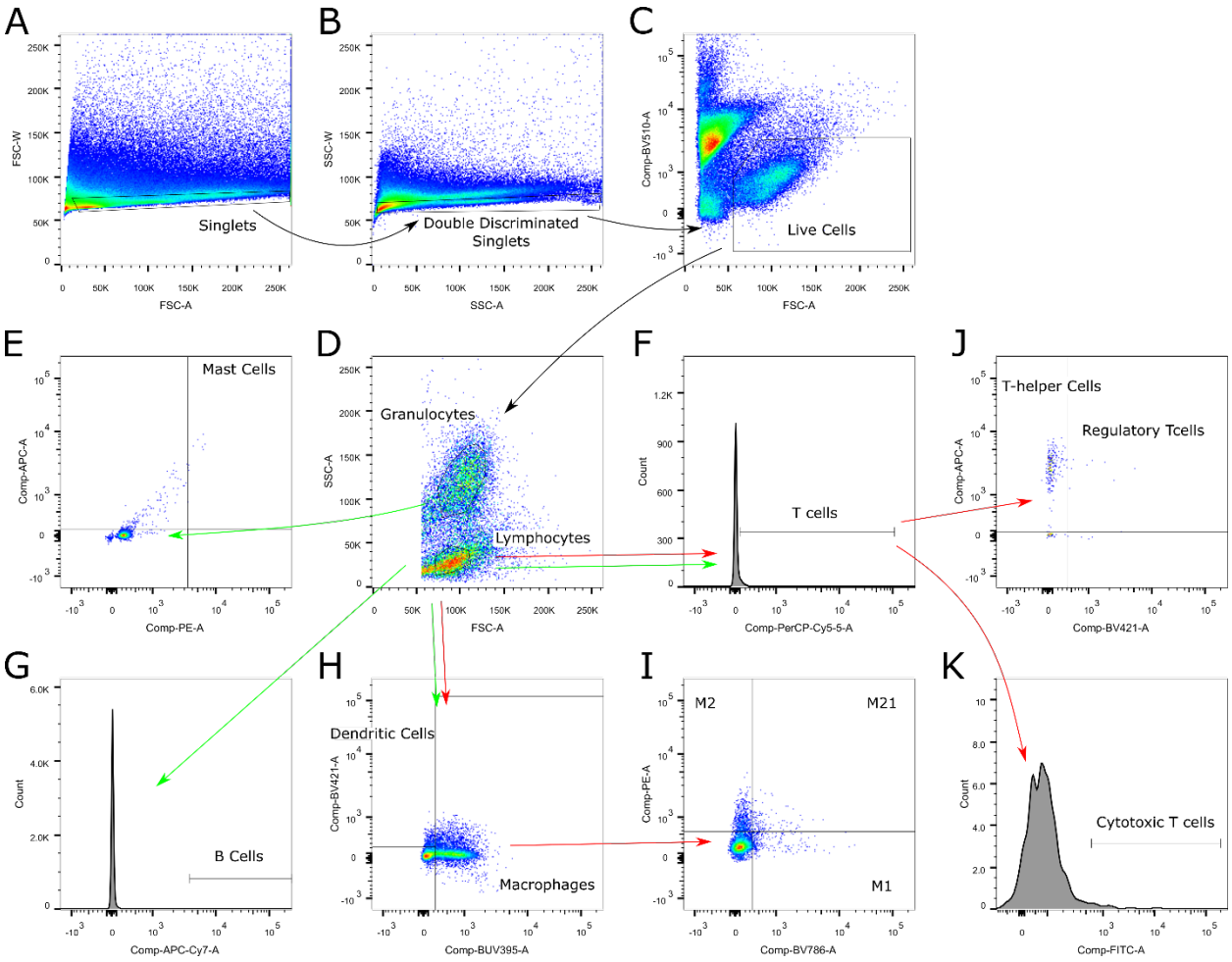

Figure S5: Gating Scheme for Flow Cytometry Analysis. Representative gating of single cell suspension isolated of subcutaneously injected ECM hydrogel. (A-B) General gating for both panels (black arrow) for double discrimination of singlets based on forward and side scatter. (C) Live cells were gated based on clustered from lack of stain uptake and forward scatter. (D) Granulocyte cluster based on forward and side scatter with (F) $CD117^{+}Fc\varepsilon RI^{+}$ gated for mast cells. (E) Lymphocyte cluster based on forward and side scatter with (F) $CD3^{+}$ gated for T cells. Total cells based on forward and side scatter distribution were utilized to differentiate (G) B cells, (H) $CD11c^{+}F4, 80^{-}$ dendritic cells, and $F4, 80^{+}$ macrophages. For Panel 2 (red arrow), macrophages were further differentiated based on (I) M1 $CD86^{+}$ and M2 $CD206^{+}$ markers. T cells were further separated into (J) $CD4^{+}$ T-helper cells, $CD4^{+}FOXP3^{+}$ Regulatory T cells, and (K) $CD8^{+}$ cytotoxic T cells.

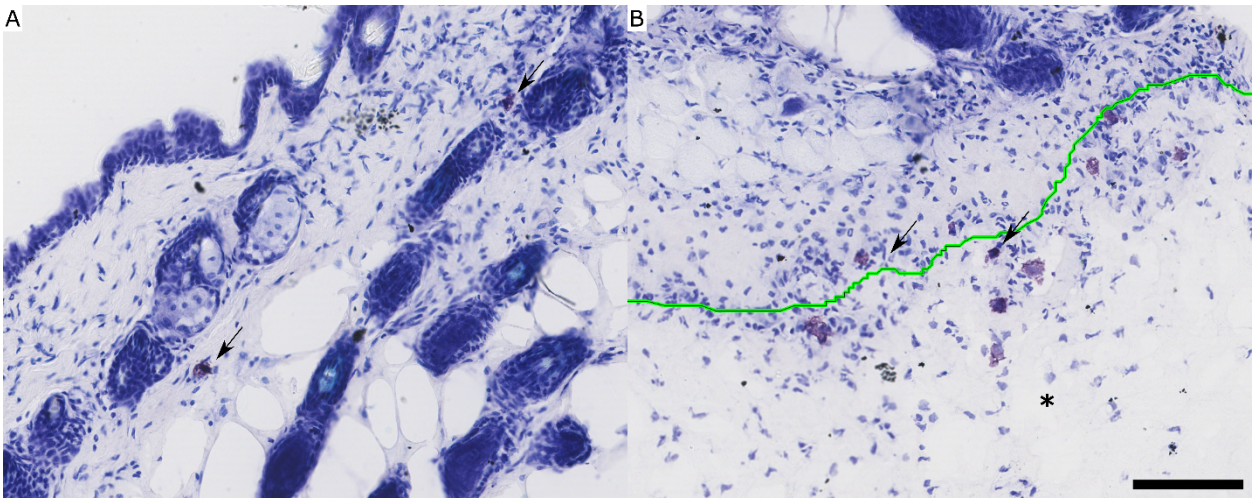

Figure S6: Mast cell engraftment in deficient mice. Representative toluidine blue staining in 9 week old deficient mice following dorsal subcutaneous injection of *in vitro* differentiated bone marrow derived mast cells at 4 weeks old showing reconstitution of mast cells in the (A) skin and infiltrating into subcutaneously injected (B, C) ECM scaffold at 3 days post-injection (material outlined in green with asterisk on side where material is present). Mast cell staining is indicated by a black arrow with both resting and degranulated mast cells observed at this timepoint. Scale bar is 100 μm.

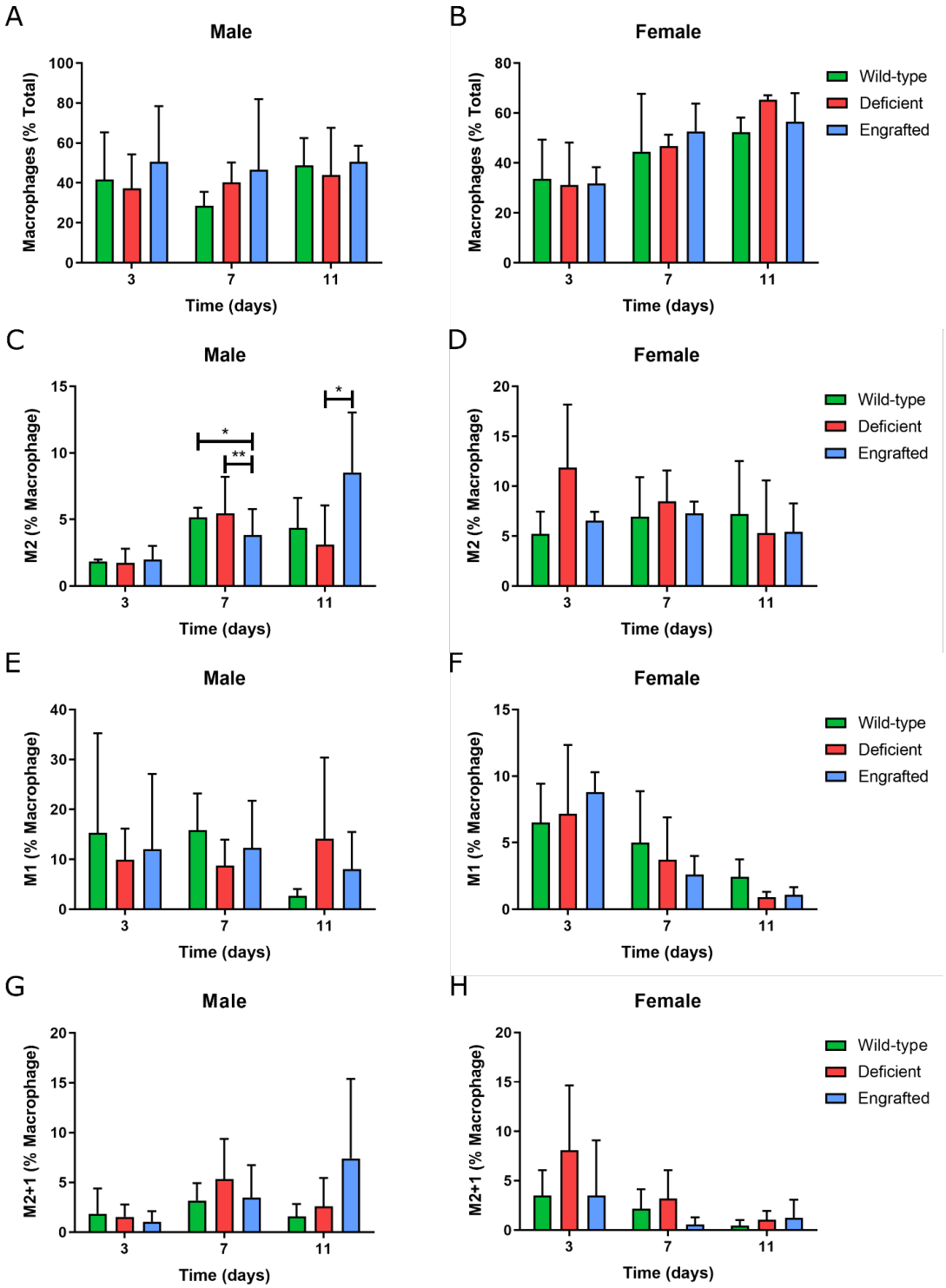

Figure S7: Flow cytometry of total and macrophage polarized subpopulations. Percentages of total F4, 80$^+$ macrophages relative to live cells (A, B), and CD206$^+$ M2 (C, D), CD86$^+$ M1 (E, F) and co-expressing CD206$^+$CD86$^+$ M2+1 (G, H) macrophages relative to total macrophages at three, seven, and eleven days post-injection between wild-type (green), deficient (red), and engrafted (blue) male (A, C, E, G) and female mice (B, D, F, H).

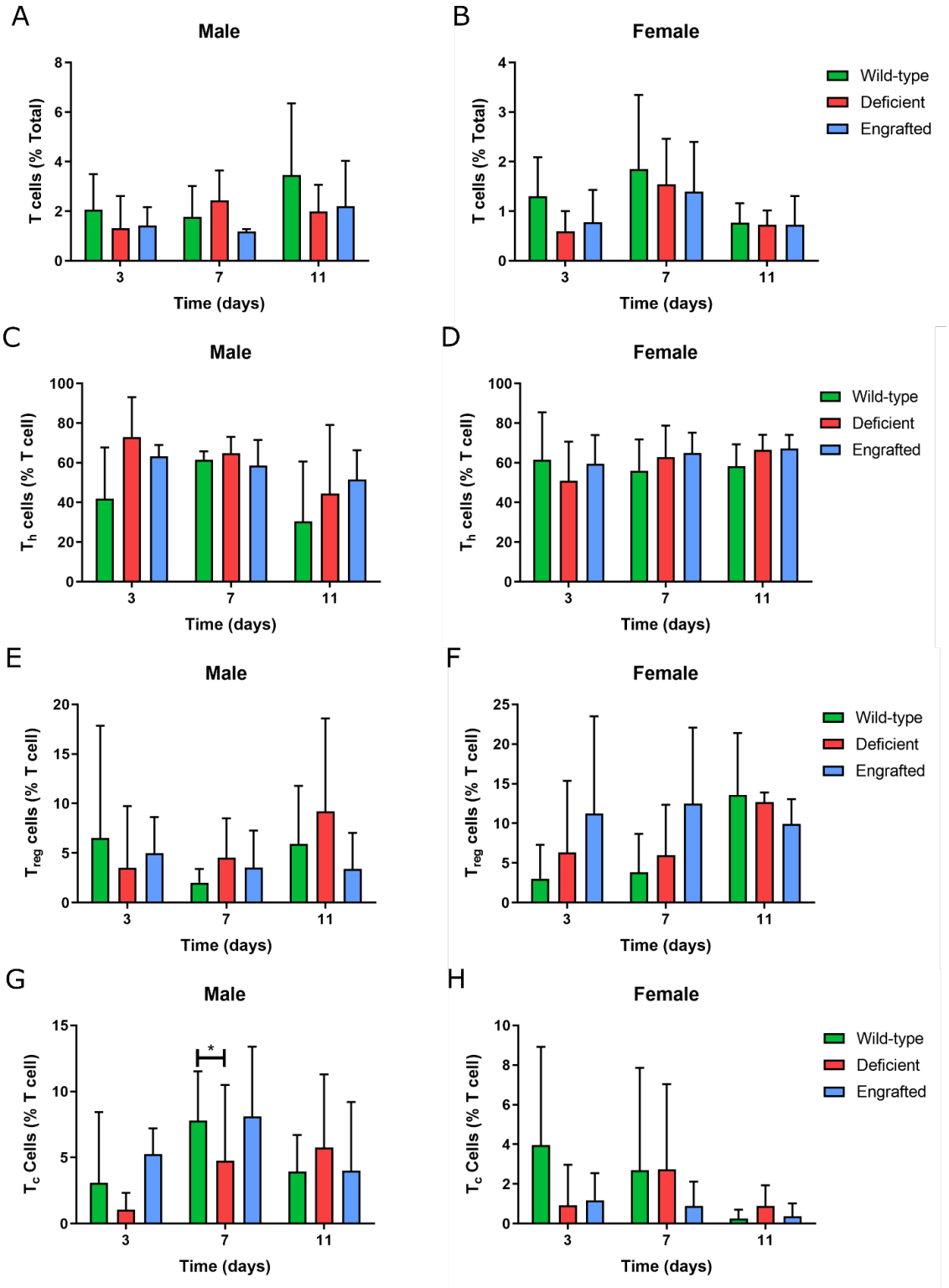

Figure S8: Flow cytometry of total T cells and differentiated subpopulations. Percentages of total $CD3^+$ T cells relative to total live cells (A, B), and $CD4^+$ T-helper (T_h) cells (C, D), $CD4^+FOXP3^+$ regulatory T (T_{reg}) cells (E, F) and $CD8^+$ cytotoxic T (T_c) cells (G, H) relative to total T cells at three, seven, and eleven days post-injection between wild-type (green), deficient (red), and engrafted (blue) male (A, C, E, G) and female mice (B, D, F, H).

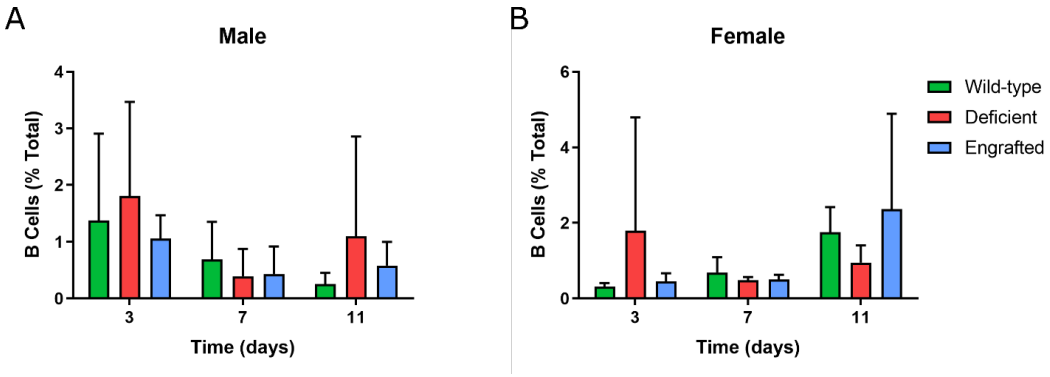

Figure S9: Flow cytometry of B-cells. Percentages of $CD19^{+}$ B cells relative to total live cells at three, seven, and eleven days post-injection between wild-type (green), deficient (red), and engrafted (blue) male (A) and female mice (B).

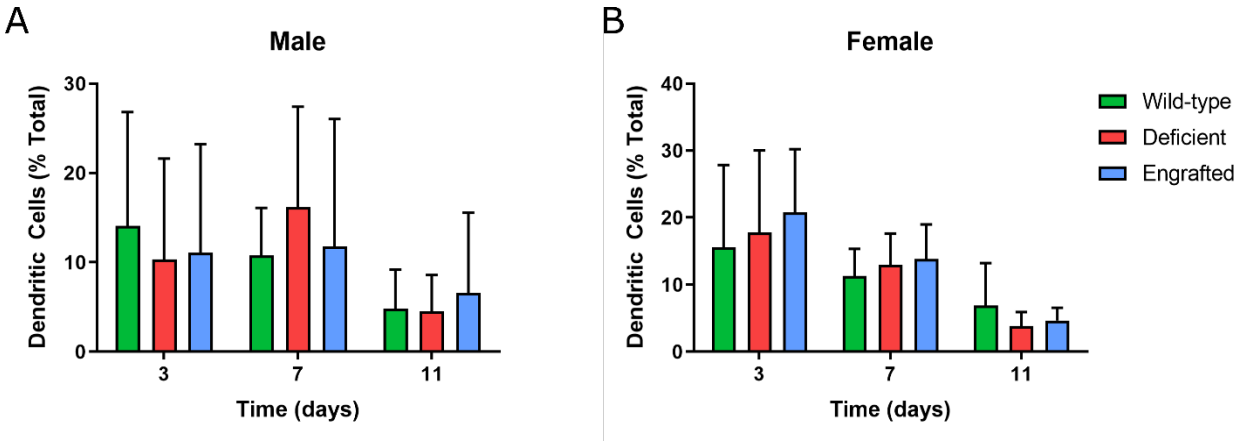

Figure S10: Flow cytometry of Dendritic Cells. Percentages of CD11c^{+}F4, 80^{-} dendritic cells relative to total live cells at three, seven, and eleven days post-injection between wild-type (green), deficient (red), and engrafted (blue) male (A) and female mice (B).

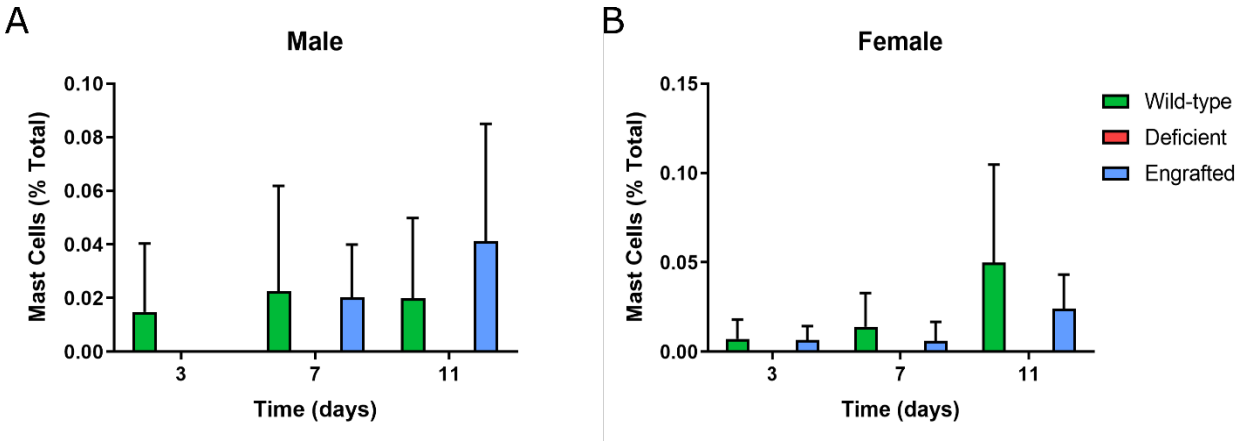

Figure S11: Flow cytometry of Mast Cells. Percentages of CD117^{+}FcƐRI^{+} mast cells relative to total live cells at three, seven, and eleven days post-injection between wild-type (green), deficient (red, not present), and engrafted (blue) male (A) and female mice (B).

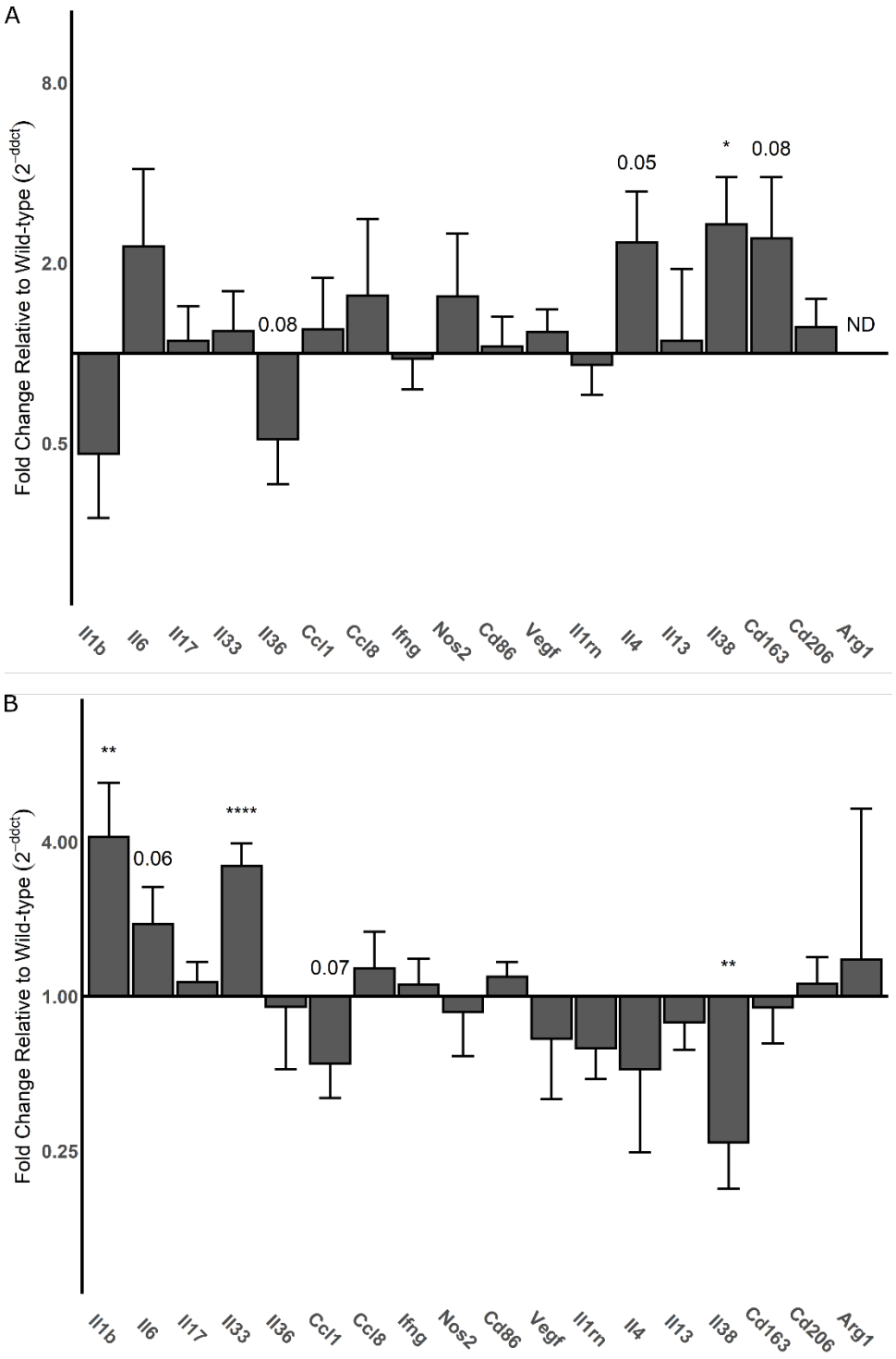

Figure S12: Screen of deficient versus wild-type gene expression in male mice. qPCR results of pro-inflammatory versus pro-remodeling immune markers at day 3 (A) and day 11 (B) in male mice. Fold change and significance of deficient mouse sample gene expression was normalized relative to wild-type gene expression. Gene expression plotted as mean ± SEM. (ND = not detected, value displayed for trend $p < 0.1$, *$p < 0.05$, **$p < 0.01$, and ****$p < 0.0001$).

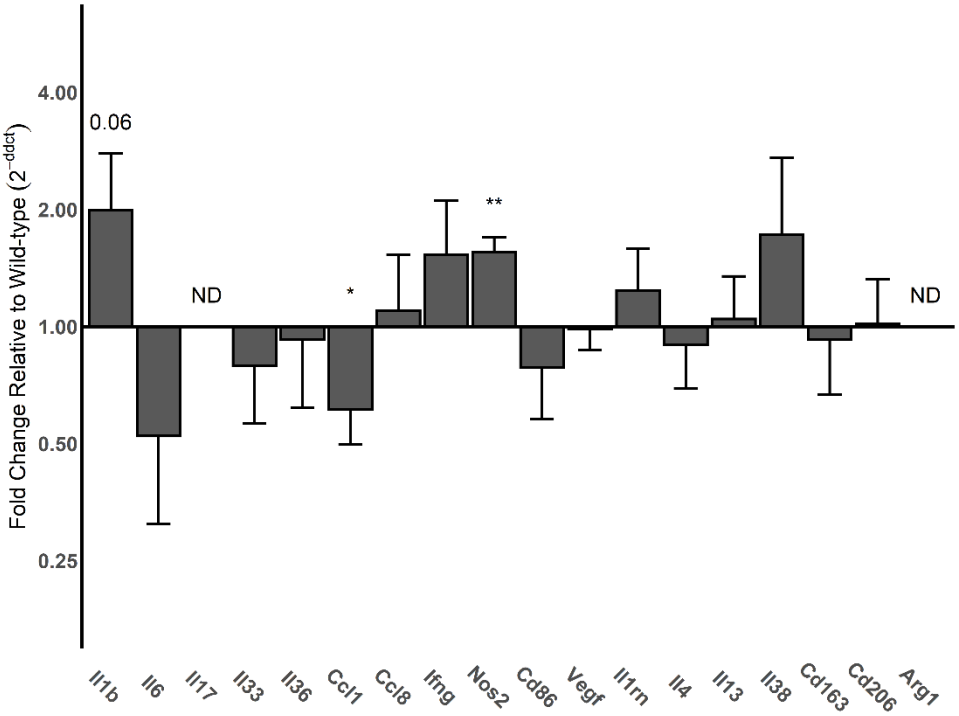

Figure S13: Screen of deficient versus wild-type gene expression in female mice. qPCR results of pro-inflammatory versus pro-remodeling immune markers at day 3 in female mice. Fold change and significance of deficient mouse sample gene expression was normalized relative to wild-type gene expression. Gene expression plotted as mean ± SEM. (ND = not detected, value displayed for trend $p < 0.1$, *$p < 0.05$, **$p < 0.01$).

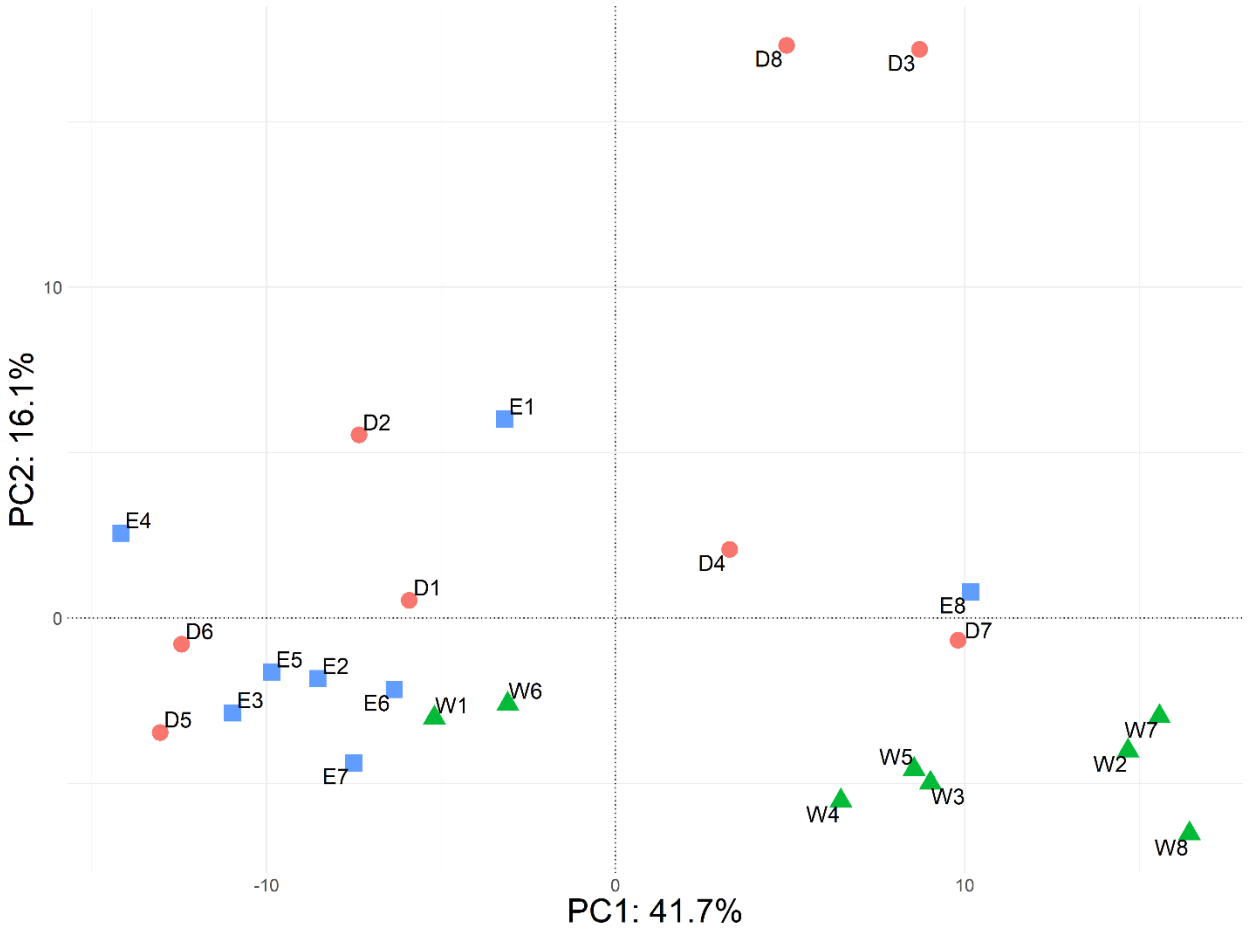

Figure S14: Principal component analysis plot of Nanostring nCounter data. PC1 (41.7% of variance) versus PC2 (16.1% of variance) of the top 50% of assessed genes sorted by variance of their normalized gene expression based on the NanostringDiff package method. Points indicate wild-type, W1-W8 (green triangles), deficient, D1-D8 (red circles), and engrafted, E1-E8 (blue squares) samples.

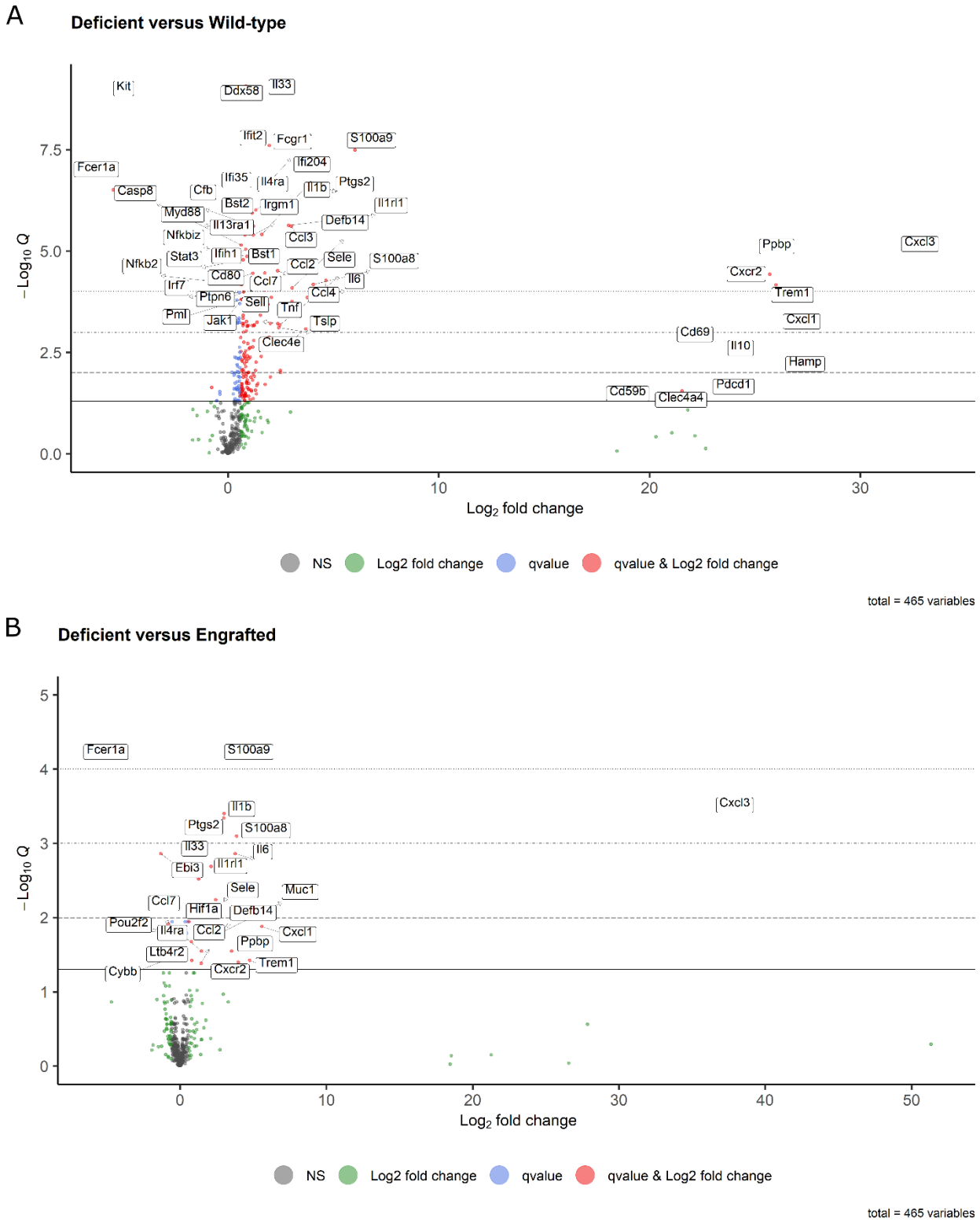

Figure S15: Volcano plots of pairwise comparisons for deficient response. Differential expression between deficient versus (A) wild-type and (B) engrafted sample groups with dots indicating false discovery rate less than 0.05 (blue, red), absolute fold change greater than 1.5 (green, red) or non-significant (black). Dashed lines indicating different significance thresholds (*$q < 0.05$, **$q < 0.01$, ***$q < 0.001$ and ****$q < 0.0001$).

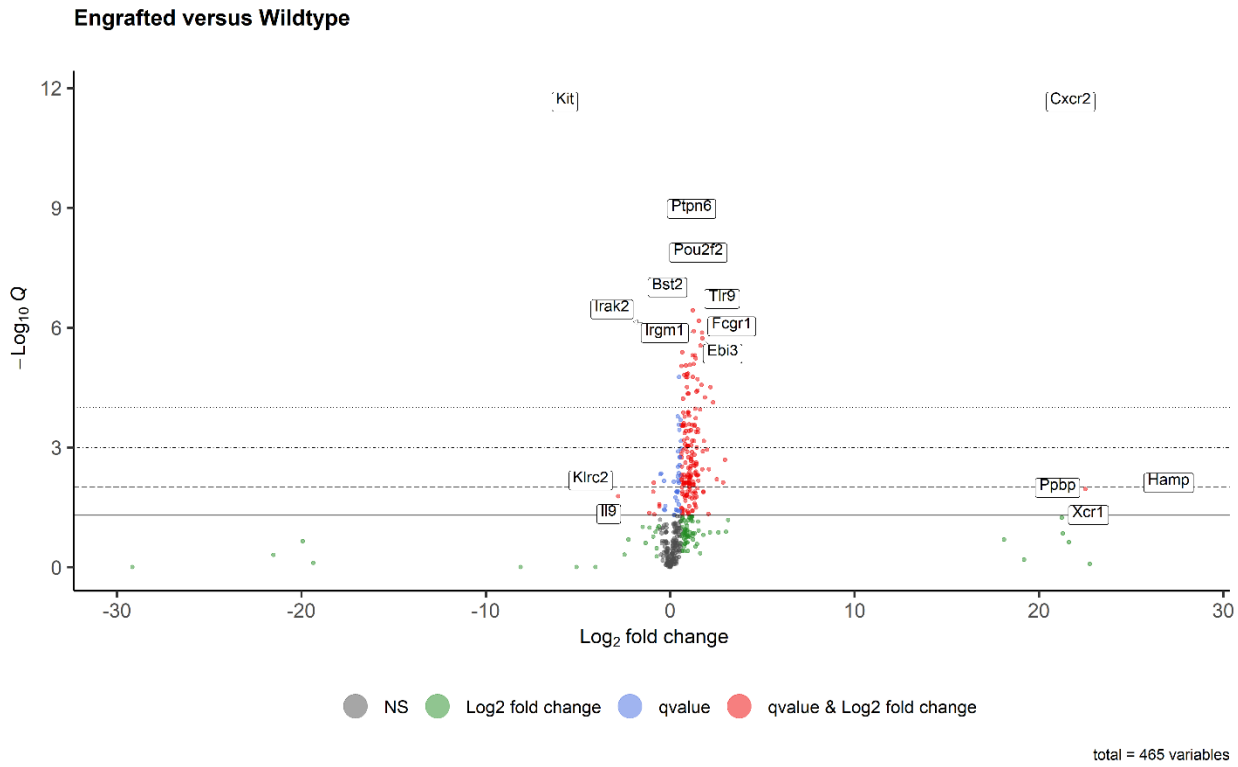

Figure S16: Volcano plot of pairwise comparison between engrafted and wild-type sample. Differential expression of engrafted sample versus wild-type with dots indicating false discovery rate less than 0.05 (blue, red), absolute fold change greater than 1.5 (green, red) or non-significant (black). Dashed lines indicating different significance thresholds (**q* < 0.05, ***q* < 0.01, ****q* < 0.001 and *****q* < 0.0001).

Table S1: Primers

Gene	Forward Primer			Reverse Primer		
Gapdh	5'	CATCAAGAAGGTGGTGAAGC	3'	5'	GTTGTCATACCAGGAAATGAGC	3'
Il1b	5'	TGCCACCTTTTGACAGTGATG	3'	5'	TGATGTGCTGCTGCGAGATT	3'
Il6	5'	TCCAGTTGCCTTCTTGGGAC	3'	5'	AGTCTCCTCTCCGGACTTGT	3'
Il17	5'	AAGCTGGACCACCACATGAA	3'	5'	CCCTGAAAGTGAAGGGGCAG	3'
Il33	5'	TCCAACTCCAAGATTTCCCCG	3'	5'	CAGTGCAGTAGACATGGCAGAA	3'
Il36	5'	AGGGCAAACCAACTTTGCAG	3'	5'	GAAGTGGAGCCCTCTATGCC	3'
Ccl1	5'	AGAAAGAGCTTCCCCTGAAGTTT	3'	5'	TGAGGCGCAGCTTTCTCTACC	3'
Ccl8	5'	CCCCTTCGGGTGCTGAAAAG	3'	5'	TCACTGACCCACTTCTGTGTG	3'
Ifng	5'	CGGCTGACTGAACTCAGATTG	3'	5'	CTGCAGCTCTGAATGTTTCTTAT	3'
Nos2	5'	CAGCTGGGCTGTACAAACCTT	3'	5'	CATTGGAAGTGAAGCGTTTCG	3'
Cd86	5'	GACTTGAACAACCAGACTCCTG	3'	5'	ATCAGCAAGACTGTCACAAAGA	3'
Vegf	5'	GCACATAGAGAGAATGAGCTTCC	3'	5'	CTCCGCTCTGAACAAGGCT	3'
Il1rn	5'	TCGGAGTACCTGTCATGCAAA	3'	5'	GCTTGCATCTTGCAGGGTCT	3'
Il4	5'	GAGACTCTTTCGGGCTTTTCG	3'	5'	CAGTGATGTGGACTTGGACTC	3'
Il13	5'	GAGCAACATCACACAAGACCAGA	3'	5'	GGCCAGGTCCACACTCCATA	3'
Il38	5'	TGCAGGAATGTGCTCCCTTC	3'	5'	GGTCTAGGCCTCGGTTAGGA	3'
Cd163	5'	GAGACACACGGAGCCATCAA	3'	5'	CGTTAGTGACAGCAGAGGCA	3'
Cd206	5'	GTGGACGCTCTAAGTGCCAT	3'	5'	GAATCTGACACCCAGCGGAA	3'
Arg1	5'	GAACACGGCAGTGGCTTTAAC	3'	5'	TGCTTAGTTCTGTCTGCTTTGC	3'

Table S2: Differential expression of mast cell deficient to other group samples

Gene	logFC	pvalue	qvalue
Bcl3	0.96	1.05E-04	1.25E-03
Bst1	1.12	1.91E-04	2.02E-03
Bst2	0.54	2.00E-03	1.56E-02
Casp8	0.42	6.35E-05	8.62E-04
Ccl12	0.73	3.00E-02	1.49E-01
Ccl2	1.90	1.15E-06	2.87E-05
Ccl20	1.24	3.55E-03	2.37E-02
Ccl3	2.00	3.42E-06	7.73E-05
Ccl4	3.21	8.32E-06	1.65E-04
Ccl7	1.76	2.57E-06	6.10E-05
Ccl9	0.89	3.35E-02	1.56E-01
Ccr5	0.73	4.67E-02	1.96E-01
Ccr9	0.50	3.52E-02	1.59E-01
Ccrl2	0.85	3.40E-02	1.56E-01
Cd14	0.79	1.08E-02	6.29E-02
Cd244	0.59	4.07E-02	1.79E-01
Cd24a	0.61	3.48E-03	2.36E-02
Cd44	0.49	9.75E-05	1.19E-03
Cd59b	10.05	1.35E-02	7.59E-02
Cd69	12.56	5.91E-05	8.26E-04
Cd80	0.72	5.34E-04	5.17E-03
Cfb	0.72	1.31E-04	1.49E-03
Clec4e	2.65	2.43E-04	2.45E-03
Csf1	0.42	1.68E-02	9.09E-02
Csf3r	0.81	9.62E-04	8.31E-03
Cxcl1	16.41	0.00E+00	0.00E+00
Cxcl10	1.45	5.63E-03	3.57E-02
Cxcl3	35.38	5.86E-12	6.85E-10
Cxcr2	14.84	1.02E-07	3.74E-06
Ddx58	0.52	6.51E-07	1.93E-05
Defb14	2.65	3.60E-07	1.14E-05
Fas	0.46	1.98E-02	1.05E-01
Fasl	0.94	2.74E-02	1.40E-01
Fcer1a	-5.26	5.77E-09	3.04E-07
Fcgr1	0.97	1.38E-04	1.52E-03
Gata3	-0.42	3.79E-02	1.70E-01
Hamp	13.87	6.40E-03	3.95E-02
Hif1a	0.49	6.30E-04	5.76E-03
Ifi204	0.89	3.68E-04	3.64E-03
Ifi35	0.53	1.98E-05	3.61E-04
Ifih1	0.42	3.28E-03	2.29E-02
Ifit2	1.21	1.08E-06	2.86E-05
Ifitm1	1.53	2.19E-05	3.86E-04
Il10	12.91	6.13E-04	5.71E-03
Il13ra1	0.72	1.15E-05	2.18E-04
Il15ra	0.55	5.56E-03	3.57E-02
Il18rap	0.90	3.06E-02	1.49E-01
Il1a	0.78	1.65E-03	1.40E-02
Il1b	3.50	6.56E-12	6.85E-10
Il1r1	0.44	2.80E-05	4.59E-04
Il1rl1	2.50	1.49E-09	1.01E-07
Il1rl2	0.50	6.40E-06	1.32E-04
Il2rg	0.47	4.26E-02	1.85E-01
Il33	1.78	8.66E-12	6.85E-10
Il4ra	1.05	8.11E-08	3.21E-06
Il6	3.76	1.84E-08	7.93E-07
Irf7	1.07	5.74E-04	5.45E-03
Irgm1	0.56	3.78E-03	2.50E-02
Itga5	0.74	1.71E-04	1.85E-03
Itga6	0.70	4.89E-05	7.04E-04
Lilrb3	0.51	4.86E-02	2.01E-01
Ltb4r1	0.63	1.87E-03	1.51E-02
Ltb4r2	0.88	3.28E-05	5.20E-04
Masp1	1.08	4.36E-05	6.47E-04
Muc1	2.38	6.79E-05	8.88E-04
Mx1	0.70	3.42E-03	2.36E-02
Myd88	0.52	6.92E-05	8.88E-04
Nfkb2	0.45	1.14E-04	1.32E-03
Nfkbiz	0.51	9.03E-04	8.09E-03
Nod2	0.85	3.06E-03	2.20E-02
Pdcd1	25.82	3.02E-03	2.20E-02
Pecam1	0.53	2.15E-03	1.65E-02
Plaur	0.86	1.93E-03	1.53E-02
Ppbp	14.78	1.14E-08	5.40E-07
Ptgs2	3.53	7.37E-12	6.85E-10
S100a8	3.96	3.41E-09	2.03E-07
S100a9	5.37	0.00E+00	0.00E+00
Sele	2.45	1.05E-06	2.86E-05
Sell	1.76	2.12E-04	2.19E-03
Socs3	1.10	8.46E-05	1.06E-03
Stat2	0.82	1.88E-03	1.51E-02
Stat3	0.51	3.53E-05	5.41E-04
Thy1	0.44	9.29E-04	8.18E-03
Tlr5	0.43	3.87E-02	1.72E-01
Tnf	2.29	2.28E-05	3.87E-04

Tnfsf14	0.81	2.19E-02	1.16E-01	Tslp	1.50	1.82E-03	1.51E-02
Trem1	15.38	1.39E-07	4.72E-06				

Table S3: Differential expression of mast cell deficient samples to wild-type

Gene	logFC	pvalue	qvalue
Ahr	0.56	1.60E-02	3.85E-02
Arhgdib	0.74	7.20E-04	3.72E-03
B2m	0.73	1.61E-04	1.01E-03
Batf	0.98	9.85E-04	4.52E-03
Bcl3	1.16	9.73E-05	6.87E-04
Bcl6	0.43	7.65E-03	2.31E-02
Bid	0.60	2.23E-04	1.36E-03
Bst1	1.75	1.98E-06	3.48E-05
Bst2	1.15	2.91E-08	1.15E-06
Btk	0.78	1.47E-02	3.65E-02
C1qa	0.83	1.28E-02	3.30E-02
C1qb	0.79	2.10E-02	4.88E-02
C1ra	0.67	7.83E-03	2.34E-02
C1s	0.65	1.10E-02	2.94E-02
C3	1.36	1.32E-02	3.36E-02
Card9	0.84	5.36E-04	2.89E-03
Casp1	0.47	7.29E-05	5.87E-04
Casp8	0.63	3.29E-07	7.10E-06
Ccbp2	1.23	2.21E-02	4.97E-02
Ccl12	1.19	2.89E-03	1.07E-02
Ccl2	2.36	1.68E-06	3.08E-05
Ccl20	1.95	2.15E-04	1.32E-03
Ccl3	3.00	7.70E-08	2.44E-06
Ccl4	4.65	3.34E-06	5.28E-05
Ccl6	1.43	5.82E-03	1.85E-02
Ccl7	2.06	1.11E-05	1.39E-04
Ccl9	1.31	9.73E-03	2.72E-02
Ccr5	1.11	1.06E-02	2.86E-02
Ccrl2	2.02	7.69E-05	6.08E-04
Cd109	0.44	4.95E-03	1.67E-02
Cd14	1.54	3.94E-05	3.82E-04
Cd163	0.99	2.52E-02	5.51E-02
Cd244	1.04	2.35E-03	9.40E-03
Cd24a	0.56	2.18E-02	4.93E-02
Cd274	0.91	7.62E-03	2.31E-02
Cd44	0.45	2.35E-03	9.40E-03
Cd53	1.11	9.79E-03	2.72E-02
Cd59b	19.10	8.29E-03	2.46E-02
Cd69	22.16	1.25E-04	8.13E-04
Cd80	1.18	2.08E-06	3.52E-05
Cd86	0.73	2.97E-03	1.10E-02
Cd97	0.73	1.04E-02	2.85E-02
Ceacam1	0.68	9.96E-03	2.75E-02
Cfb	1.21	7.26E-08	2.44E-06
Cfh	0.81	1.40E-02	3.50E-02
Cfp	1.08	3.74E-03	1.30E-02
Cish	-0.45	4.89E-02	9.56E-02
Clec4a4	21.55	1.04E-02	2.85E-02
Clec4e	3.69	1.29E-04	8.26E-04
Clec5a	0.89	5.71E-03	1.84E-02
Cmklr1	0.65	6.06E-03	1.91E-02
Crlf2	0.66	3.81E-02	7.83E-02
Csf1	0.90	1.31E-05	1.55E-04
Csf2rb	0.99	2.62E-03	9.94E-03
Csf3r	1.29	1.34E-05	1.55E-04
Cxcl1	27.22	4.22E-05	3.93E-04
Cxcl10	1.77	6.25E-03	1.95E-02
Cxcl13	2.49	2.60E-03	9.94E-03
Cxcl3	32.83	2.04E-07	4.85E-06
Cxcr2	25.70	2.29E-06	3.75E-05
Ddx58	0.85	5.37E-12	8.51E-10
Defb14	3.05	5.83E-06	8.15E-05
Emr1	0.80	4.39E-02	8.83E-02
Entpd1	0.87	1.47E-04	9.30E-04
Ets1	0.55	6.90E-05	5.75E-04
Fas	0.79	6.38E-04	3.33E-03
Fasl	1.20	1.86E-02	4.40E-02
Fcer1a	-5.44	5.91E-09	3.12E-07
Fcer1g	0.95	2.60E-03	9.94E-03
Fcgr1	1.83	3.94E-09	2.34E-07
Fcgr2b	0.91	2.53E-02	5.51E-02
Fcgr4	1.57	7.88E-04	3.98E-03
Fcgrt	0.64	3.36E-02	7.02E-02
Fkbp5	0.80	2.13E-02	4.90E-02
Gata3	-0.52	2.17E-02	4.93E-02
Gm10499	0.75	3.07E-04	1.78E-03
H2-K1	0.54	4.22E-04	2.36E-03
H2-Q10	2.49	2.15E-03	8.82E-03
Hamp	27.39	9.20E-04	4.37E-03
Hlx	0.50	4.35E-02	8.80E-02
Icam1	0.58	8.70E-04	4.22E-03
Ifi204	1.61	1.40E-07	3.91E-06
Ifi35	0.84	1.20E-08	5.72E-07
Ifih1	0.85	4.35E-07	8.98E-06
Ifit2	1.96	2.10E-10	2.49E-08

Ifitm1	1.89	2.10E-05	2.08E-04	Jak1	0.66	1.43E-05	1.56E-04
Ifnar2	0.66	2.11E-03	8.72E-03	Jak2	0.45	1.60E-03	6.84E-03
Ifngr1	0.73	8.91E-03	2.55E-02	Jak3	0.65	1.07E-02	2.86E-02
Ikbke	0.74	7.97E-05	6.10E-04	Kir3dl1	2.97	4.77E-02	9.39E-02
Ikzf1	0.98	8.76E-03	2.54E-02	Kit	-4.96	0.00E+00	0.00E+00
Il10	24.33	3.06E-04	1.78E-03	Lcp2	1.33	1.26E-03	5.55E-03
Il10ra	0.72	1.78E-02	4.25E-02	Lilrb3	1.14	2.31E-04	1.39E-03
Il10rb	0.63	1.24E-02	3.22E-02	Lilrb4	1.03	5.76E-03	1.85E-02
Il11ra1	-0.64	3.28E-02	6.90E-02	Litaf	0.52	6.96E-03	2.15E-02
Il12a	-1.67	3.96E-02	8.11E-02	Lta	-0.81	2.47E-02	5.43E-02
Il13ra1	1.03	1.27E-07	3.78E-06	Ltb4r1	0.80	8.30E-04	4.11E-03
Il15ra	0.91	1.10E-04	7.34E-04	Ltb4r2	0.97	1.01E-04	6.88E-04
Il16	0.61	1.52E-02	3.73E-02	Ly96	0.72	4.08E-05	3.87E-04
Il17ra	0.49	9.50E-04	4.47E-03	Masp1	1.25	9.03E-05	6.61E-04
Il18	0.54	1.21E-02	3.18E-02	Ms4a1	1.44	4.50E-02	8.98E-02
Il18r1	0.68	3.25E-02	6.85E-02	Msr1	1.30	2.17E-03	8.82E-03
Il18rap	1.36	6.65E-03	2.06E-02	Muc1	2.01	3.60E-03	1.28E-02
Il1a	0.88	2.85E-03	1.07E-02	Mx1	0.99	4.70E-04	2.57E-03
Il1b	3.98	3.93E-09	2.34E-07	Myd88	0.82	1.54E-07	4.02E-06
Il1r1	0.50	5.79E-05	5.09E-04	Ncf4	0.87	1.52E-02	3.73E-02
Il1rl1	2.88	6.36E-08	2.32E-06	Nfatc1	0.71	9.50E-05	6.84E-04
Il1rl2	0.55	1.95E-05	1.97E-04	Nfatc2	0.55	3.68E-03	1.29E-02
Il1rn	0.42	1.54E-05	1.62E-04	Nfkb1	0.44	7.17E-05	5.87E-04
Il2rg	0.89	1.19E-03	5.30E-03	Nfkb2	0.64	4.40E-06	6.67E-05
Il33	2.28	2.98E-12	7.08E-10	Nfkbia	0.55	4.76E-03	1.62E-02
Il4ra	1.32	2.25E-08	9.70E-07	Nfkbiz	0.90	6.90E-07	1.37E-05
Il6	3.76	1.15E-05	1.40E-04	Nod2	1.39	6.75E-05	5.73E-04
Il6ra	0.70	1.06E-02	2.86E-02	Notch1	-0.53	2.17E-02	4.93E-02
Il6st	0.43	9.36E-03	2.65E-02	Nox4	0.99	5.66E-03	1.84E-02
Irak2	0.54	8.28E-06	1.06E-04	Pdcd1	23.80	5.39E-03	1.78E-02
Irak3	0.68	1.17E-03	5.24E-03	Pdgfrb	0.49	2.07E-02	4.85E-02
Irak4	0.71	4.96E-05	4.53E-04	Pecam1	0.67	1.08E-03	4.87E-03
Irf1	0.45	2.37E-02	5.25E-02	Pla2g2e	-0.98	4.53E-02	9.00E-02
Irf5	0.66	7.32E-03	2.24E-02	Plau	0.73	1.48E-02	3.66E-02
Irf7	1.72	6.80E-06	9.23E-05	Plaur	1.18	4.15E-04	2.35E-03
Irf8	0.87	5.14E-03	1.72E-02	Pml	0.63	1.45E-05	1.56E-04
Irgm1	1.20	1.61E-07	4.02E-06	Pou2f2	0.71	2.04E-03	8.48E-03
Itga4	0.81	9.81E-04	4.52E-03	Ppbp	26.04	2.45E-07	5.53E-06
Itga5	0.91	1.01E-04	6.88E-04	Prdm1	-0.49	3.70E-02	7.65E-02
Itga6	0.89	1.42E-05	1.56E-04	Psmb10	0.76	2.42E-03	9.59E-03
Itgal	0.79	1.35E-03	5.88E-03	Psmb9	0.62	8.40E-03	2.46E-02
Itgam	1.16	4.41E-03	1.51E-02	Ptafr	0.91	4.43E-03	1.51E-02
Itgb1	0.53	5.10E-05	4.57E-04	Ptgs2	4.07	3.16E-09	2.34E-07
Itgb2	0.93	2.42E-02	5.35E-02	Ptpn22	0.99	9.42E-03	2.65E-02

Ptpn6	0.74	7.75E-06	1.02E-04	Tlr1	1.06	8.29E-04	4.11E-03
Ptprc	0.78	1.57E-02	3.82E-02	Tlr2	1.05	4.41E-04	2.44E-03
Relb	0.51	2.52E-03	9.83E-03	Tlr3	0.46	9.21E-03	2.62E-02
S100a8	4.05	4.49E-06	6.67E-05	Tlr4	0.90	5.19E-03	1.72E-02
S100a9	6.03	3.42E-10	3.25E-08	Tlr5	0.67	6.00E-03	1.90E-02
Sele	2.47	9.05E-05	6.61E-04	Tlr8	0.98	1.58E-02	3.82E-02
Sell	2.37	8.24E-05	6.21E-04	Tlr9	0.84	1.68E-03	7.11E-03
Serping1	0.48	4.78E-02	9.39E-02	Tmem173	0.58	1.38E-02	3.48E-02
Socs3	1.23	2.70E-04	1.60E-03	Tnf	3.05	1.69E-05	1.75E-04
Stat1	0.88	6.39E-05	5.52E-04	Tnfaip3	0.70	7.83E-05	6.10E-04
Stat2	1.23	9.84E-05	6.87E-04	Tnfrsf11a	0.94	3.33E-04	1.91E-03
Stat3	0.72	8.62E-07	1.64E-05	Tnfrsf13b	0.57	2.66E-02	5.68E-02
Stat5a	0.56	1.81E-03	7.62E-03	Tnfrsf14	0.64	1.36E-02	3.43E-02
Stat5b	0.45	2.11E-02	4.90E-02	Tnfrsf1b	0.82	1.60E-02	3.85E-02
Syk	0.85	3.45E-03	1.23E-02	Tnfrsf4	0.57	5.95E-04	3.14E-03
Tagap	1.06	1.96E-02	4.60E-02	Tnfsf10	0.61	3.54E-02	7.38E-02
Tap1	0.62	5.64E-04	3.01E-03	Tnfsf12	0.64	3.59E-02	7.45E-02
Tapbp	0.49	3.38E-03	1.22E-02	Tnfsf14	1.25	3.40E-03	1.22E-02
Tcf7	-0.78	7.83E-03	2.34E-02	Trem1	26.00	4.78E-06	6.88E-05
Tgfb1	0.55	8.84E-03	2.54E-02	Tslp	2.40	1.18E-04	7.78E-04
Tgfbi	0.92	7.51E-04	3.84E-03	Tyrobp	0.79	2.86E-02	6.08E-02
Tgfbr2	0.72	3.68E-03	1.29E-02	Vcam1	0.82	1.23E-02	3.20E-02
Thy1	0.52	9.89E-04	4.52E-03	Xcr1	21.82	4.07E-02	8.26E-02
Tirap	0.44	1.45E-03	6.26E-03	Zeb1	0.55	1.13E-02	2.97E-02

Table S4: Differential expression of mast cell deficient to engrafted samples

Gene	logFC	pvalue	qvalue
Bcl3	0.76	1.03E-02	1.13E-01
Blnk	-0.56	1.26E-02	1.27E-01
Ccl2	1.44	2.62E-03	4.15E-02
Ccl4	1.77	4.03E-02	2.42E-01
Ccl7	1.47	1.37E-03	2.84E-02
Ccr9	0.72	1.71E-02	1.38E-01
Cd24a	0.65	8.09E-03	9.61E-02
Cd44	0.53	3.45E-04	1.14E-02
Cd69	2.96	9.38E-03	1.09E-01
Cd79b	-0.98	3.71E-02	2.32E-01
Cd82	-0.54	3.53E-04	1.14E-02
Cd83	-1.04	1.94E-02	1.44E-01
Cd86	-0.49	4.46E-02	2.60E-01
Cebpb	0.43	3.99E-03	5.59E-02
Cx3cr1	-1.14	3.85E-03	5.59E-02
Cxcl1	5.59	4.72E-04	1.32E-02
Cxcl3	37.92	1.61E-06	2.55E-04
Cxcl9	-1.57	1.31E-02	1.27E-01
Cxcr2	3.98	2.43E-03	3.98E-02
Cybb	-1.07	2.20E-03	3.77E-02
Defb14	2.24	5.68E-04	1.50E-02
Ebi3	-1.32	2.32E-05	1.38E-03
Emr1	-0.89	2.61E-02	1.85E-01
Fcamr	0.82	1.29E-02	1.27E-01
Fcer1a	-5.07	2.06E-07	4.90E-05
H2-Aa	-1.08	1.70E-02	1.38E-01
H2-Ab1	-0.95	2.83E-02	1.98E-01
H2-DMa	-0.90	3.88E-02	2.36E-01
H2-Eb1	-1.02	2.39E-02	1.72E-01
Hif1a	0.60	3.43E-04	1.14E-02
Ifitm1	1.16	8.03E-03	9.61E-02
Il10ra	-0.64	3.26E-02	2.21E-01
Il12rb2	-0.97	3.77E-02	2.33E-01
Il16	-0.72	3.77E-03	5.59E-02
Il1a	0.69	2.15E-02	1.57E-01
Il1b	3.01	3.34E-06	3.97E-04
Il1rl1	2.12	3.88E-05	2.05E-03
Il1rl2	0.44	6.85E-04	1.63E-02
Il33	1.27	6.34E-05	3.01E-03
Il4ra	0.77	9.36E-04	2.12E-02
Il6	3.76	2.22E-05	1.38E-03
Il9	3.30	1.70E-02	1.38E-01
Irf8	-0.61	4.74E-02	2.67E-01
Itga5	0.57	1.50E-02	1.37E-01
Itga6	0.51	1.26E-02	1.27E-01
Ltb4r2	0.80	2.22E-03	3.77E-02
Ly86	-0.87	1.63E-02	1.38E-01
Marco	-4.70	1.53E-02	1.37E-01
Masp1	0.92	4.12E-03	5.59E-02
Muc1	2.75	6.46E-04	1.61E-02
Nos2	0.80	3.72E-02	2.32E-01
Pou2f2	-0.81	4.09E-04	1.21E-02
Pparg	-0.59	1.36E-02	1.30E-01
Ppbp	3.53	1.36E-03	2.84E-02
Ptgs2	2.99	4.81E-06	4.57E-04
Ptpn6	-0.42	1.18E-02	1.24E-01
Rorc	-0.60	4.28E-02	2.54E-01
S100a8	3.87	1.01E-05	7.97E-04
S100a9	4.71	1.81E-07	4.90E-05
Sele	2.43	1.33E-04	5.74E-03
Sell	1.16	4.49E-02	2.60E-01
Slamf7	-0.98	6.70E-03	8.37E-02
Socs3	0.97	4.02E-03	5.59E-02
Spn	-1.10	5.78E-03	7.63E-02
Tagap	-1.13	1.05E-02	1.13E-01
Tgfbr1	-0.41	1.85E-03	3.54E-02
Tlr2	-0.59	4.62E-02	2.65E-01
Tlr9	-0.72	6.64E-03	8.37E-02
Tnf	1.53	1.89E-02	1.44E-01
Trem1	4.76	2.16E-03	3.77E-02
Trp53	0.42	9.81E-03	1.11E-01

Table S5: Differential expression of mast cell engrafted to wild-type samples

Gene	logFC	pvalue	qvalue
Ahr	0.75	1.35E-03	4.99E-03
Arhgdib	0.96	1.29E-05	1.43E-04
B2m	0.97	6.04E-07	1.44E-05
Batf	1.14	1.45E-04	8.85E-04
Bcl6	0.71	1.19E-05	1.34E-04
Bid	0.60	2.87E-04	1.47E-03
Blnk	0.84	1.87E-04	1.06E-03
Bst1	1.26	5.37E-04	2.41E-03
Bst2	1.22	3.87E-09	3.67E-07
Btk	1.06	1.04E-03	4.13E-03
C1qa	1.30	1.11E-04	6.96E-04
C1qb	1.40	5.74E-05	4.07E-04
C1ra	0.80	1.62E-03	5.58E-03
C1s	0.96	1.98E-04	1.09E-03
C2	0.77	6.26E-03	1.57E-02
C3	1.20	2.74E-02	5.42E-02
C4a	0.68	3.14E-02	6.05E-02
Card9	0.93	1.58E-04	9.24E-04
Casp1	0.61	3.68E-07	9.20E-06
Casp8	0.42	7.14E-04	3.03E-03
Ccbp2	1.95	3.41E-04	1.69E-03
Ccl12	0.94	1.90E-02	4.01E-02
Ccl20	1.42	7.00E-03	1.73E-02
Ccl3	2.00	2.09E-04	1.14E-03
Ccl4	2.87	2.44E-03	7.60E-03
Ccl5	1.18	2.70E-02	5.37E-02
Ccl6	1.21	1.82E-02	3.90E-02
Ccr2	1.08	1.52E-03	5.33E-03
Ccr6	22.53	3.53E-02	6.69E-02
Ccrl1	0.75	8.54E-03	2.03E-02
Ccrl2	2.33	5.85E-06	7.51E-05
Cd109	0.47	2.58E-03	7.72E-03
Cd14	1.50	6.01E-05	4.20E-04
Cd22	0.93	4.89E-03	1.30E-02
Cd226	1.16	2.97E-02	5.78E-02
Cd244	0.90	8.51E-03	2.03E-02
Cd274	1.04	2.47E-03	7.61E-03
Cd36	1.03	3.49E-03	9.86E-03
Cd3e	1.13	3.61E-02	6.81E-02
Cd4	0.81	1.74E-02	3.78E-02
Cd40	0.68	2.33E-02	4.79E-02
Cd48	1.07	1.90E-03	6.36E-03
Cd53	0.99	2.13E-02	4.45E-02
Cd7	0.76	3.51E-02	6.66E-02
Cd74	1.32	4.82E-03	1.29E-02
Cd79b	1.77	2.37E-04	1.26E-03
Cd80	0.92	2.50E-04	1.31E-03
Cd83	1.18	8.00E-03	1.92E-02
Cd86	1.23	8.76E-07	1.73E-05
Cd97	0.77	7.04E-03	1.73E-02
Ceacam1	0.64	1.85E-02	3.95E-02
Cfb	0.99	1.11E-05	1.32E-04
Cfd	1.34	7.71E-03	1.86E-02
Cfh	1.03	1.84E-03	6.23E-03
Cfp	1.07	4.07E-03	1.12E-02
Ciita	1.03	1.31E-02	2.98E-02
Clec4a4	21.92	2.69E-02	5.37E-02
Clec4e	2.07	2.26E-02	4.67E-02
Clec5a	1.11	6.89E-04	2.95E-03
Cmklr1	1.03	1.50E-05	1.62E-04
Crlf2	1.13	4.18E-04	1.97E-03
Csf1	0.96	3.24E-06	4.53E-05
Csf1r	1.18	2.55E-04	1.32E-03
Csf2rb	0.90	6.23E-03	1.57E-02
Csf3r	0.96	1.29E-03	4.90E-03
Ctnnb1	-0.49	1.16E-03	4.51E-03
Ctsc	0.51	3.65E-04	1.77E-03
Ctss	1.53	2.09E-03	6.85E-03
Cul9	0.64	5.70E-03	1.46E-02
Cx3cr1	1.88	4.11E-06	5.57E-05
Cxcl12	0.66	3.60E-05	2.94E-04
Cxcl13	2.97	4.41E-04	2.05E-03
Cxcl9	1.79	4.95E-03	1.30E-02
Cxcr2	21.72	6.11E-15	1.45E-12
Cxcr3	0.86	6.54E-03	1.64E-02
Cxcr4	0.74	2.45E-03	7.60E-03
Cybb	1.70	1.61E-06	2.73E-05
Ddx58	0.66	1.05E-07	4.15E-06
Ebi3	1.74	3.90E-08	1.85E-06
Emr1	1.69	3.24E-05	2.78E-04
Entpd1	1.21	1.46E-07	4.97E-06
Fas	0.66	4.75E-03	1.29E-02
Fcamr	-0.92	4.79E-03	1.29E-02
Fcer1g	1.32	3.25E-05	2.78E-04
Fcgr1	1.73	2.54E-08	1.34E-06

Fcgr2b	1.22	2.87E-03	8.36E-03
Fcgr3	1.41	5.37E-04	2.41E-03
Fcgr4	1.83	1.09E-04	6.92E-04
Fcgrt	0.95	1.62E-03	5.58E-03
Fkbp5	1.11	1.51E-03	5.33E-03
Gm10499	0.86	5.42E-05	3.90E-04
Gpi1	0.55	3.81E-02	7.15E-02
Gpr183	1.03	2.58E-03	7.72E-03
H2-Aa	1.47	1.38E-03	5.00E-03
H2-Ab1	1.30	2.96E-03	8.51E-03
H2-DMa	1.42	1.34E-03	4.99E-03
H2-DMb2	1.35	1.22E-02	2.80E-02
H2-Eb1	1.25	5.70E-03	1.46E-02
H2-K1	0.77	7.08E-07	1.53E-05
H2-Q10	2.53	1.89E-03	6.36E-03
Hamp	27.04	1.41E-03	5.07E-03
Hcst	1.39	1.45E-02	3.24E-02
Hfe	0.91	6.13E-03	1.56E-02
Hlx	0.61	1.50E-02	3.34E-02
Icam1	0.56	1.44E-03	5.16E-03
Ifi204	1.42	2.72E-06	4.04E-05
Ifi35	0.61	3.27E-05	2.78E-04
Ifih1	0.86	3.38E-07	8.91E-06
Ifit2	1.49	1.11E-06	1.95E-05
Ifnar1	0.48	8.88E-07	1.73E-05
Ifnar2	1.00	3.23E-06	4.53E-05
Ifngr1	1.17	2.94E-05	2.69E-04
Ifngr2	0.58	1.08E-04	6.92E-04
Ikbke	0.93	9.59E-07	1.75E-05
Ikzf1	1.06	4.79E-03	1.29E-02
Ikzf2	0.90	2.49E-03	7.64E-03
Il10	22.84	4.16E-02	7.65E-02
Il10ra	1.36	8.63E-06	1.08E-04
Il10rb	1.03	5.22E-05	3.87E-04
Il12rb2	0.98	3.47E-02	6.62E-02
Il13ra1	0.63	1.25E-03	4.78E-03
Il15	0.66	1.58E-02	3.50E-02
Il15ra	0.72	2.81E-03	8.24E-03
Il16	1.33	1.42E-07	4.97E-06
Il17ra	0.51	6.30E-04	2.77E-03
Il18r1	1.16	3.34E-04	1.67E-03
Il1r2	0.66	2.13E-02	4.45E-02
Il22ra2	2.10	8.72E-04	3.54E-03
Il2rg	0.83	2.43E-03	7.60E-03

Il33	1.02	1.35E-03	4.99E-03
Il4ra	0.55	1.90E-02	4.01E-02
Il6ra	1.12	4.91E-05	3.70E-04
Il7r	1.37	5.34E-03	1.38E-02
Il9	-3.34	1.35E-02	3.06E-02
Irak2	0.69	1.52E-08	1.03E-06
Irak3	1.07	3.07E-07	8.57E-06
Irak4	0.62	3.73E-04	1.77E-03
Irf1	0.83	3.40E-05	2.83E-04
Irf3	-0.55	3.38E-02	6.51E-02
Irf5	1.03	2.80E-05	2.66E-04
Irf7	1.29	6.54E-04	2.85E-03
Irf8	1.48	2.48E-06	3.80E-05
Irgm1	1.29	2.06E-08	1.22E-06
Itga4	1.27	2.78E-07	8.24E-06
Itgal	0.95	1.52E-04	9.16E-04
Itgam	1.25	2.33E-03	7.41E-03
Itgb1	0.41	1.52E-03	5.33E-03
Itgb2	1.22	3.18E-03	9.09E-03
Jak1	0.70	4.63E-06	6.10E-05
Jak2	0.47	1.13E-03	4.45E-03
Jak3	0.53	3.95E-02	7.30E-02
Kir3dl1	3.14	3.45E-02	6.60E-02
Kit	-5.72	0.00E+00	0.00E+00
Klra8	1.16	2.62E-02	5.30E-02
Klrc1	1.32	1.08E-02	2.52E-02
Klrc2	-2.83	6.70E-03	1.67E-02
Klrd1	0.97	2.23E-02	4.62E-02
Klrk1	1.03	7.13E-03	1.75E-02
Lair1	1.52	1.33E-03	4.99E-03
Lcp2	1.43	5.96E-04	2.64E-03
Lilra5	1.07	2.86E-02	5.64E-02
Lilrb3	1.26	5.39E-05	3.90E-04
Lilrb4	1.49	8.73E-05	5.91E-04
Litaf	0.75	1.00E-04	6.62E-04
Ltb	1.00	2.76E-03	8.16E-03
Ly86	1.49	4.55E-05	3.54E-04
Ly96	0.87	9.10E-07	1.73E-05
Map4k1	1.19	1.82E-02	3.90E-02
Mapkapk2	0.41	1.59E-05	1.68E-04
Mbp	1.74	8.64E-04	3.54E-03
Msr1	1.40	1.01E-03	4.06E-03
Mx1	0.59	3.82E-02	7.15E-02
Myd88	0.58	1.94E-04	1.08E-03

Ncf4	1.15	1.36E-03	4.99E-03
Nfatc1	0.68	2.23E-04	1.20E-03
Nfatc2	0.91	1.95E-06	3.10E-05
Nfkb1	0.46	2.94E-05	2.69E-04
Nfkbia	0.78	6.36E-05	4.38E-04
Nfkbiz	0.78	1.66E-05	1.72E-04
Nod2	1.07	2.76E-03	8.16E-03
Nos2	-0.86	2.34E-02	4.79E-02
Notch1	-0.59	1.15E-02	2.68E-02
Nox4	1.06	3.32E-03	9.43E-03
Pdgfb	0.61	1.92E-03	6.36E-03
Pla2g2e	-1.13	2.08E-02	4.37E-02
Plau	0.65	2.95E-02	5.76E-02
Pml	0.52	3.58E-04	1.75E-03
Pou2f2	1.52	7.36E-11	8.74E-09
Pparg	0.82	5.33E-04	2.41E-03
Ppbp	22.51	4.02E-03	1.12E-02
Prdm1	-0.59	1.31E-02	2.98E-02
Prkcd	0.65	7.24E-04	3.04E-03
Psmb10	0.95	1.61E-04	9.30E-04
Psmb9	0.93	8.84E-05	5.91E-04
Ptafr	1.39	1.86E-05	1.88E-04
Ptpn22	1.44	1.77E-04	1.01E-03
Ptpn6	1.16	4.39E-12	6.95E-10
Ptprc	1.13	4.73E-04	2.18E-03
Rela	0.43	2.41E-04	1.27E-03
Relb	0.71	3.00E-05	2.69E-04
Rorc	0.79	7.35E-03	1.79E-02
Sell	1.21	3.84E-02	7.16E-02
Serping1	0.54	2.65E-02	5.33E-02
Slamf7	1.63	9.36E-06	1.14E-04
Spn	1.36	6.69E-04	2.89E-03
Stat1	0.97	1.15E-05	1.33E-04
Stat2	0.83	9.20E-03	2.17E-02
Stat3	0.42	4.56E-03	1.25E-02
Stat5a	0.43	1.82E-02	3.90E-02
Stat5b	0.61	1.98E-03	6.53E-03
Stat6	0.49	4.78E-05	3.66E-04
Syk	0.98	7.92E-04	3.30E-03
Tagap	2.19	1.96E-06	3.10E-05
Tap1	0.90	6.48E-07	1.47E-05
Tapbp	0.70	3.66E-05	2.94E-04
Tbk1	0.44	2.15E-03	6.96E-03
Tcf7	-0.89	2.56E-03	7.72E-03
Tgfb1	0.81	1.36E-04	8.38E-04
Tgfbi	0.98	3.71E-04	1.77E-03
Tgfbr1	0.56	2.08E-05	2.06E-04
Tgfbr2	0.75	2.43E-03	7.60E-03
Tlr1	1.31	3.73E-05	2.95E-04
Tlr2	1.64	6.61E-08	2.85E-06
Tlr3	0.47	1.17E-02	2.71E-02
Tlr4	0.98	2.53E-03	7.69E-03
Tlr8	1.34	1.10E-03	4.35E-03
Tlr9	1.56	8.49E-09	6.72E-07
Tnf	1.52	3.87E-02	7.18E-02
Tnfaip3	0.75	2.57E-05	2.50E-04
Tnfrsf11a	1.38	1.85E-07	5.86E-06
Tnfrsf13b	0.77	2.89E-03	8.38E-03
Tnfrsf14	0.99	1.56E-04	9.24E-04
Tnfrsf1b	1.07	1.67E-03	5.71E-03
Tnfsf12	1.20	1.06E-04	6.87E-04
Tnfsf13b	1.04	3.02E-02	5.86E-02
Tnfsf14	0.87	4.31E-02	7.90E-02
Trem1	21.24	2.95E-02	5.76E-02
Trem2	1.48	3.77E-03	1.05E-02
Trp53	-0.53	1.22E-03	4.72E-03
Tslp	1.80	5.05E-03	1.32E-02
Tyrobp	1.31	3.03E-04	1.53E-03
Vcam1	1.10	8.05E-04	3.33E-03
Xcr1	22.61	1.39E-02	3.13E-02
Zeb1	0.64	3.57E-03	1.00E-02

Table S6: KEGG Pathway Enrichment between mast cell deficient to other group samples

ID	Description	pvalue	qvalue	Gene ID	Count
mmu04668	TNF signaling pathway	2.66E-04	2.53E-02	Bcl3, Ccl2, Ccl20, Cxcl1, Cxcl10, Cxcl3, Il1b, Il6, Nod2, Ptgs2, Sele, Socs3, Tnf	13
mmu04657	IL-17 signaling pathway	1.37E-03	6.51E-02	Ccl2, Ccl20, Ccl7, Cxcl1, Cxcl10, Cxcl3, Il1b, Il6, Ptgs2, S100a8, S100a9, Tnf	12
mmu04621	NOD-like receptor signaling pathway	9.57E-03	1.83E-01	Ccl2, Cxcl1, Cxcl3, Defb14, Ifi204, Il1b, Il6, Irf7, Nod2, Stat2, Tnf	11
mmu04061	Viral protein interaction with cytokine and cytokine receptor	1.05E-02	1.83E-01	Ccl2, Ccl20, Ccl3, Ccl4, Ccl7, Cxcl1, Cxcl10, Cxcl3, Cxcr2, Il10, Il6, Ppbp, Tnf	13
mmu04623	Cytosolic DNA-sensing pathway	1.88E-02	2.23E-01	Ccl4, Cxcl10, Il1b, Il33, Il6, Irf7	6
mmu04062	Chemokine signaling pathway	3.26E-02	3.21E-01	Ccl2, Ccl20, Ccl3, Ccl4, Ccl7, Cxcl1, Cxcl10, Cxcl3, Cxcr2, Ppbp, Stat2	11
mmu04625	C-type lectin receptor signaling pathway	3.72E-02	3.21E-01	Bcl3, Clec4e, Il10, Il1b, Il6, Ptgs2, Stat2, Tnf	8
mmu04640	Hematopoietic cell lineage	4.92E-02	3.43E-01	Cd24a, Csf3r, Fcgr1, Il1a, Il1b, Il4ra, Il6, Itga5, Itga6, Tnf	10
mmu04060	Cytokine-cytokine receptor interaction	5.01E-02	3.43E-01	Ccl2, Ccl20, Ccl3, Ccl4, Ccl7, Csf3r, Cxcl1, Cxcl10, Cxcl3, Cxcr2, Il10, Il13ra1, Il1a, Il1b, Il1rl1, Il33, Il4ra, Il6, Ppbp, Tnf, Tslp	21

Table S7: KEGG Pathway Enrichment between mast cell deficient to wild-type

ID	Description	pvalue	qvalue	Gene ID	Count
mmu04620	Toll-like receptor signaling pathway	4.70E-03	1.35E-01	Casp8, Ccl3, Ccl4, Cd14, Cd80, Cd86, Cxcl10, Ifnar2, Ikbke, Il1b, Il6, Irak4, Irf5, Irf7, Ly96, Myd88, Stat1, Tlr1, Tlr2, Tlr4, Tlr5, Tlr8, Tlr9, Tnf	24
mmu04621	NOD-like receptor signaling pathway	1.82E-02	2.31E-01	Card9, Casp8, Ccl12, Ccl2, Cxcl1, Cxcl3, Defb14, Ifi204, Ifnar2, Ikbke, Il1b, Il6, Irak4, Irf7, Jak1, Myd88, Nod2, Stat1, Stat2, Tlr4, Tnf, Tnfaip3	22
mmu04061	Viral protein interaction with cytokine and cytokine receptor	1.99E-02	2.31E-01	Ccl12, Ccl2, Ccl20, Ccl3, Ccl4, Ccl6, Ccl7, Ccl9, Ccr5, Csf1, Cxcl1, Cxcl10, Cxcl13, Cxcl3, Cxcr2, Il10, Il10ra, Il10rb, Il18rap, Il2rg, Il6, Il6ra, Ppbp, Tnf, Tnfrsf14, Tnfrsf1b, Tnfsf14	27
mmu04668	TNF signaling pathway	2.21E-02	2.31E-01	Bcl3, Casp8, Ccl12, Ccl2, Ccl20, Csf1, Cxcl1, Cxcl10, Cxcl3, Fas, Il1b, Il6, Nod2, Ptgs2, Sele, Socs3, Tnf, Tnfaip3, Tnfrsf1b, Vcam1	20
mmu04217	Necroptosis	3.37E-02	2.58E-01	Bid, Casp8, Fas, Fasl, Ifnar2, Ifngr1, Il1a, Il1b, Il33, Jak1, Jak3, Stat1, Stat2, Stat3, Tlr4, Tnf, Tnfaip3	17

Table S8: KEGG Pathway Enrichment between mast cell deficient to engrafted

ID	Description	pvalue	qvalue	Gene ID	Count
mmu04657	IL-17 signaling pathway	7.07E-05	5.09E-03	Ccl2, Ccl7, Cxcl1, Cxcl3, Il1b, Il6, Ptgs2, S100a8, S100a9	9
mmu04668	TNF signaling pathway	2.59E-03	9.32E-02	Ccl2, Cxcl1, Cxcl3, Il1b, Il6, Ptgs2, Sele	7
mmu04621	NOD-like receptor signaling pathway	4.83E-03	1.16E-01	Ccl2, Cxcl1, Cxcl3, Cybb, Defb14, Il1b, Il6	7
mmu04060	Cytokine-cytokine receptor interaction	1.49E-02	2.13E-01	Ccl2, Ccl7, Cxcl1, Cxcl3, Cxcr2, Ebi3, Il1b, Il1rl1, Il33, Il4ra, Il6, Ppbp	12
mmu04061	Viral protein interaction with cytokine and cytokine receptor	2.07E-02	2.13E-01	Ccl2, Ccl7, Cxcl1, Cxcl3, Cxcr2, Il6, Ppbp	7
mmu04066	HIF-1 signaling pathway	4.31E-02	2.58E-01	Cybb, Hif1a, Il6	3
mmu04062	Chemokine signaling pathway	4.35E-02	2.58E-01	Ccl2, Ccl7, Cxcl1, Cxcl3, Cxcr2, Ppbp	6

Table S9: KEGG Pathway Enrichment between mast cell engrafted to wild-type

ID	Description	pvalue	qvalue	Gene ID	Count
mmu04145	Phagosome	3.34E-06	3.91E-04	C1ra, Cd14, Cd36, Ctss, Cybb, Fcgr1, Fcgr2b, Fcgr3, Fcgr4, Gm10499, H2-Aa, H2-Ab1, H2-DMa, H2-DMb2, H2-Eb1, H2-K1, H2-Q10, Itgam, Itgb2, Msr1, Ncf4, Tap1, Tlr2, Tlr4	24
mmu04612	Antigen processing and presentation	1.95E-04	1.14E-02	B2m, Cd4, Cd74, Ciita, Ctss, Gm10499, H2-Aa, H2-Ab1, H2-DMa, H2-DMb2, H2-Eb1, H2-K1, H2-Q10, Klrc1, Klrd1, Tap1, Tapbp	17
mmu04380	Osteoclast differentiation	3.06E-02	4.68E-01	Blnk, Btk, Csf1, Csf1r, Fcgr1, Fcgr2b, Fcgr3, Fcgr4, Ifnar2, Ifngr1, Jak1, Lcp2, Ncf4, Nfatc1, Nfatc2, Nfkbia, Pparg, Relb, Stat1, Stat2, Syk, Tgfb1, Tgfbr2, Tnfrsf11a, Trem2, Tyrobp	26

Table S10: Non-reduced enriched GO Terms between deficient and other groups

ID	Description	pvalue	qvalue	Gene ID	Count
GO:0030593	neutrophil chemotaxis	5.50E-08	7.18E-05	Bst1, Ccl2, Ccl20, Ccl3, Ccl4, Ccl7, Csf3r, Cxcl1, Cxcl10, Cxcl3, Cxcr2, Il1b, Nod2, Ppbp, S100a8, S100a9, Sell, Trem1	18
GO:1990266	neutrophil migration	9.51E-08	7.18E-05	Bst1, Ccl2, Ccl20, Ccl3, Ccl4, Ccl7, Csf3r, Cxcl1, Cxcl10, Cxcl3, Cxcr2, Il1a, Il1b, Nod2, Ppbp, S100a8, S100a9, Sell, Trem1	19
GO:0071621	granulocyte chemotaxis	2.04E-06	1.03E-03	Bst1, Ccl2, Ccl20, Ccl3, Ccl4, Ccl7, Csf3r, Cxcl1, Cxcl10, Cxcl3, Cxcr2, Il1b, Nod2, Ppbp, S100a8, S100a9, Sell, Trem1	18
GO:0097530	granulocyte migration	3.27E-06	1.24E-03	Bst1, Ccl2, Ccl20, Ccl3, Ccl4, Ccl7, Csf3r, Cxcl1, Cxcl10, Cxcl3, Cxcr2, Il1a, Il1b, Nod2, Ppbp, S100a8, S100a9, Sell, Trem1	19
GO:0006954	inflammatory response	8.85E-06	2.68E-03	Bst1, Ccl2, Ccl20, Ccl3, Ccl4, Ccl7, Cd24a, Cxcl1, Cxcl10, Cxcl3, Cxcr2, Fcer1a, Fcgr1, Hamp, Il10, Il1a, Il1b, Il1rl1, Il33, Il4ra, Il6, Ltb4r1, Ltb4r2, Nod2, Ppbp, Ptgs2, S100a8, S100a9, Sele, Socs3, Tnf, Trem1, Tslp	33
GO:0050900	leukocyte migration	2.76E-05	6.95E-03	Bst1, Ccl2, Ccl20, Ccl3, Ccl4, Ccl7, Cd24a, Csf3r, Cxcl1, Cxcl10, Cxcl3, Cxcr2, Il1a, Il1b, Il33, Itga6, Nod2, Ppbp, S100a8, S100a9, Sele, Sell, Tnf, Trem1	24
GO:0006952	defense response	5.68E-05	1.11E-02	Bcl3, Bst1, Ccl2, Ccl20, Ccl3, Ccl4, Ccl7, Cd24a, Cfb, Clec4e, Cxcl1, Cxcl10, Cxcl3, Cxcr2, Defb14, Fcer1a, Fcgr1, Hamp, Ifi204, Ifit2, Ifitm1, Il10, Il1a, Il1b, Il1rl1, Il33, Il4ra, Il6, Irf7, Ltb4r1, Ltb4r2, Masp1, Nod2, Ppbp, Ptgs2, S100a8, S100a9, Sele, Socs3, Stat2, Tnf, Trem1, Tslp	43
GO:0097529	myeloid leukocyte migration	5.90E-05	1.11E-02	Bst1, Ccl2, Ccl20, Ccl3, Ccl4, Ccl7, Csf3r, Cxcl1, Cxcl10, Cxcl3, Cxcr2, Il1a, Il1b, Nod2, Ppbp, S100a8, S100a9, Sell, Trem1	19
GO:0030595	leukocyte chemotaxis	8.77E-05	1.47E-02	Bst1, Ccl2, Ccl20, Ccl3, Ccl4, Ccl7, Csf3r, Cxcl1, Cxcl10, Cxcl3, Cxcr2, Il1b, Nod2, Ppbp, S100a8, S100a9, Sell, Trem1	18
GO:0019730	antimicrobial humoral response	1.23E-04	1.86E-02	Bcl3, Ccl2, Ccl20, Cxcl1, Cxcl10, Cxcl3, Nod2, Ppbp, S100a9, Tslp	10
GO:0032103	positive regulation of response to external stimulus	2.10E-04	2.75E-02	Ccl2, Ccl3, Ccl4, Cd24a, Cxcl1, Cxcl10, Cxcr2, Fcer1a, Fcgr1, Ifi204, Il1b, Il1rl1, Il33, Il6, Irf7, Nod2, Ptgs2, S100a8, S100a9, Sell, Tnf, Tslp	22
GO:0010573	vascular endothelial growth factor production	2.18E-04	2.75E-02	Ccl2, Il1a, Il1b, Il6, Ptgs2, Tnf	6
GO:0060326	cell chemotaxis	3.44E-04	3.77E-02	Bst1, Ccl2, Ccl20, Ccl3, Ccl4, Ccl7, Csf3r, Cxcl1, Cxcl10, Cxcl3, Cxcr2, Defb14, Il1b, Nod2, Ppbp, S100a8, S100a9, Sell, Trem1	19
GO:0050729	positive regulation of inflammatory response	3.76E-04	3.77E-02	Ccl3, Cd24a, Fcer1a, Fcgr1, Il1b, Il1rl1, Il33, Il6, Nod2, Ptgs2, S100a8, S100a9, Tnf, Tslp	14

GO:0061844	antimicrobial humoral immune response mediated by antimicrobial peptide	3.76E-04	3.77E-02	Ccl2, Ccl20, Cxcl1, Cxcl10, Cxcl3, Nod2, Ppbp, S100a9, Tslp	9
GO:0009617	response to bacterium	4.04E-04	3.77E-02	Bcl3, Ccl2, Cd24a, Cd80, Clec4e, Cxcl1, Cxcl10, Cxcl3, Defb14, Fcgr1, Hamp, Ifi204, Il10, Il1a, Il1b, Il6, Nod2, Ppbp, Ptgs2, S100a8, S100a9, Tnf, Trem1, Tslp	24
GO:0002526	acute inflammatory response	4.42E-04	3.77E-02	Cxcl1, Cxcr2, Fcer1a, Fcgr1, Il1a, Il1b, Il6, Ptgs2, Tnf, Trem1	10
GO:0031349	positive regulation of defense response	4.64E-04	3.77E-02	Ccl3, Cd24a, Cxcl1, Fcer1a, Fcgr1, Ifi204, Il1b, Il1rl1, Il33, Il6, Irf7, Nod2, Ptgs2, S100a8, S100a9, Tnf, Tslp	17
GO:0009605	response to external stimulus	4.74E-04	3.77E-02	Bcl3, Bst1, Ccl2, Ccl20, Ccl3, Ccl4, Ccl7, Cd24a, Cd80, Cfb, Clec4e, Csf3r, Cxcl1, Cxcl10, Cxcl3, Cxcr2, Defb14, Fcer1a, Fcgr1, Hamp, Ifi204, Ifit2, Ifitm1, Il10, Il1a, Il1b, Il1rl1, Il33, Il4ra, Il6, Irf7, Itga6, Masp1, Nod2, Ppbp, Ptgs2, S100a8, S100a9, Sell, Socs3, Stat2, Tnf, Trem1, Tslp	44

Table S11: Non-reduced enriched GO Terms between deficient and wild-type

ID	Description	pvalue	qvalue	Gene ID	Count
GO:0009607	response to biotic stimulus	1.05E-05	5.57E-03	B2m, Batf, Bcl3, Bid, Bst2, Btk, C1qa, C1qb, C1ra, C3, Card9, Ccl12, Ccl2, Ccl20, Ccl3, Ccl4, Ccl6, Ccl7, Ccl9, Cd14, Cd274, Cd80, Cd86, Ceacam1, Cfb, Cfh, Cfp, Clec4e, Clec5a, Csf1, Cxcl1, Cxcl10, Cxcl13, Cxcl3, Ddx58, Defb14, Fcer1g, Fcgr1, Fcgr4, Fkbp5, Hamp, Ifi204, Ifih1, Ifit2, Ifitm1, Ifnar2, Ifngr1, Ikbke, Il10, Il10rb, Il18rap, Il1a, Il1b, Il33, Il4ra, Il6, Irak3, Irak4, Irf5, Irf7, Irf8, Irgm1, Jak3, Ly96, Masp1, Myd88, Nod2, Pml, Pou2f2, Ppbp, Psmb9, Ptafr, Ptgs2, Ptpn22, Ptpn6, Ptprc, S100a8, S100a9, Stat1, Stat2, Syk, Tagap, Tap1, Tlr1, Tlr2, Tlr4, Tlr5, Tlr8, Tlr9, Tnf, Tnfaip3, Tnfrsf11a, Tnfrsf14, Tnfrsf1b, Trem1, Tslp	96
GO:0043207	response to external biotic stimulus	1.18E-05	5.57E-03	B2m, Batf, Bcl3, Bst2, Btk, C1qa, C1qb, C1ra, C3, Card9, Ccl12, Ccl2, Ccl20, Ccl3, Ccl4, Ccl6, Ccl7, Ccl9, Cd14, Cd274, Cd80, Cd86, Ceacam1, Cfb, Cfh, Cfp, Clec4e, Clec5a, Csf1, Cxcl1, Cxcl10, Cxcl13, Cxcl3, Ddx58, Defb14, Fcer1g, Fcgr1, Fcgr4, Fkbp5, Hamp, Ifi204, Ifih1, Ifit2, Ifitm1, Ifnar2, Ifngr1, Ikbke, Il10, Il10rb, Il18rap, Il1a, Il1b, Il33, Il4ra, Il6, Irak3, Irak4, Irf5, Irf7, Irf8, Irgm1, Jak3, Ly96, Masp1, Myd88, Nod2, Pml, Pou2f2, Ppbp, Psmb9, Ptafr, Ptgs2, Ptpn22, Ptpn6, Ptprc, S100a8, S100a9, Stat1, Stat2, Syk, Tagap, Tap1, Tlr1, Tlr2, Tlr4, Tlr5, Tlr8, Tlr9, Tnf, Tnfaip3, Tnfrsf11a, Tnfrsf14, Tnfrsf1b, Trem1, Tslp	95
GO:0051707	response to other organism	1.18E-05	5.57E-03	B2m, Batf, Bcl3, Bst2, Btk, C1qa, C1qb, C1ra, C3, Card9, Ccl12, Ccl2, Ccl20, Ccl3, Ccl4, Ccl6, Ccl7, Ccl9, Cd14, Cd274, Cd80, Cd86, Ceacam1, Cfb, Cfh, Cfp, Clec4e, Clec5a, Csf1, Cxcl1, Cxcl10, Cxcl13, Cxcl3, Ddx58, Defb14, Fcer1g, Fcgr1, Fcgr4, Fkbp5, Hamp, Ifi204, Ifih1, Ifit2, Ifitm1, Ifnar2, Ifngr1, Ikbke, Il10, Il10rb, Il18rap, Il1a, Il1b, Il33, Il4ra, Il6, Irak3, Irak4, Irf5, Irf7, Irf8, Irgm1, Jak3, Ly96, Masp1, Myd88, Nod2, Pml, Pou2f2, Ppbp, Psmb9, Ptafr, Ptgs2, Ptpn22, Ptpn6, Ptprc, S100a8, S100a9, Stat1, Stat2, Syk, Tagap, Tap1, Tlr1, Tlr2, Tlr4, Tlr5, Tlr8, Tlr9, Tnf, Tnfaip3, Tnfrsf11a, Tnfrsf14, Tnfrsf1b, Trem1, Tslp	95
GO:0032675	regulation of interleukin-6 production	1.40E-05	5.57E-03	Card9, Ccr5, Ddx58, Fcer1g, Ifih1, Il10, Il16, Il1a, Il1b, Il33, Il6, Il6ra, Irak3, Myd88, Nod2, Pou2f2, Ptafr, Ptpn22, Ptpn6, Stat3, Syk, Tlr1, Tlr2, Tlr4, Tlr8, Tlr9, Tnf, Tnfaip3, Tslp	29
GO:0032755	positive regulation of interleukin-6 production	1.63E-05	5.57E-03	Card9, Ccr5, Ddx58, Fcer1g, Ifih1, Il16, Il1a, Il1b, Il33, Il6, Il6ra, Myd88,	24

				Nod2, Pou2f2, Ptafr, Stat3, Syk, Tlr1, Tlr2, Tlr4, Tlr8, Tlr9, Tnf, Tslp	
GO:0098542	defense response to other organism	2.11E-05	6.01E-03	B2m, Batf, Bcl3, Bst2, Btk, C1qa, C1qb, C1ra, C3, Card9, Ccl12, Ccl2, Ccl20, Ccl3, Ccl4, Ccl6, Ccl7, Ccl9, Cd14, Cd86, Ceacam1, Cfb, Cfh, Cfp, Clec4e, Clec5a, Csf1, Cxcl1, Cxcl10, Cxcl13, Ddx58, Defb14, Fcer1g, Fcgr1, Hamp, Ifi204, Ifih1, Ifit2, Ifitm1, Ifnar2, Ifngr1, Ikbke, Il10, Il10rb, Il18rap, Il1b, Il33, Il4ra, Il6, Irak3, Irak4, Irf5, Irf7, Irf8, Irgm1, Jak3, Ly96, Masp1, Myd88, Nod2, Pml, Ptpn22, Ptpn6, Ptprc, S100a8, S100a9, Stat1, Stat2, Syk, Tagap, Tap1, Tlr1, Tlr2, Tlr4, Tlr5, Tlr8, Tlr9, Tnf, Tnfaip3, Tnfrsf14, Trem1, Tslp	82
GO:0032635	interleukin-6 production	2.88E-05	6.47E-03	Card9, Ccr5, Ddx58, Fcer1g, Ifih1, Il10, Il16, Il18rap, Il1a, Il1b, Il33, Il6, Il6ra, Irak3, Myd88, Nod2, Pou2f2, Ptafr, Ptpn22, Ptpn6, Stat3, Syk, Tlr1, Tlr2, Tlr4, Tlr8, Tlr9, Tnf, Tnfaip3, Tslp	30
GO:0044419	interspecies interaction between organisms	3.07E-05	6.47E-03	B2m, Batf, Bcl3, Bst2, Btk, C1qa, C1qb, C1ra, C3, Card9, Ccl12, Ccl2, Ccl20, Ccl3, Ccl4, Ccl6, Ccl7, Ccl9, Ccr5, Cd14, Cd274, Cd80, Cd86, Ceacam1, Cfb, Cfh, Cfp, Clec4e, Clec5a, Csf1, Cxcl1, Cxcl10, Cxcl13, Cxcl3, Ddx58, Defb14, Fcer1g, Fcgr1, Fcgr4, Fkbp5, Hamp, Ifi204, Ifih1, Ifit2, Ifitm1, Ifnar2, Ifngr1, Ikbke, Il10, Il10rb, Il18rap, Il1a, Il1b, Il33, Il4ra, Il6, Irak3, Irak4, Irf5, Irf7, Irf8, Irgm1, Jak3, Ly96, Masp1, Myd88, Nod2, Pml, Pou2f2, Ppbp, Psmb9, Ptafr, Ptgs2, Ptpn22, Ptpn6, Ptprc, S100a8, S100a9, Stat1, Stat2, Syk, Tagap, Tap1, Tlr1, Tlr2, Tlr4, Tlr5, Tlr8, Tlr9, Tnf, Tnfaip3, Tnfrsf11a, Tnfrsf14, Tnfrsf1b, Trem1, Tslp, Vcam1	97
GO:0009605	response to external stimulus	3.40E-05	6.47E-03	B2m, Batf, Bcl3, Bst1, Bst2, Btk, C1qa, C1qb, C1ra, C3, Card9, Ccl12, Ccl2, Ccl20, Ccl3, Ccl4, Ccl6, Ccl7, Ccl9, Ccr5, Ccrl2, Cd14, Cd274, Cd80, Cd86, Ceacam1, Cfb, Cfh, Cfp, Clec4e, Clec5a, Cmklr1, Csf1, Csf3r, Cxcl1, Cxcl10, Cxcl13, Cxcl3, Cxcr2, Ddx58, Defb14, Fas, Fcer1a, Fcer1g, Fcgr1, Fcgr4, Fkbp5, Hamp, Ifi204, Ifih1, Ifit2, Ifitm1, Ifnar2, Ifngr1, Ikbke, Il10, Il10rb, Il16, Il18rap, Il1a, Il1b, Il1rl1, Il33, Il4ra, Il6, Irak3, Irak4, Irf5, Irf7, Irf8, Irgm1, Itga4, Itga6, Itgam, Jak3, Kit, Ly96, Masp1, Myd88, Nfkbiz, Nod2, Plau, Pml, Pou2f2, Ppbp, Psmb9, Ptafr, Ptgs2, Ptpn22, Ptpn6, Ptprc, S100a8, S100a9, Sell, Socs3, Stat1, Stat2, Stat3, Syk, Tagap, Tap1, Tlr1, Tlr2, Tlr4, Tlr5, Tlr8, Tlr9, Tnf, Tnfaip3, Tnfrsf11a, Tnfrsf14, Tnfrsf1b, Tnfsf14, Trem1, Tslp, Vcam1	116

GO:0032677	regulation of interleukin-8 production	5.94E-05	1.02E-02	Bcl3, Cd14, Ddx58, Il1b, Il6, Myd88, Nod2, Ptpn22, Ptprc, Stat3, Syk, Tlr1, Tlr2, Tlr4, Tlr5, Tlr8, Tlr9, Tnf	18
GO:0051179	localization	6.88E-05	1.07E-02	Arhgdib, B2m, Bid, Bst1, Bst2, Btk, C3, Ccl12, Ccl2, Ccl20, Ccl3, Ccl4, Ccl6, Ccl7, Ccl9, Ccr5, Ccrl2, Cd14, Cd274, Ceacam1, Cfh, Clec4e, Clec5a, Cmklr1, Csf1, Csf3r, Cxcl1, Cxcl10, Cxcl13, Cxcl3, Cxcr2, Ddx58, Defb14, Entpd1, Fas, Fasl, Fcer1a, Fcer1g, Fcgr1, Hamp, Ifngr1, Ikbke, Ikzf1, Il10, Il10ra, Il15ra, Il16, Il1a, Il1b, Il2rg, Il33, Il4ra, Il6, Irak4, Irf8, Itga4, Itga5, Itga6, Itgal, Itgam, Jak3, Kit, Lcp2, Ltb4r2, Msr1, Mx1, Myd88, Ncf4, Nfatc1, Nod2, Nox4, Pecam1, Plau, Pml, Pou2f2, Ppbp, Ptafr, Ptgs2, Ptpn22, Ptpn6, Ptprc, S100a8, S100a9, Sele, Sell, Stat3, Syk, Tap1, Tgfbr2, Tlr1, Tlr2, Tlr4, Tlr5, Tlr8, Tlr9, Tnf, Tnfaip3, Tnfrsf11a, Tnfrsf14, Tnfrsf1b, Tnfsf14, Trem1, Vcam1	103
GO:1990266	neutrophil migration	9.46E-05	1.35E-02	Bst1, Ccl12, Ccl2, Ccl20, Ccl3, Ccl4, Ccl6, Ccl7, Ccl9, Csf3r, Cxcl1, Cxcl10, Cxcl13, Cxcl3, Cxcr2, Fcer1g, Il1a, Il1b, Irak4, Itgam, Myd88, Nod2, Pecam1, Ppbp, S100a8, S100a9, Sell, Syk, Trem1	29
GO:0006952	defense response	1.08E-04	1.43E-02	B2m, Batf, Bcl3, Bst1, Bst2, Btk, C1qa, C1qb, C1ra, C3, Card9, Ccl12, Ccl2, Ccl20, Ccl3, Ccl4, Ccl6, Ccl7, Ccl9, Ccr5, Ccrl2, Cd14, Cd86, Ceacam1, Cfb, Cfh, Cfp, Clec4e, Clec5a, Cmklr1, Csf1, Cxcl1, Cxcl10, Cxcl13, Cxcl3, Cxcr2, Ddx58, Defb14, Fcer1a, Fcer1g, Fcgr1, Hamp, Ifi204, Ifih1, Ifit2, Ifitm1, Ifnar2, Ifngr1, Ikbke, Il10, Il10rb, Il16, Il18rap, Il1a, Il1b, Il1rl1, Il33, Il4ra, Il6, Irak3, Irak4, Irf5, Irf7, Irf8, Irgm1, Itgam, Jak3, Kit, Ltb4r1, Ltb4r2, Ly96, Masp1, Myd88, Nfkbiz, Nod2, Nox4, Pml, Ppbp, Ptafr, Ptgs2, Ptpn22, Ptpn6, Ptprc, S100a8, S100a9, Sele, Socs3, Stat1, Stat2, Stat3, Syk, Tagap, Tap1, Tlr1, Tlr2, Tlr4, Tlr5, Tlr8, Tlr9, Tnf, Tnfaip3, Tnfrsf11a, Tnfrsf14, Tnfrsf1b, Trem1, Tslp	106
GO:0032637	interleukin-8 production	1.18E-04	1.44E-02	Bcl3, Cd14, Ddx58, Il1b, Il6, Myd88, Nod2, Ptpn22, Ptprc, Stat3, Syk, Tlr1, Tlr2, Tlr4, Tlr5, Tlr8, Tlr9, Tnf	18
GO:0002444	myeloid leukocyte mediated immunity	2.49E-04	2.85E-02	Btk, C3, Cxcl1, Ddx58, Fcer1a, Fcer1g, Fcgr1, Il4ra, Irak4, Itgam, Kit, Ptafr, Syk, Trem1	14
GO:0009617	response to bacterium	3.17E-04	3.23E-02	B2m, Bcl3, C3, Card9, Ccl12, Ccl2, Cd14, Cd274, Cd80, Cd86, Clec4e, Cxcl1, Cxcl10, Cxcl13, Cxcl3, Defb14, Fcer1g, Fcgr1, Fcgr4, Fkbp5, Hamp, Ifi204, Il10, Il1a, Il1b, Il6, Irak3, Irf5, Irf8, Irgm1, Ly96, Myd88, Nod2, Ppbp, Psmb9, Ptafr, Ptgs2, Ptpn22, S100a8, S100a9, Stat1, Syk, Tlr1, Tlr2, Tlr4,	54

				Tlr5, Tlr9, Tnf, Tnfaip3, Tnfrsf11a, Tnfrsf14, Tnfrsf1b, Trem1, Tslp	
GO:0002755	MyD88-dependent toll-like receptor signaling pathway	3.40E-04	3.23E-02	Irak3, Irf7, Myd88, Tlr1, Tlr2, Tlr4, Tlr5, Tlr8, Tlr9	9
GO:0051770	positive regulation of nitric-oxide synthase biosynthetic process	3.40E-04	3.23E-02	Ccl2, Ccl20, Il33, Jak3, Nod2, Stat1, Tlr2, Tlr4, Tlr9	9
GO:0032757	positive regulation of interleukin-8 production	4.22E-04	3.70E-02	Cd14, Ddx58, Il1b, Il6, Myd88, Nod2, Stat3, Syk, Tlr1, Tlr2, Tlr4, Tlr5, Tlr8, Tlr9, Tnf	15
GO:0030593	neutrophil chemotaxis	4.32E-04	3.70E-02	Bst1, Ccl12, Ccl2, Ccl20, Ccl3, Ccl4, Ccl6, Ccl7, Ccl9, Csf3r, Cxcl1, Cxcl10, Cxcl13, Cxcl3, Cxcr2, Fcer1g, Il1b, Itgam, Nod2, Ppbp, S100a8, S100a9, Sell, Syk, Trem1	25

Table S12: Non-reduced enriched GO Terms between deficient and engrafted

ID	Description	pvalue	qvalue	Gene ID	Count
GO:0006954	inflammatory response	1.27E-07	1.69E-04	Ccl2, Ccl7, Cxcl1, Cxcl3, Cxcr2, Cybb, Fcer1a, Hif1a, Il1b, Il1rl1, Il33, Il4ra, Il6, Ltb4r2, Ppbp, Ptgs2, S100a8, S100a9, Sele, Trem1	20
GO:0030593	neutrophil chemotaxis	7.35E-06	4.88E-03	Ccl2, Ccl7, Cxcl1, Cxcl3, Cxcr2, Il1b, Ppbp, S100a8, S100a9, Trem1	10
GO:1990266	neutrophil migration	2.69E-05	1.18E-02	Ccl2, Ccl7, Cxcl1, Cxcl3, Cxcr2, Il1b, Ppbp, S100a8, S100a9, Trem1	10
GO:0010573	vascular endothelial growth factor production	3.55E-05	1.18E-02	Ccl2, Hif1a, Il1b, Il6, Ptgs2	5
GO:0071621	granulocyte chemotaxis	5.17E-05	1.37E-02	Ccl2, Ccl7, Cxcl1, Cxcl3, Cxcr2, Il1b, Ppbp, S100a8, S100a9, Trem1	10
GO:0051179	localization	9.79E-05	2.17E-02	Ccl2, Ccl7, Cxcl1, Cxcl3, Cxcr2, Cybb, Defb14, Fcer1a, Hif1a, Il1b, Il33, Il4ra, Il6, Ltb4r2, Pou2f2, Ppbp, Ptgs2, S100a8, S100a9, Sele, Trem1	21
GO:0097530	granulocyte migration	1.64E-04	2.47E-02	Ccl2, Ccl7, Cxcl1, Cxcl3, Cxcr2, Il1b, Ppbp, S100a8, S100a9, Trem1	10
GO:0002526	acute inflammatory response	1.68E-04	2.47E-02	Cxcl1, Cxcr2, Fcer1a, Il1b, Il6, Ptgs2, Trem1	7
GO:0016477	cell migration	2.06E-04	2.47E-02	Ccl2, Ccl7, Cxcl1, Cxcl3, Cxcr2, Defb14, Hif1a, Il1b, Il33, Ltb4r2, Ppbp, Ptgs2, S100a8, S100a9, Sele, Trem1	16
GO:0048870	cell motility	2.06E-04	2.47E-02	Ccl2, Ccl7, Cxcl1, Cxcl3, Cxcr2, Defb14, Hif1a, Il1b, Il33, Ltb4r2, Ppbp, Ptgs2, S100a8, S100a9, Sele, Trem1	16
GO:0051674	localization of cell	2.06E-04	2.47E-02	Ccl2, Ccl7, Cxcl1, Cxcl3, Cxcr2, Defb14, Hif1a, Il1b, Il33, Ltb4r2, Ppbp, Ptgs2, S100a8, S100a9, Sele, Trem1	16
GO:0006952	defense response	2.31E-04	2.47E-02	Ccl2, Ccl7, Cxcl1, Cxcl3, Cxcr2, Cybb, Defb14, Fcer1a, Hif1a, Il1b, Il1rl1, Il33, Il4ra, Il6, Ltb4r2, Ppbp, Ptgs2, S100a8, S100a9, Sele, Trem1	21
GO:0006928	movement of cell or subcellular component	2.60E-04	2.47E-02	Ccl2, Ccl7, Cxcl1, Cxcl3, Cxcr2, Defb14, Hif1a, Il1b, Il33, Ltb4r2, Ppbp, Ptgs2, S100a8, S100a9, Sele, Trem1	16
GO:0040011	locomotion	2.60E-04	2.47E-02	Ccl2, Ccl7, Cxcl1, Cxcl3, Cxcr2, Defb14, Hif1a, Il1b, Il33, Ltb4r2, Ppbp, Ptgs2, S100a8, S100a9, Sele, Trem1	16
GO:0060326	cell chemotaxis	4.27E-04	3.54E-02	Ccl2, Ccl7, Cxcl1, Cxcl3, Cxcr2, Defb14, Il1b, Ppbp, S100a8, S100a9, Trem1	11
GO:0030595	leukocyte chemotaxis	4.40E-04	3.54E-02	Ccl2, Ccl7, Cxcl1, Cxcl3, Cxcr2, Il1b, Ppbp, S100a8, S100a9, Trem1	10
GO:0002523	leukocyte migration involved in inflammatory response	4.53E-04	3.54E-02	Ccl2, Ppbp, S100a8, S100a9	4
GO:0051050	positive regulation of transport	6.00E-04	4.43E-02	Ccl2, Cxcl1, Fcer1a, Hif1a, Il1b, Il33, Il4ra, Il6, Ptgs2, S100a8, S100a9, Sele	12
GO:0051047	positive regulation of secretion	7.04E-04	4.92E-02	Fcer1a, Hif1a, Il1b, Il33, Il4ra, Il6, S100a8, S100a9	8
GO:0097529	myeloid leukocyte migration	7.63E-04	4.95E-02	Ccl2, Ccl7, Cxcl1, Cxcl3, Cxcr2, Il1b, Ppbp, S100a8, S100a9, Trem1	10
GO:0050900	leukocyte migration	7.83E-04	4.95E-02	Ccl2, Ccl7, Cxcl1, Cxcl3, Cxcr2, Il1b, Il33, Ppbp, S100a8, S100a9, Sele, Trem1	12

Table S13: Non-reduced enriched GO Terms between engrafted and wild-type

ID	Description	pvalue	qvalue	Gene ID	Count
GO:0002478	antigen processing and presentation of exogenous peptide antigen	8.40E-07	9.86E-04	B2m, Cd74, Ctss, Fcer1g, Fcgr1, Fcgr2b, Fcgr3, H2-Aa, H2-Ab1, H2-DMa, H2-DMb2, H2-Eb1, H2-K1, Tap1, Tapbp	15
GO:0048002	antigen processing and presentation of peptide antigen	1.15E-06	9.86E-04	B2m, Cd74, Ctss, Fcer1g, Fcgr1, Fcgr2b, Fcgr3, H2-Aa, H2-Ab1, H2-DMa, H2-DMb2, H2-Eb1, H2-K1, H2-Q10, Hfe, Tap1, Tapbp, Trem2	18
GO:0019882	antigen processing and presentation	1.99E-05	8.90E-03	B2m, Cd74, Ctss, Fcer1g, Fcgr1, Fcgr2b, Fcgr3, H2-Aa, H2-Ab1, H2-DMa, H2-DMb2, H2-Eb1, H2-K1, H2-Q10, Hfe, Nod2, Psmb9, Relb, Tap1, Tapbp, Trem2	21
GO:0019884	antigen processing and presentation of exogenous antigen	2.07E-05	8.90E-03	B2m, Cd74, Ctss, Fcer1g, Fcgr1, Fcgr2b, Fcgr3, H2-Aa, H2-Ab1, H2-DMa, H2-DMb2, H2-Eb1, H2-K1, Tap1, Tapbp	15
GO:0002376	immune system process	9.55E-05	3.28E-02	Ahr, B2m, Batf, Bcl6, Blnk, Bst1, Bst2, Btk, C1qa, C1qb, C1ra, C2, Card9, Casp1, Ccl12, Ccl20, Ccl3, Ccl4, Ccl6, Ccr2, Ccrl2, Cd14, Cd22, Cd274, Cd36, Cd4, Cd40, Cd48, Cd74, Cd79b, Cd80, Cd83, Cd86, Ceacam1, Cfb, Cfd, Cfh, Cfp, Ciita, Clec4e, Clec5a, Cmklr1, Crlf2, Csf1, Csf1r, Csf3r, Ctss, Cx3cr1, Cxcl12, Cxcl13, Cxcl9, Cxcr2, Cxcr3, Cxcr4, Cybb, Ddx58, Ebi3, Fas, Fcamr, Fcer1g, Fcgr1, Fcgr2b, Fcgr3, Fcgr4, Fcgrt, Gpr183, H2-Aa, H2-Ab1, H2-DMa, H2-DMb2, H2-Eb1, H2-K1, H2-Q10, Hamp, Hcst, Hfe, Hlx, Ifi204, Ifih1, Ifit2, Ifnar2, Ifngr1, Ikbke, Ikzf1, Il10rb, Il15, Il15ra, Il16, Il18r1, Il2rg, Il33, Il6ra, Il7r, Il9, Irak3, Irak4, Irf1, Irf5, Irf7, Irf8, Irgm1, Itga4, Itgal, Itgam, Itgb2, Kit, Klrd1, Klrk1, Lcp2, Ltb, Ly86, Ly96, Nfatc1, Nfatc2, Nfkbia, Nfkbiz, Nod2, Nos2, Notch1, Pdgfb, Pou2f2, Pparg, Ppbp, Prdm1, Prkcd, Psmb10, Psmb9, Ptafr, Ptpn22, Ptpn6, Ptprc, Relb, Rorc, Slamf7, Spn, Stat1, Stat2, Stat5b, Syk, Tagap, Tap1, Tapbp, Tcf7, Tgfb1, Tgfbr2, Tlr1, Tlr2, Tlr4, Tlr8, Tlr9, Tnfaip3, Tnfrsf11a, Tnfrsf13b, Tnfrsf14, Tnfrsf1b, Tnfsf12, Trem2, Tslp, Tyrobp, Vcam1, Xcr1, Zeb1	162
GO:0006955	immune response	1.21E-04	3.46E-02	B2m, Batf, Bcl6, Blnk, Bst2, Btk, C1qa, C1qb, C1ra, C2, Card9, Casp1, Ccl12, Ccl20, Ccl3, Ccl4, Ccl6, Ccr2, Ccrl2, Cd14, Cd22, Cd274, Cd36, Cd4, Cd40, Cd48, Cd74, Cd79b, Cd80, Cd86, Ceacam1, Cfb, Cfd, Cfh, Cfp, Ciita, Clec4e, Clec5a, Cmklr1, Crlf2, Csf1, Csf1r, Ctss, Cx3cr1, Cxcl12, Cxcl13, Cxcl9, Cxcr2, Cxcr3, Cxcr4, Cybb, Ddx58, Fas, Fcamr, Fcer1g, Fcgr1, Fcgr2b, Fcgr3, Fcgr4, Fcgrt,	137

				Gpr183, H2-Aa, H2-Ab1, H2-DMa, H2-Eb1, H2-K1, H2-Q10, Hcst, Hfe, Hlx, Ifi204, Ifih1, Ifit2, Ifnar2, Ikbke, Il15, Il18r1, Il33, Il6ra, Il7r, Il9, Irak3, Irak4, Irf1, Irf5, Irf7, Irf8, Irgm1, Itgal, Itgam, Itgb2, Kit, Klrd1, Klrk1, Lcp2, Ltb, Ly86, Ly96, Nfatc2, Nfkbiz, Nod2, Nos2, Notch1, Pou2f2, Pparg, Ppbp, Prdm1, Prkcd, Ptafr, Ptpn22, Ptpn6, Ptprc, Relb, Rorc, Slamf7, Spn, Stat1, Stat2, Stat5b, Syk, Tap1, Tgfb1, Tlr1, Tlr2, Tlr4, Tlr8, Tlr9, Tnfaip3, Tnfrsf11a, Tnfrsf13b, Tnfrsf14, Tnfrsf1b, Tnfsf12, Trem2, Tslp, Tyrobp, Xcr1	
GO:0043207	response to external biotic stimulus	1.93E-04	3.60E-02	B2m, Batf, Bst2, Btk, C1qa, C1qb, C1ra, C2, Card9, Casp1, Ccl12, Ccl20, Ccl3, Ccl4, Ccl6, Cd14, Cd274, Cd36, Cd4, Cd40, Cd74, Cd79b, Cd80, Cd86, Ceacam1, Cfb, Cfd, Cfh, Cfp, Ciita, Clec4e, Clec5a, Csf1, Csf1r, Cx3cr1, Cxcl12, Cxcl13, Cxcl9, Cybb, Ddx58, Fcer1g, Fcgr1, Fcgr2b, Fcgr4, Fkbp5, H2-Aa, H2-Ab1, H2-Eb1, H2-K1, Hamp, Ifi204, Ifih1, Ifit2, Ifnar2, Ifngr1, Ikbke, Il10rb, Il15, Il33, Il7r, Irak2, Irak3, Irak4, Irf1, Irf5, Irf7, Irf8, Irgm1, Klrd1, Klrk1, Litaf, Ly86, Ly96, Nfkbia, Nod2, Nos2, Pou2f2, Pparg, Ppbp, Prdm1, Prkcd, Psmb9, Ptafr, Ptpn22, Ptpn6, Ptprc, Relb, Slamf7, Spn, Stat1, Stat2, Stat5b, Syk, Tagap, Tap1, Tgfb1, Tlr1, Tlr2, Tlr4, Tlr8, Tlr9, Tnfaip3, Tnfrsf11a, Tnfrsf14, Tnfrsf1b, Trem2, Tslp	107
GO:0051707	response to other organism	1.93E-04	3.60E-02	B2m, Batf, Bst2, Btk, C1qa, C1qb, C1ra, C2, Card9, Casp1, Ccl12, Ccl20, Ccl3, Ccl4, Ccl6, Cd14, Cd274, Cd36, Cd4, Cd40, Cd74, Cd79b, Cd80, Cd86, Ceacam1, Cfb, Cfd, Cfh, Cfp, Ciita, Clec4e, Clec5a, Csf1, Csf1r, Cx3cr1, Cxcl12, Cxcl13, Cxcl9, Cybb, Ddx58, Fcer1g, Fcgr1, Fcgr2b, Fcgr4, Fkbp5, H2-Aa, H2-Ab1, H2-Eb1, H2-K1, Hamp, Ifi204, Ifih1, Ifit2, Ifnar2, Ifngr1, Ikbke, Il10rb, Il15, Il33, Il7r, Irak2, Irak3, Irak4, Irf1, Irf5, Irf7, Irf8, Irgm1, Klrd1, Klrk1, Litaf, Ly86, Ly96, Nfkbia, Nod2, Nos2, Pou2f2, Pparg, Ppbp, Prdm1, Prkcd, Psmb9, Ptafr, Ptpn22, Ptpn6, Ptprc, Relb, Slamf7, Spn, Stat1, Stat2, Stat5b, Syk, Tagap, Tap1, Tgfb1, Tlr1, Tlr2, Tlr4, Tlr8, Tlr9, Tnfaip3, Tnfrsf11a, Tnfrsf14, Tnfrsf1b, Trem2, Tslp	107
GO:0009607	response to biotic stimulus	1.98E-04	3.60E-02	B2m, Batf, Bid, Bst2, Btk, C1qa, C1qb, C1ra, C2, Card9, Casp1, Ccl12, Ccl20, Ccl3, Ccl4, Ccl6, Cd14, Cd274, Cd36, Cd4, Cd40, Cd74, Cd79b, Cd80, Cd86, Ceacam1, Cfb, Cfd, Cfh, Cfp, Ciita, Clec4e, Clec5a, Csf1, Csf1r, Cx3cr1, Cxcl12, Cxcl13, Cxcl9, Cybb,	108

				Ddx58, Fcer1g, Fcgr1, Fcgr2b, Fcgr4, Fkbp5, H2-Aa, H2-Ab1, H2-Eb1, H2-K1, Hamp, Ifi204, Ifih1, Ifit2, Ifnar2, Ifngr1, Ikbke, Il10rb, Il15, Il33, Il7r, Irak2, Irak3, Irak4, Irf1, Irf5, Irf7, Irf8, Irgm1, Klrd1, Klrk1, Litaf, Ly86, Ly96, Nfkbia, Nod2, Nos2, Pou2f2, Pparg, Ppbp, Prdm1, Prkcd, Psmb9, Ptafr, Ptpn22, Ptpn6, Ptprc, Relb, Slamf7, Spn, Stat1, Stat2, Stat5b, Syk, Tagap, Tap1, Tgfb1, Tlr1, Tlr2, Tlr4, Tlr8, Tlr9, Tnfaip3, Tnfrsf11a, Tnfrsf14, Tnfrsf1b, Trem2, Tslp	
GO:0010033	response to organic substance	2.23E-04	3.60E-02	Ahr, B2m, Bst2, Btk, Card9, Casp1, Ccl12, Ccl20, Ccl3, Ccl4, Ccl6, Ccr2, Cd14, Cd274, Cd36, Cd4, Cd40, Cd74, Cd80, Cd83, Cd86, Ceacam1, Cfb, Ciita, Crlf2, Csf1, Csf1r, Csf2rb, Csf3r, Cx3cr1, Cxcl12, Cxcl13, Cxcl9, Cxcr2, Cxcr4, Ddx58, Ebi3, Fas, Fcer1g, Fcgr2b, Fcgr4, H2-Aa, H2-Ab1, H2-Eb1, Hfe, Ifi204, Ifih1, Ifit2, Ifnar2, Ifngr1, Ikbke, Il10ra, Il10rb, Il13ra1, Il15, Il15ra, Il16, Il18r1, Il1r2, Il22ra2, Il2rg, Il33, Il6ra, Irak2, Irak3, Irak4, Irf1, Irf5, Irf7, Irf8, Irgm1, Itga4, Itgb2, Jak1, Kit, Klrk1, Litaf, Ly86, Ly96, Map4k1, Nfkbia, Nod2, Nos2, Notch1, Nox4, Pdgfb, Pparg, Ppbp, Prdm1, Prkcd, Ptafr, Ptpn22, Ptpn6, Ptprc, Relb, Rorc, Stat1, Stat2, Stat5b, Syk, Tgfb1, Tgfbr2, Tlr1, Tlr2, Tlr4, Tlr9, Tnfaip3, Tnfrsf11a, Tnfrsf1b, Trem2, Tslp, Vcam1, Xcr1, Zeb1	114
GO:0002274	myeloid leukocyte activation	2.30E-04	3.60E-02	Batf, Btk, C1qa, Casp1, Ccr2, Cd48, Crlf2, Cx3cr1, Cxcr2, Fcer1g, Fcgr3, Fcgr4, Hamp, Ifngr1, Il15, Il16, Il33, Itgam, Itgb2, Kit, Klrk1, Lcp2, Pparg, Prkcd, Ptafr, Relb, Syk, Tgfb1, Tgfbr2, Tlr1, Tlr2, Tlr4, Tlr8, Tlr9, Trem2, Tslp, Tyrobp	37
GO:0006909	phagocytosis	2.69E-04	3.85E-02	C2, Ccr2, Cd36, Fcer1g, Fcgr1, Fcgr2b, Fcgr3, Il15, Il15ra, Il2rg, Irf8, Itgal, Itgam, Itgb2, Msr1, Ncf4, Nod2, Pparg, Ptprc, Syk, Tgfb1, Tlr2, Tlr4, Trem2, Tyrobp	25
GO:0044419	interspecies interaction between organisms	3.31E-04	4.35E-02	B2m, Batf, Bst2, Btk, C1qa, C1qb, C1ra, C2, Card9, Casp1, Ccl12, Ccl20, Ccl3, Ccl4, Ccl6, Cd14, Cd274, Cd36, Cd4, Cd40, Cd74, Cd79b, Cd80, Cd86, Ceacam1, Cfb, Cfd, Cfh, Cfp, Ciita, Clec4e, Clec5a, Csf1, Csf1r, Cx3cr1, Cxcl12, Cxcl13, Cxcl9, Cxcr4, Cybb, Ddx58, Fcer1g, Fcgr1, Fcgr2b, Fcgr4, Fkbp5, H2-Aa, H2-Ab1, H2-Eb1, H2-K1, Hamp, Ifi204, Ifih1, Ifit2, Ifnar2, Ifngr1, Ikbke, Il10rb, Il15, Il33, Il7r, Irak2, Irak3, Irak4, Irf1, Irf5, Irf7, Irf8, Irgm1, Klrd1, Klrk1, Litaf, Ly86, Ly96, Nfkbia, Nod2, Nos2, Notch1, Pou2f2, Pparg, Ppbp, Prdm1, Prkcd, Psmb9, Ptafr, Ptpn22, Ptpn6, Ptprc,	110

				Relb, Slamf7, Spn, Stat1, Stat2, Stat5b, Syk, Tagap, Tap1, Tgfb1, Tlr1, Tlr2, Tlr4, Tlr8, Tlr9, Tnfaip3, Tnfrsf11a, Tnfrsf14, Tnfrsf1b, Trem2, Tslp, Vcam1	
GO:0002474	antigen processing and presentation of peptide antigen via MHC class I	4.13E-04	4.35E-02	B2m, Fcer1g, Fcgr1, Fcgr3, H2-K1, H2-Q10, Hfe, Tap1, Tapbp	9
GO:0019886	antigen processing and presentation of exogenous peptide antigen via MHC class II	4.13E-04	4.35E-02	Cd74, Ctss, Fcer1g, Fcgr2b, H2-Aa, H2-Ab1, H2-DMa, H2-DMb2, H2-Eb1	9
GO:0009605	response to external stimulus	4.27E-04	4.35E-02	B2m, Batf, Bcl6, Bst1, Bst2, Btk, C1qa, C1qb, C1ra, C2, Card9, Casp1, Ccl12, Ccl20, Ccl3, Ccl4, Ccl6, Ccr2, Ccrl2, Cd14, Cd274, Cd36, Cd4, Cd40, Cd74, Cd79b, Cd80, Cd86, Ceacam1, Cfb, Cfd, Cfh, Cfp, Ciita, Clec4e, Clec5a, Cmklr1, Csf1, Csf1r, Csf3r, Ctss, Cx3cr1, Cxcl12, Cxcl13, Cxcl9, Cxcr2, Cxcr3, Cxcr4, Cybb, Ddx58, Fas, Fcer1g, Fcgr1, Fcgr2b, Fcgr3, Fcgr4, Fkbp5, Gpr183, H2-Aa, H2-Ab1, H2-Eb1, H2-K1, Hamp, Hfe, Ifi204, Ifih1, Ifit2, Ifnar2, Ifngr1, Ikbke, Il10rb, Il15, Il16, Il1r2, Il22ra2, Il33, Il7r, Irak2, Irak3, Irak4, Irf1, Irf5, Irf7, Irf8, Irgm1, Itga4, Itgam, Itgb2, Kit, Klrd1, Klrk1, Litaf, Ly86, Ly96, Nfkbia, Nfkbiz, Nod2, Nos2, Notch1, Pdgfb, Pou2f2, Pparg, Ppbp, Prdm1, Prkcd, Psmb9, Ptafr, Ptpn22, Ptpn6, Ptprc, Relb, Slamf7, Spn, Stat1, Stat2, Stat5b, Syk, Tagap, Tap1, Tgfb1, Tlr1, Tlr2, Tlr4, Tlr8, Tlr9, Tnfaip3, Tnfrsf11a, Tnfrsf14, Tnfrsf1b, Trem2, Tslp, Vcam1, Xcr1	133
GO:0098542	defense response to other organism	4.45E-04	4.35E-02	B2m, Batf, Bst2, Btk, C1qa, C1qb, C1ra, C2, Card9, Casp1, Ccl12, Ccl20, Ccl3, Ccl4, Ccl6, Cd14, Cd36, Cd4, Cd40, Cd74, Cd86, Ceacam1, Cfb, Cfd, Cfh, Cfp, Ciita, Clec4e, Clec5a, Csf1, Csf1r, Cx3cr1, Cxcl13, Cxcl9, Cybb, Ddx58, Fcer1g, Fcgr1, H2-Aa, H2-Ab1, H2-Eb1, H2-K1, Hamp, Ifi204, Ifih1, Ifit2, Ifnar2, Ifngr1, Ikbke, Il10rb, Il15, Il33, Il7r, Irak3, Irak4, Irf1, Irf5, Irf7, Irf8, Irgm1, Klrd1, Klrk1, Ly86, Ly96, Nod2, Nos2, Pparg, Prdm1, Prkcd, Ptpn22, Ptpn6, Ptprc, Relb, Slamf7, Spn, Stat1, Stat2, Stat5b, Syk, Tagap, Tap1, Tgfb1, Tlr1, Tlr2, Tlr4, Tlr8, Tlr9, Tnfaip3, Tnfrsf14, Trem2, Tslp	91
GO:0071310	cellular response to organic substance	5.21E-04	4.35E-02	Ahr, B2m, Btk, Casp1, Ccl12, Ccl20, Ccl3, Ccl4, Ccl6, Ccr2, Cd14, Cd274, Cd36, Cd4, Cd40, Cd74, Cd80, Cd86, Ceacam1, Crlf2, Csf1, Csf1r, Csf2rb, Csf3r, Cx3cr1, Cxcl12, Cxcl13, Cxcl9, Cxcr2, Cxcr4, Ddx58, Ebi3, Fcer1g,	101

				Fcgr2b, Fcgr4, H2-Ab1, Hfe, Ifi204, Ifih1, Ifit2, Ifnar2, Ifngr1, Ikbke, Il10ra, Il10rb, Il13ra1, Il15, Il15ra, Il16, Il18r1, Il1r2, Il22ra2, Il2rg, Il33, Il6ra, Irak2, Irak3, Irak4, Irf1, Irf5, Irf7, Irf8, Irgm1, Itga4, Jak1, Kit, Klrk1, Litaf, Ly86, Ly96, Map4k1, Nfkbia, Nod2, Nos2, Notch1, Nox4, Pdgfb, Pparg, Ppbp, Prdm1, Prkcd, Ptpn22, Ptpn6, Ptprc, Rorc, Stat1, Stat2, Stat5b, Syk, Tgfb1, Tgfbr2, Tlr2, Tlr4, Tlr9, Tnfaip3, Tnfrsf11a, Tnfrsf1b, Trem2, Tslp, Vcam1, Zeb1	
GO:0006952	defense response	5.82E-04	4.35E-02	B2m, Batf, Bcl6, Bst1, Bst2, Btk, C1qa, C1qb, C1ra, C2, Card9, Casp1, Ccl12, Ccl20, Ccl3, Ccl4, Ccl6, Ccr2, Ccrl2, Cd14, Cd36, Cd4, Cd40, Cd74, Cd86, Ceacam1, Cfb, Cfd, Cfh, Cfp, Ciita, Clec4e, Clec5a, Cmklr1, Crlf2, Csf1, Csf1r, Ctss, Cx3cr1, Cxcl12, Cxcl13, Cxcl9, Cxcr2, Cxcr3, Cybb, Ddx58, Fcer1g, Fcgr1, Fcgr2b, Fcgr3, H2-Aa, H2-Ab1, H2-Eb1, H2-K1, Hamp, Ifi204, Ifih1, Ifit2, Ifnar2, Ifngr1, Ikbke, Il10rb, Il15, Il16, Il18r1, Il1r2, Il22ra2, Il33, Il7r, Irak2, Irak3, Irak4, Irf1, Irf5, Irf7, Irf8, Irgm1, Itgam, Itgb2, Kit, Klrd1, Klrk1, Ly86, Ly96, Nfkbia, Nfkbiz, Nod2, Nos2, Notch1, Nox4, Pla2g2e, Pparg, Ppbp, Prdm1, Prkcd, Ptafr, Ptpn22, Ptpn6, Ptprc, Relb, Slamf7, Spn, Stat1, Stat2, Stat5b, Syk, Tagap, Tap1, Tapbp, Tgfb1, Tlr1, Tlr2, Tlr4, Tlr8, Tlr9, Tnfaip3, Tnfrsf11a, Tnfrsf14, Tnfrsf1b, Trem2, Tslp, Tyrobp	122
GO:0045087	innate immune response	5.91E-04	4.35E-02	B2m, Bst2, Btk, C1qa, C1qb, C1ra, C2, Card9, Casp1, Ccl12, Ccl20, Ccl3, Ccl4, Ccl6, Cd14, Cd40, Cd74, Ceacam1, Cfb, Cfd, Cfh, Cfp, Ciita, Clec4e, Clec5a, Csf1, Csf1r, Cx3cr1, Cybb, Ddx58, Fcer1g, Fcgr1, H2-Aa, H2-Ab1, H2-Eb1, Ifi204, Ifih1, Ifit2, Ifnar2, Ikbke, Irak3, Irak4, Irf1, Irf5, Irf7, Irf8, Irgm1, Klrd1, Klrk1, Ly86, Ly96, Nod2, Nos2, Pparg, Prdm1, Ptpn6, Relb, Slamf7, Stat1, Stat2, Stat5b, Syk, Tap1, Tgfb1, Tlr1, Tlr2, Tlr4, Tlr8, Tlr9, Tnfaip3, Tnfrsf14, Trem2	72
GO:0002495	antigen processing and presentation of peptide antigen via MHC class II	6.33E-04	4.35E-02	Cd74, Ctss, Fcer1g, Fcgr2b, H2-Aa, H2-Ab1, H2-DMa, H2-DMb2, H2-Eb1, Trem2	10
GO:0002504	antigen processing and presentation of peptide or polysaccharide antigen via MHC class II	6.33E-04	4.35E-02	Cd74, Ctss, Fcer1g, Fcgr2b, H2-Aa, H2-Ab1, H2-DMa, H2-DMb2, H2-Eb1, Trem2	10
GO:0006911	phagocytosis, engulfment	6.33E-04	4.35E-02	Cd36, Fcer1g, Fcgr1, Fcgr2b, Fcgr3, Itgam, Itgb2, Msr1, Pparg, Trem2	10

GO:0010324	membrane invagination	6.33E-04	4.35E-02	Cd36, Fcer1g, Fcgr1, Fcgr2b, Fcgr3, Itgam, Itgb2, Msr1, Pparg, Trem2	10
GO:0099024	plasma membrane invagination	6.33E-04	4.35E-02	Cd36, Fcer1g, Fcgr1, Fcgr2b, Fcgr3, Itgam, Itgb2, Msr1, Pparg, Trem2	10